

UNCLASSIFIED

AD 408 799

DEFENSE DOCUMENTATION CENTER

FOR

SCIENTIFIC AND TECHNICAL INFORMATION

CAMERON STATION, ALEXANDRIA, VIRGINIA



UNCLASSIFIED

NOTICE: When government or other drawings, specifications or other data are used for any purpose other than in connection with a definitely related government procurement operation, the U. S. Government thereby incurs no responsibility, nor any obligation whatsoever; and the fact that the Government may have formulated, furnished, or in any way supplied the said drawings, specifications, or other data is not to be regarded by implication or otherwise as in any manner licensing the holder or any other person or corporation, or conveying any rights or permission to manufacture, use or sell any patented invention that may in any way be related thereto.

(5) 574 190

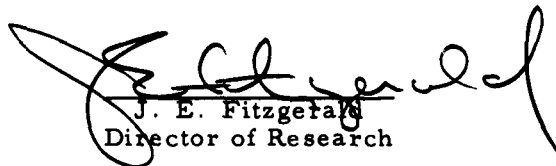
(4) 11.50

(14)
LPC Report No. 578/556/Ff3
copy 62

(6) ENGINEERING METHODS FOR GRAIN STRUCTURAL
INTEGRITY ANALYSIS . (7) - (11) . A

(11) May 1963, (12) 10. (13) NA

Approved by:


J. E. Fitzgerald
Director of Research

(15)
This research was partially supported by the Space
Systems Division, Air Force Systems Command,
United States Air Force, Edwards Air Force Base,
California, under Contract No. AF 04(611) 28013 and
by the Propulsion Laboratory, Army Missile Com-
mand, Redstone Arsenal, Alabama under Contract
No. DA 04-4957 ORD 3260.

(16) - (17) 111 (18) 11 (19) 11

LOCKHEED PROPULSION COMPANY
P. O. Box 111
Redlands, California

agw

*Flaming Content
7/29/64*

CONTENTS

	Page
FOREWORD	iv
1. ENGINEERING PROCEDURES FOR PROPELLANT PHYSICAL CHARACTERIZATION	1-3
1.1 MASTER STRESS RELAXATION MODULUS	1-4
1.2 CONSTANT CROSSHEAD RATE ULTIMATE PROPERTIES	1-15
1.3 CONSTANT LOAD ULTIMATE PROPERTIES	1-21
1.4 CONSTANT STRAIN ULTIMATE PROPERTIES	1-24
1.5 PROPELLANT-LINER-SUBSTRATE BONDING ULTIMATE PROPERTIES	1-25
1.6 REDUCED LINEAR COEFFICIENT OF THERMAL EXPANSION	1-30
2. ENGINEERING METHODS FOR GRAIN STRUCTURAL ANALYSIS	2-2
2.1 THERMAL STRAIN ANALYSIS - PROBLEM 1	2-3
2.2 THERMAL STRAIN FAILURE ANALYSIS - PROBLEM 1A	2-7
2.3 GRAIN SLUMP DEFLECTIONS - PROBLEM 2	2-9
2.4 GRAIN PRESSURIZATION - PROBLEM 3	2-16
2.5 PRESSURIZATION STRAIN FAILURE ANALYSIS - PROBLEM 3A	2-18
3. BACKGROUND AND MATHEMATICAL PROCEDURES	3-2
3.1 PROPELLANT VISCOELASTIC PROPERTIES	3-3
3.2 CONSTANT CROSSHEAD RATE FAILURE PROPERTIES	3-21
3.3 CONSTANT LOAD PROPERTIES	3-22

CONTENTS (Continued)

	Page
3.4 CONSTANT STRAIN PROPERTIES	3-23
3.5 PROPELLANT-LINER-SUBSTRATE BOND PROPERTIES	3-23
3.6 REDUCED LINEAR COEFFICIENT OF EXPANSION	3-24
3.7 BIAXIAL TESTING OF TOXIC OR RARE MATERIALS	3-25
3.8 ANALOG MOTOR TESTS	3-20
4. GRAIN STRUCTURAL ANALYSIS METHODS DISCUSSION, ALTERNATE METHODS, AND LIMIT DESIGN CONSIDERATIONS	4-2
4.1 THERMAL STRAIN ANALYSIS	4-2
4.2 THERMAL STRAIN FAILURE ANALYSIS	4-4
4.3 GRAIN SLUMP DEFLECTIONS	4-6
4.4 GRAIN PRESSURIZATION	4-8
4.5 PRESSURIZATION FAILURE ANALYSIS	4-9
4.6 STORAGE AND LAUNCH STRESSES	4-10
4.7 GRAIN TERMINATIONS	4-11
4.8 STAR POINT DEFLECTION DURING HORIZONTAL STORAGE	4-15
APPENDIX A TEST SPECIMEN PREPARATION	A-1
APPENDIX B OPERATOR EQUATION - PRONY SERIES COEFFICIENTS	B-1
APPENDIX C UNIAXIAL TENSILE CREEP COMPLIANCE TEST	C-1
APPENDIX D REFERENCE FIGURES FOR GRAIN STRAIN AND SLUMP CALCULATIONS	D-1

REFERENCES

FOREWORD

During the past five years, the specialized engineering analysis techniques required in solid propellant grain structural integrity evaluation have received increasing attention. Following the Joint Services Physical Property Panel Meeting in 1958, where the need for research in this area was emphasized, intensified effort resulted in development of engineering methods for analysis of viscoelastic propellant grains. A program of research under the direction of Dr. M. L. Williams at the California Institute of Technology resulted in the publication of "Fundamental Studies Relating to Systems Analysis of Solid Propellants" (GALCIT SM 61-5) in 1961. The report rapidly gained the status of a reference text for the solid propellant industry, and, with the permission of the authors, has been excerpted extensively in this handbook. Indeed, the present handbook is regarded as an extension of the GALCIT SM 61-5 report, with primary attention directed at presentation of engineering methods in propellant grain structural analysis.

The physical behavior of solid propellant, in contrast to elastic solids, is significantly affected by small changes in the temperature and characteristic time scale under consideration. For this reason, the methods of linear viscoelastic stress analysis are used to quantitatively assess the behavior of a grain under pressure, temperature and environmental loading. This handbook does not attempt to treat the complexities of viscoelastic structural analysis theory in detail, but rather to describe engineering methods that have been found useful in applying this theory in grain analysis. With exceptions as noted in the text, the engineering methods described herein have been verified in motor structural models, static test motors, and flight motors in programs at Lockheed Propulsion Company.

The handbook has been compiled for engineering use. Section 1 describes, without extensive background, methods for laboratory characterization of propellants. Section 2 treats state-of-the-art engineering grain analysis methods, also without extensive background. More specialized aspects of these problem areas are discussed in Sections 3 and 4 and pertinent literature source references are given. The references cited are mainly those to which convenient access is possible; no priority of publication is implied. Reference data, propellant specimens preparation techniques, and auxiliary laboratory methods are included in the Appendices. The information presented in this handbook is comprehensive only in that sufficient information has been included to permit complete engineering analysis of grain structural problems presently regarded as having been reduced to practice. Grain structural problems associated with complex motor designs and complex material properties require highly specialized engineering and mathematical treatments that are considered beyond the present scope of the handbook.

Advantage has been taken of the fact that extensive information concerning propellant physical characterization will be available about mid 1963 in the "ICRPG Solid Propellant Mechanical Behavior Manual". Summary information concerning certain test procedures has been included herein with reference to more extensive discussions in the ICRPG Manual, as appropriate.

This handbook has been compiled and edited under the direction of J. W. Jones by the Lockheed Propulsion Company Structural Integrity Department.

Section 1

ENGINEERING PROCEDURES FOR PROPELLANT
PHYSICAL CHARACTERIZATION

CONTENTS

	Page
1. ENGINEERING PROCEDURES FOR PROPELLANT PHYSICAL CHARACTERIZATION	1-3
1.1 MASTER STRESS RELAXATION MODULUS	1-4
1.1.1 Reduced Variable Data Reduction	1-9
1.2 CONSTANT CROSSHEAD RATE ULTIMATE PROPERTIES	1-15
1.3 CONSTANT LOAD ULTIMATE PROPERTIES	1-21
1.4 CONSTANT STRAIN ULTIMATE PROPERTIES	1-24
1.5 PROPELLANT-LINER-SUBSTRATE BONDING ULTIMATE PROPERTIES	1-25
1.6 REDUCED LINEAR COEFFICIENT OF THERMAL EXPANSION	1-30

TABLES

1-1 COMPUTATION SHEET - STRESS RELAXATION MODULUS, $E(t)$	1-7
1-2 COMPUTATION SHEET - SHIFT FACTOR a_T	1-11
1-3 COMPUTATION SHEET - STRESS RELAXATION MODULUS, $E(t)$	1-13

FIGURES

	Page
1-1 Tab End Tensile Specimen, Schematic	1-4
1-2 Tab End Tensile Specimen Under Test	1-5
1-3 Force and Displacement versus Time, Ramp Stress Relaxation Test	1-6
1-4 Stress Relaxation Data for Temperatures Between -110°F and +174°F, Polycarbutene-R Propellant Batch 7958 . . .	1-8
1-5 Temperature-Time Shift Relationships, $T < T_g$	1-9
1-6 Temperature-Time Shift Relationships, $T > T_g$	1-10
1-7 Master Stress Relaxation Modulus at $T = 70^\circ$, 150° , and -68°F and Shift Factor, Polycarbutene-R Propellant Batch 7958	1-14
1-8 JANAF Tensile Specimen with Plastic Strain Gage	1-16
1-9 Typical Tensile Test Force-Time Curves	1-17
1-10 Constant Crosshead Rate Properties, Polycarbutene-R Propellant Batch 7958, JANAF Measured Strain Technique	1-19
1-11 Time-Temperature Data Conversion Procedure	1-20
1-12 Constant Load Data	1-21
1-13 Master Curve for Constant Load Strength versus Time to Rupture	1-23
1-14 Bond in Tension Specimen	1-26
1-15 Bond Test Specimen Showing Cohesive Propellant Failure	1-27
1-16 Constant Rate Liner/Propellant/Substrate Bond Data, Polycarbutene-R Propellant	1-28
1-17 Quartz Tube Dilatometer	1-31
1-18 Reduced Propellant Linear Coefficient of Thermal Expansion versus Temperature	1-32

Section 1

ENGINEERING PROCEDURES FOR PROPELLANT PHYSICAL CHARACTERIZATION

The following subsections describe methods for determining those specific propellant physical properties used in performing the grain structural analyses given in Sections 2 and 4. Engineering techniques for viscoelastic property, failure criteria and propellant thermal expansion coefficient determination are described and examples presented. The methods of testing and data handling described have been selected such that only conventional laboratory apparatus is required for execution of the tests and only slide rule or desk calculation methods need be used in data reduction.

Each of the mechanical tests described can be performed using a conventional tensile testing apparatus, such as the Instron Universal Tester. The determination of the coefficient of thermal expansion of propellant requires a linear dilatometer. Alternate and in some instances more economical methods exist for conducting the various tests. The test procedures described are, therefore, representative of the general method, and illustrative of their basic simplicity. Description of preferred methods for propellant test specimen preparation and handling is included in Appendix A of the handbook.

General background information pertinent to the tests is discussed in Section 3 and additional, more specialized methods of test and data handling are described. The subsection organization of Sections 1 and 3 correspond numerically and topically for convenience in cross referencing.

1.1 MASTER STRESS RELAXATION MODULUS (Reference Section 3.1)

Purpose: Determination of the stress relaxation modulus by ramp strain, stress relaxation techniques. Isothermal and reduced variable data reduction methods are described and illustrated. The time-temperature correspondence concept, used in reduced variable treatments, is emphasized as an engineering method for obtaining the broad spectrum master relaxation moduli needed in grain analysis (Section 1.1.1).

Test Equipment: Instron Universal Tester with temperature conditioning chamber, or equivalent apparatus.

Test Specimen: Machined tab-end tensile specimen (Appendix A) as shown schematically in Figure 1-1:

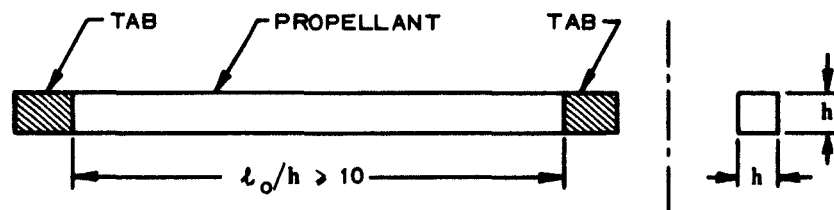


Figure 1-1 Tab End Tensile Specimen, Schematic

with dimensions

$$\text{Propellant length} = l_0 \text{ (in.)}$$

$$\text{Cross section area} = h^2 \text{ (in.}^2\text{)} = A_0$$

in the unstrained state.

Test Method: The tab-end specimen, conditioned at a constant temperature is clamped in the jaws of the tester (Figure 1-2) and extended at a constant crosshead speed to a predetermined length where the crosshead is stopped.

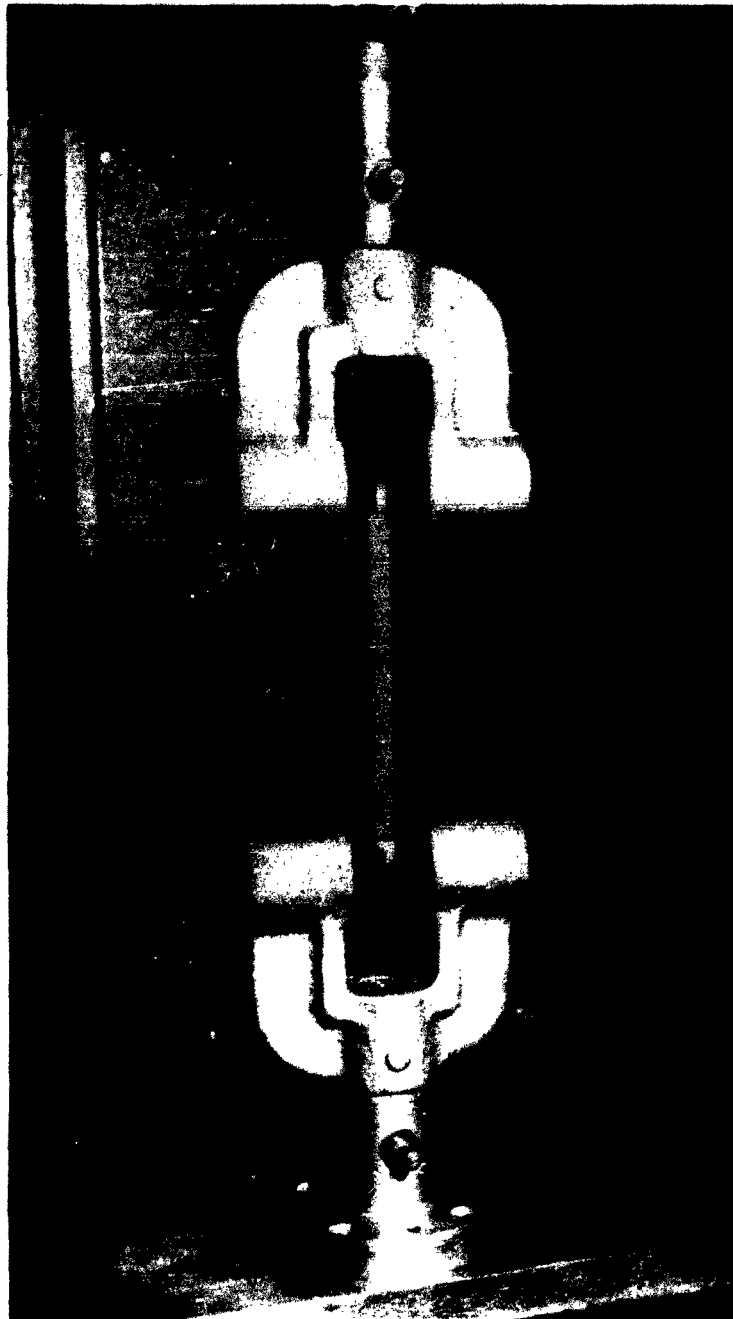


Figure 1-2 Tab End Tensile Specimen Under Test

The decay of force at the extended length is measured as time progresses. With reference to Figure 1-1 and Figure 1-3, the following constants for the test analysis are defined:

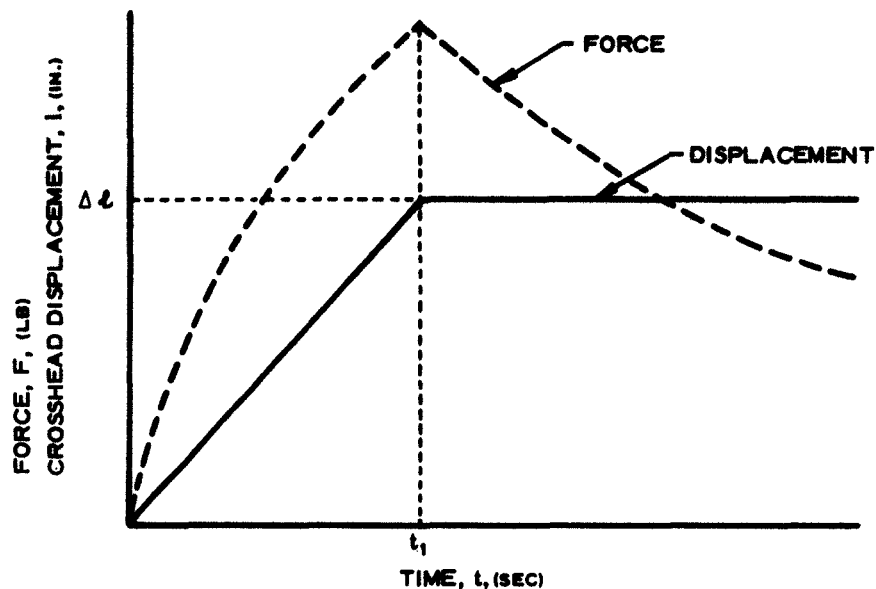


Figure 1-3 Force and Displacement versus Time, Ramp Stress Relaxation Test

$$\text{Strain at time } t_1 = \epsilon_1 = \frac{\Delta l}{l_0} \text{ (in./in.)}$$

$$\text{True stress (for } t > t_1) = \frac{F(1 + \epsilon_1)}{A_0} \text{ (psi)}$$

$$\text{Relaxation Modulus} = E(t) = \frac{F(1 + \epsilon_1)}{A_0 \epsilon_1}$$

Strain levels ϵ_1 between 0.01 and 0.10 are commonly employed in this test.

Reduction of Isothermal Data: The relaxation modulus at a given temperature for times greater than $10 t_1$ only is calculated and plotted on log-log graph paper. Table 1-1 illustrates calculation of the relaxation modulus at $T = 70^\circ\text{F}$. Figure 1-4 depicts the data of Table 1-1 in addition to data for several other temperatures.

PREPARED BY LC
 CHECKED BY MB
 APPROVED BY T

PAGE 1 OF 1
 DATE 6-16-63
 REPORT NO. 578-F-3

COMPUTATION SHEET - STRESS RELAXATION MODULUS, E (t)

REMARKS _____ PROPELLANT Polycarbonate R
 BATCH 7958

TEMPERATURE 70°

SPECIMEN GAGE LENGTH, l_0 = 4.00 (IN.)

SPECIMEN X-SECTION AREA, A_0 = 0.160 (IN.²)

TESTER X-HEAD DISPLACEMENT, Δl = 0.200 (IN.)

STRAIN LEVEL, ϵ_1 = $\frac{\Delta l}{l_0} = \frac{0.200}{4.00} = 0.050$ (IN./IN.)

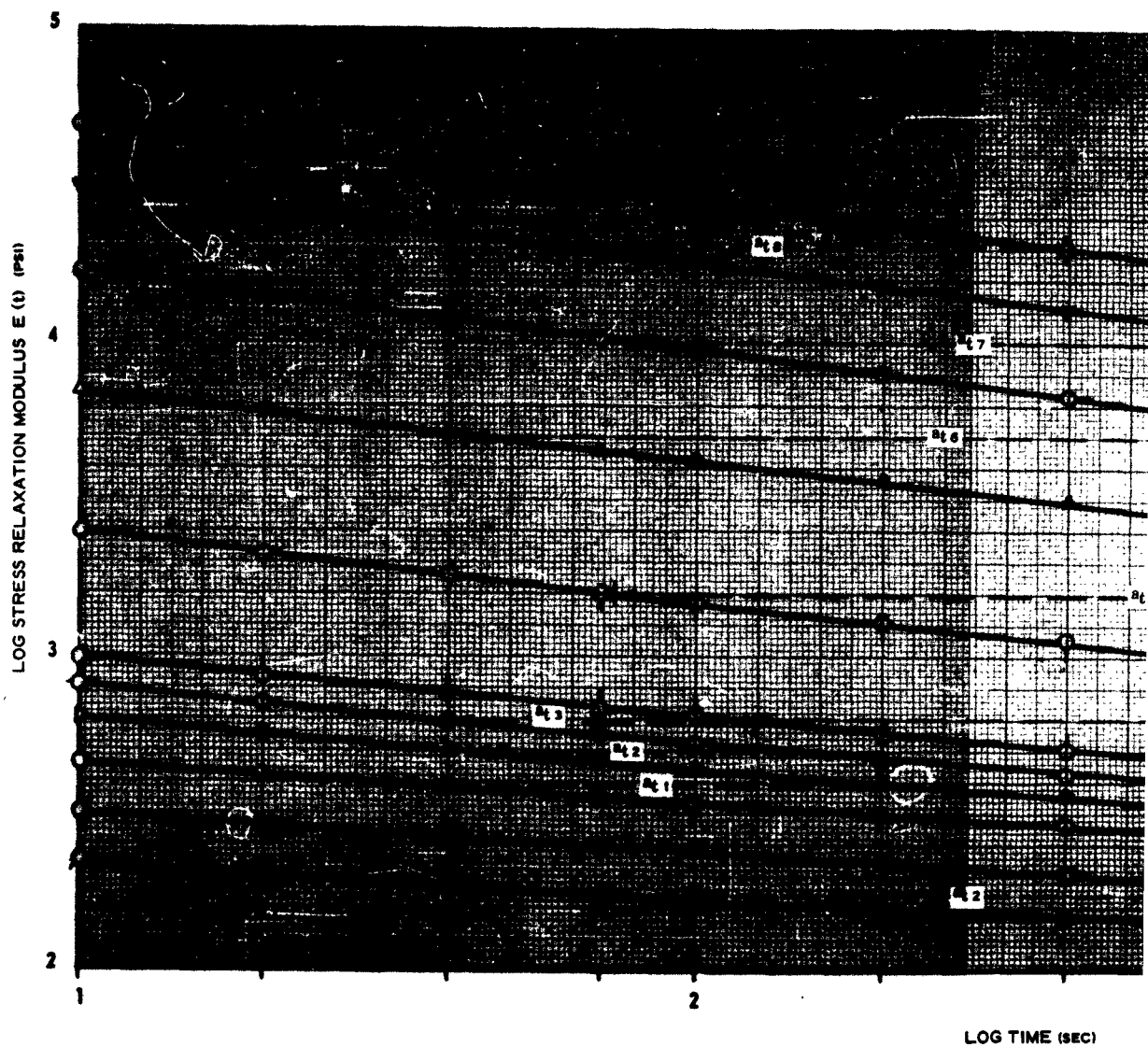
$$E(t) = \frac{F(1 + \epsilon_1)}{A_0 \epsilon_1}$$

F = FORCE, LBS

$$\frac{1 + \epsilon_1}{A_0 \epsilon_1} = \frac{1.05}{0.008} = 131; \text{LOG } \frac{1 + \epsilon_1}{A_0 \epsilon_1} = 2.117$$

= LOG a_T

TIME t (SEC)	LOG t	LOG t - LOG a_T	F (LBS)	LOG F	LOG $\frac{1 + \epsilon_1}{A_0 \epsilon_1}$	LOG E (t)	E (t) (PSI)
10	1.000		3.58	0.554	2.117	2.671	468
20	1.301		3.26	0.513	2.117	2.630	427
40	1.602		2.98	0.475	2.117	2.592	391
70	1.845		2.81	0.449	2.117	2.566	368
100	2.000		2.67	0.427	2.117	2.544	350
200	2.301		2.46	0.391	2.117	2.508	322
400	2.602		2.28	0.358	2.117	2.475	298
700	2.845		2.13	0.328	2.117	2.445	279
1000	3.000		2.02	0.306	2.117	2.423	265
2000	3.301		1.88	0.274	2.117	2.391	246
4000	3.602		1.70	0.231	2.117	2.348	223
7000	3.845		1.60	0.205	2.117	2.322	210
10000	4.000		1.53	0.184	2.117	2.301	200



Stress Relaxation Data for Temperature
Polycarbonate-R Propellant Batch 7958

TAB END TENSILE SPECIMENS

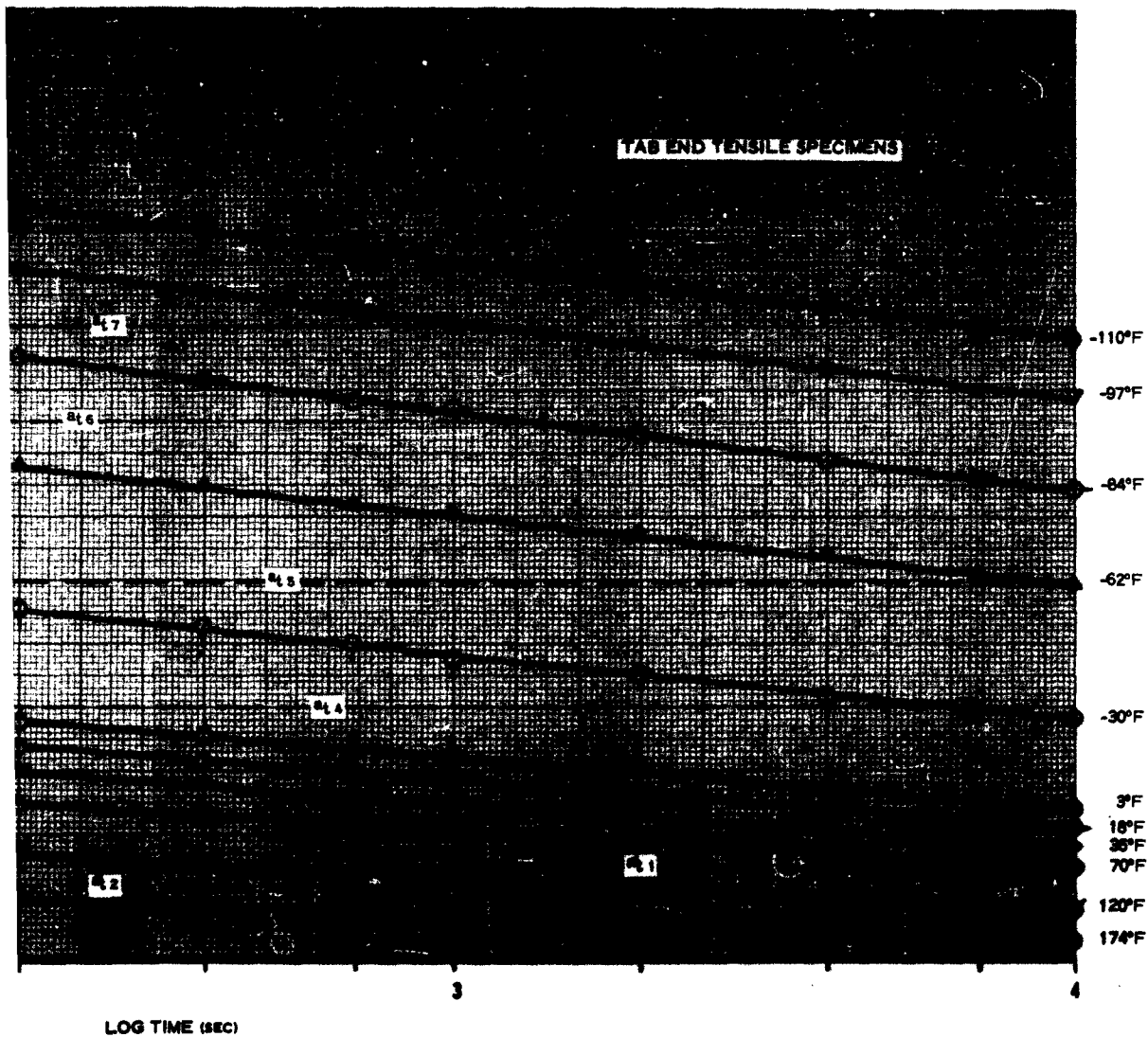


Figure 1-4

Data for Temperatures Between -110°F and +174°F,
Propellant Batch 7958

1.1.1 Reduced Variable Data Reduction

Determination of the Time-Temperature Shift Factor: An arbitrary reference temperature T_s is selected. Conveniently, the test temperature nearest the ambient laboratory room temperature is chosen.

For data at test temperatures T less than T_s , data such as those of Figure 1-4, are shifted to the left. The relative shift a_{T_n} necessary to bring adjacent curves into superposition is determined.

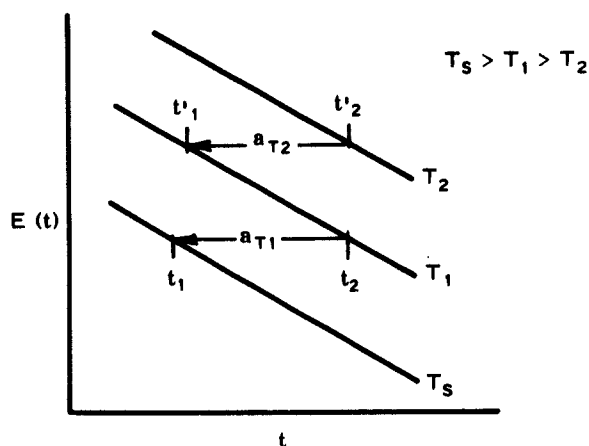


Figure 1-5 Temperature-Time Shift Relationships, $T < T_s$

For example, from Figure 1-5,

$$a_{T_1} = \frac{t_2}{t_1} \text{ or } \log a_{T_1} = \log t_2 - \log t_1$$

$$a_{T_2} = \frac{t'_2}{t'_1} \text{ or } \log a_{T_2} = \log t'_2 - \log t'_1$$

The shift factor a_T for temperature T_1 is a_{T_1} as given. The shift factor for temperature T_2 is $a_{T_1} \times a_{T_2}$ (or $\log a_{T_1} + \log a_{T_2}$). The process is repeated for each temperature; the shift factor for data at the lowest temperature is given by the product of the a_{T_n} (or the sum of the $\log a_{T_n}$).

For data at a test-temperature T greater than T_s , data are shifted to the right. The relative shift a_{T_N} necessary to bring adjacent curves into superposition is determined.

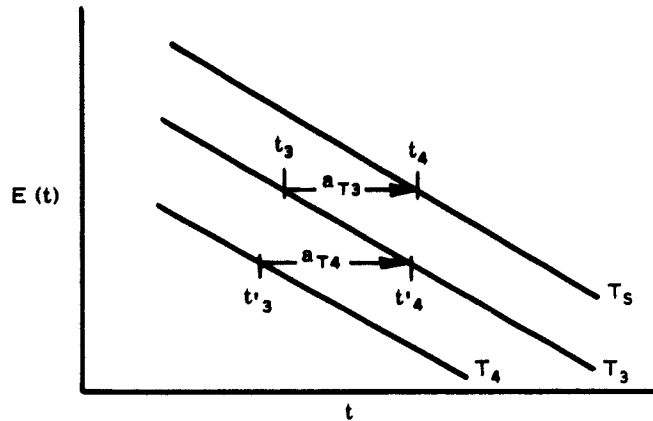


Figure 1-6 Temperature-Time Shift Relationships, $T > T_s$

For example, with reference to Figure 1-6,

$$a_{T_3} = \frac{t_3}{t_4} \text{ or } \log a_{T_3} = \log t_3 - \log t_4$$

$$a_{T_4} = \frac{t'_3}{t'_4} \text{ or } \log a_{T_4} = \log t'_3 - \log t'_4$$

The shift factor a_T for temperature T_3 is as given. The shift factor for temperature T_4 is $a_{T_3} \times a_{T_4}$ (or $\log a_{T_3} + \log a_{T_4} = \log a_T$).

The shifts a_{T_N} are shown on Figure 1-4 and the associated calculations for determination of $\log a_T$ are shown in Table 1-2. The circled notations in the " $\log a_{T_N}$ " column of Table 1-2 identify the shifts shown on Figure 1-4.

Conversion of the data of Figure 1-4 to master curve form is accomplished by performing the shift a_T for the data at each temperature. This corresponds to division of the time scale for the data at each temperature by the value of a_T for that temperature. More conveniently, the operation is conducted logarithmically ($\log t/a_T = \log t - \log a_T$).

PREPARED BY LC
 CHECKED BY MB
 APPROVED BY [Signature]

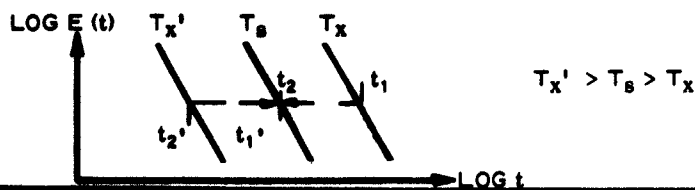
PAGE 1 OF 1
 DATE 6-16-63
 REPORT NO. 578-F-3

COMPUTATION SHEET - SHIFT FACTOR a_T

REMARKS _____

PROPELLANT Polycarbonate RBATCH 7958

T_1	T_2	LOG t_1	LOG t_2	= LOG a_{Tn}	LOG a_T for T_1
35	T_s 70	2.32	1.51	0.81 (✓) =	0.81 35
18	35	2.15	1.66	+0.49 (✓) =	1.30 18
3	18	2.10	1.60	+0.50 (✓) =	1.80 3
-30	3	3.82	2.09	+1.73 (✓) =	3.53 -30
-62	-30	3.96	1.86	+2.10 (✓) =	5.63 -62
-84	-62	3.15	1.64	+1.51 (✓) =	7.14 -84
-97	-84	3.08	1.90	+1.18 (✓) =	8.32 -97
-110	-97	2.60	1.75	+0.84 (✓) =	9.16 -110
				+	=
				+	=
				+	=

 $\uparrow T_x < T_s \uparrow$  $\uparrow T_x > T_s \uparrow$

T_1	T_2	LOG t_2	LOG t_2	= LOG a_{Tn}	LOG a_T for T_2
T_s 70	120	273	396	+ -1.23 (✓) =	-1.23 120
120	174	186	317	+ -1.31 (✓) =	-2.54 174
				+	=
				+	=
				+	=
				+	=
				+	=

The calculation of t/a_T is illustrated in Table 1-3, Column 3 and the reduced master relaxation modulus curve is shown in Figure 1-7. The master relaxation modulus curve displays the modulus versus time behavior of the propellant at the temperature $T_s = 70^\circ$. The relaxation curve for another temperature is obtained by shifting the master time scale. The shift for the temperature of interest is achieved by multiplication along the time scale by the value of a_T for the given temperature, or logarithmically, by adding $\log a_T$ to the master time scale. Shifted time scales for temperatures of 150°F and -68°F are shown in Figure 1-7.

By convention, master data obtained by reduced variable techniques is indicated by the notation, for example, $E(\tau)$ where τ is equivalent to t/a_T .

PREPARED BY LC
 CHECKED BY MB
 APPROVED BY [Signature]

PAGE 1 OF 1
 DATE 6-16-63
 REPORT NO. 578-F-3

COMPUTATION SHEET - STRESS RELAXATION MODULUS, E (t)

REMARKS _____ PROPELLANT Polycarbonate R
 BATCH 7958

TEMPERATURE 174°F

SPECIMEN GAGE LENGTH, l_0 = 4.00 (IN.)

SPECIMEN X-SECTION AREA, A_0 = 0.160 (IN.²)

TESTER X-HEAD DISPLACEMENT, Δl = 0.200 (IN.)

STRAIN LEVEL, ϵ_1 , = $\frac{\Delta l}{l_0} = \frac{0.200}{4.00} = 0.050$ (IN./IN.)

$$E(t) = \frac{F(1 + \epsilon_1)}{A_0 \epsilon_1}$$

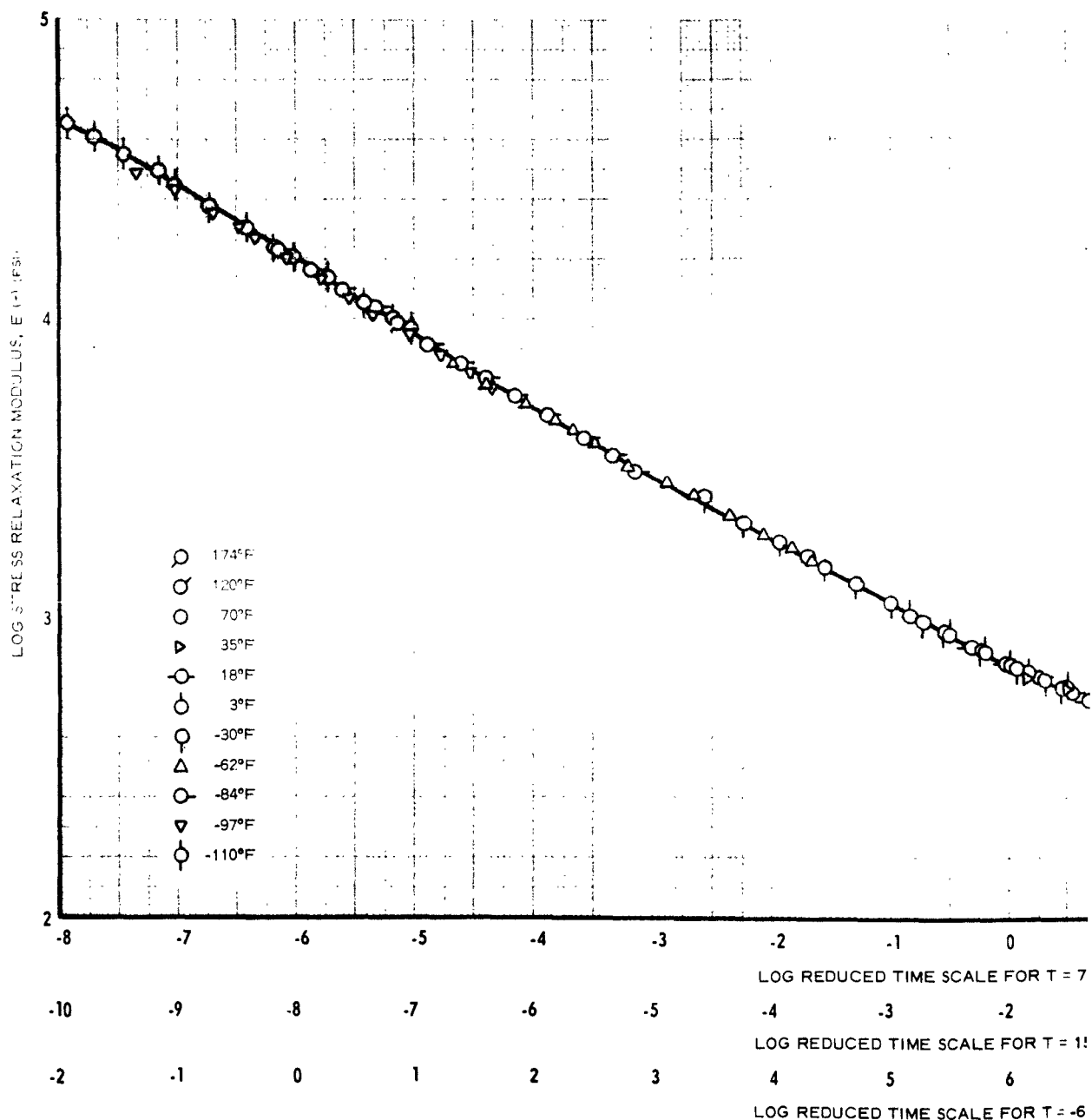
F = FORCE, LBS

$$\frac{1 + \epsilon_1}{A_0 \epsilon_1} = \frac{1.05}{0.008} = 1.31; \text{LOG } \frac{1 + \epsilon_1}{A_0 \epsilon_1} = 2.117$$

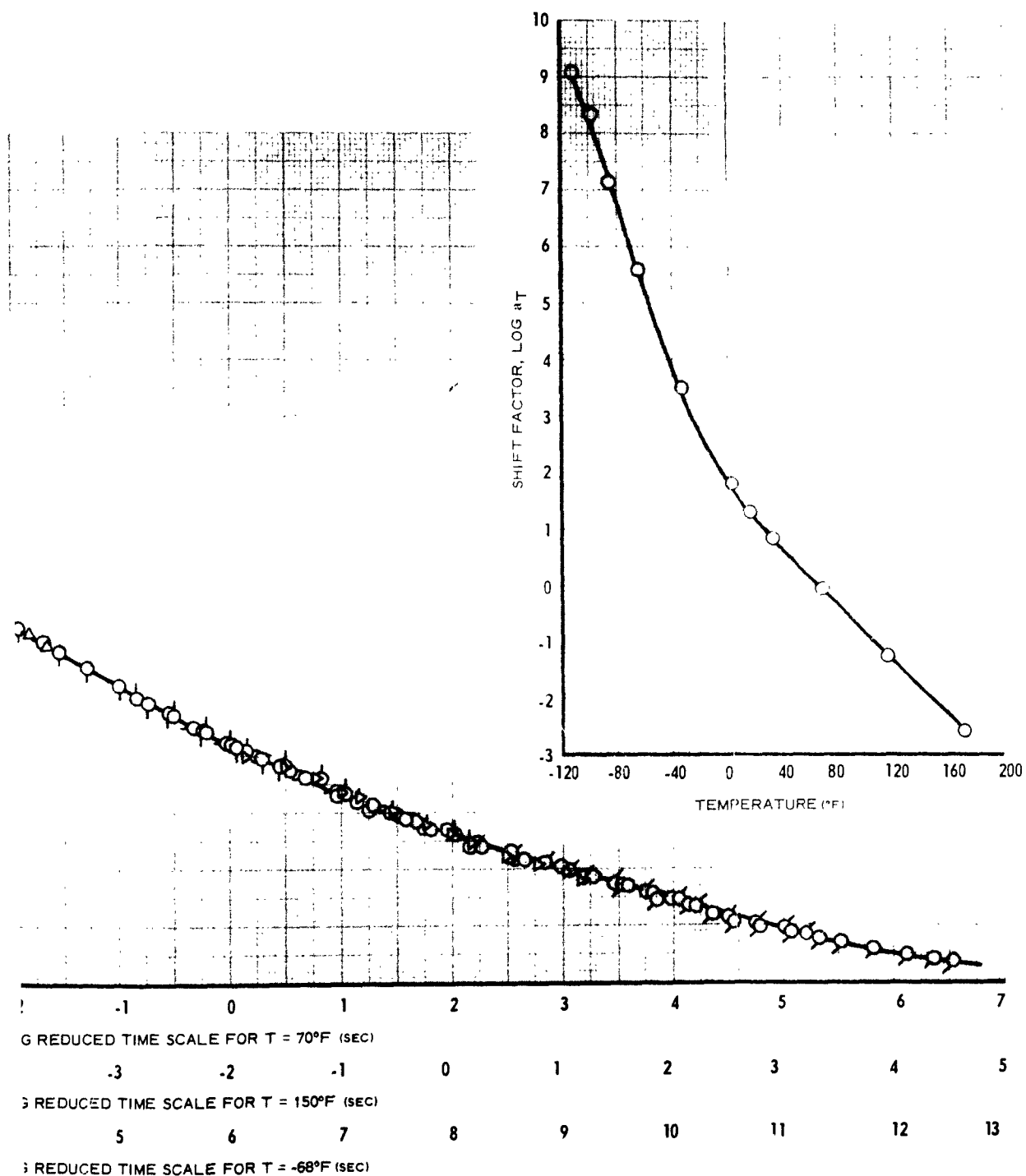
$$= \text{LOG } a_T$$

TIME t (SEC)	LOG t	LOG t - LOG a_T	F (LB)	LOG F	LOG $\frac{1 + \epsilon_1}{A_0 \epsilon_1}$	LOG E (t)	E (t) (PSI)
10	1.000	3.54	1.72	0.235	2.117	2.352	225
20	1.301	3.841	1.56	0.193	2.117	2.310	204
40	1.602	4.142	1.46	0.163	2.117	2.280	191
70	1.845	4.385	1.36	0.133	2.117	2.250	178
100	2.000	4.54	1.32	0.121	2.117	2.238	173
200	2.301	4.841	1.22	0.085	2.117	2.202	159
400	2.602	5.142	1.14	0.053	2.117	2.175	150
700	2.845	5.385	1.10	0.041	2.117	2.158	144
1000	3.000	5.54	1.07	0.029	2.117	2.146	140
2000	3.301	5.841	1.01	0.003	2.117	2.120	132
4000	3.602	6.142	0.958	-0.019	2.117	2.098	125
7000	3.845	6.385	0.916	-0.038	2.117	2.079	120
10000	4.000	6.54	0.879	-0.056	2.117	2.061	115

1



Master Stress Relaxation Modulus at $T = 70^\circ$,
Shift Factor, Polycarbuthene-R Propellant Batch



tion Modulus at T = 70°, 150°, and -68°F, and
butene-R Propellant Batch 7958

Figure 1-7



1.2 CONSTANT CROSSHEAD RATE ULTIMATE PROPERTIES (Reference Section 3.2)¹

Purpose: Determination of the strain at nominal maximum load and the true stress at nominal maximum load as measured under constant crosshead rate test conditions.

Test Equipment: Instron Universal Tester with temperature conditioning chamber or equivalent apparatus.

Test Specimen: Machined tab-end specimen (Figure 1-1, Section 1.1) or machined JANAF "dumbbell" with provision for strain measurement in the gage section (Figure 1-8 and Appendix A). The tab-end specimen is preferred. The common availability of JANAF specimens, however, requires their present use. Uniaxial failure data in this handbook were obtained in tests of JANAF samples.

Test Method: The specimen is fixed in the grips of the tester and extended at a constant tester crosshead speed until rupture occurs. Samples are pre-conditioned and tested at various temperatures. Although any crosshead speed may be selected, two inches per minute is a useful standard laboratory rate.

Data Reduction: The force versus time record of the Instron test is interpreted for the nominal maximum load, F_m , point. Figure 1-9 shows typical forms of the Instron record with the interpretation of F_m indicated. The strain at F_m is the strain at nominal maximum stress σ_m . The strain ϵ_m is either read directly from the data of the strain measuring device (Appendix A) or for the tab-end specimen is given by

$$\epsilon_m = \frac{R}{l_0} t_m$$

where R is the Instron crosshead speed (in./sec) and t_m (sec) is the time at which F_m occurs. l_0 is the unstrained length of the propellant bar (Figure 1-1, Section 1.1). The nominal maximum true stress σ_m for either specimen is given by

$$\sigma_m = \frac{F_m}{A_0} (1 + \epsilon_m)$$

¹ The test procedure conforms to the Recommended Uniaxial Tensile Test Procedure of Section 4.3.5 of the "ICRPG Solid Propellant Mechanical Behavior Manual", July, 1963, for JANAF Type Specimens.

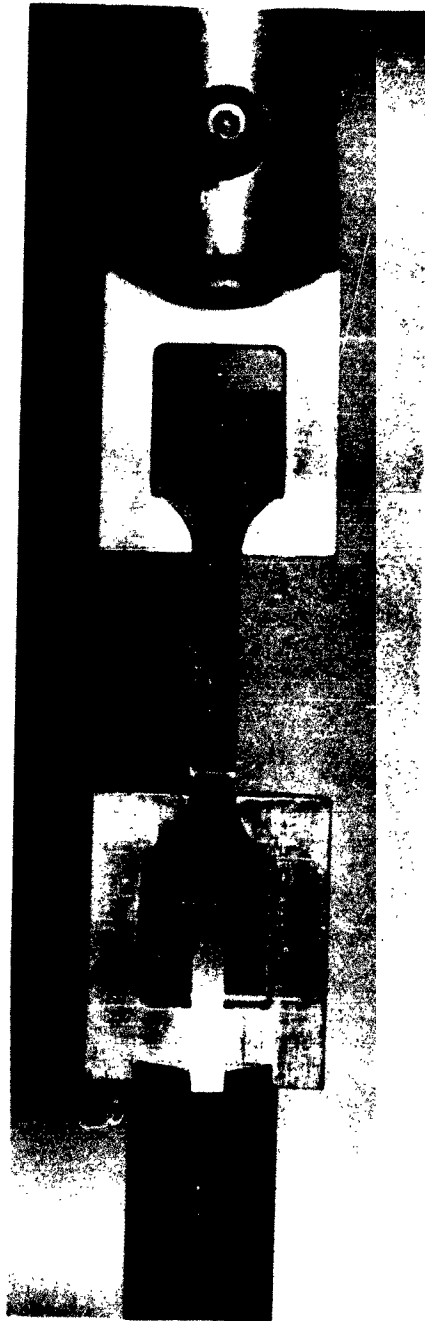


Figure 1-8 JANA F Tensile Specimen with Plastic Strain Gage

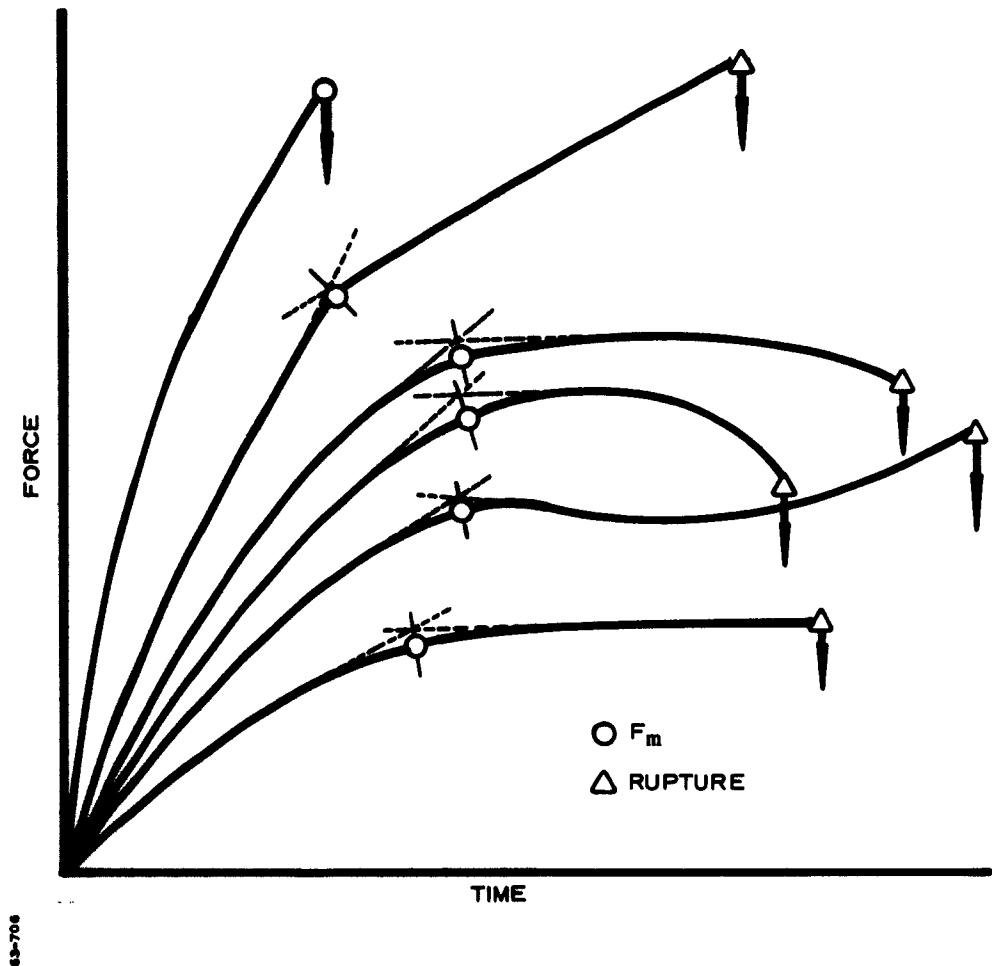


Figure 1-9 Typical Tensile Test Force-Time Curves

where A_0 is the unstrained cross section area of the specimen. The associated strain rate $\dot{\epsilon}$ is

$$\dot{\epsilon} = \epsilon_m / t_m$$

where t_m is the time at which the nominal maximum force F_m is observed. The nominal value of $\dot{\epsilon}$ for a tester crosshead speed of two inches per minute for a JANAF specimen is 0.7 in./in./min. Tabular data for the tests are more conveniently represented graphically as in Figure 1-10.

Figure 1-10 also shows data for other strain rates obtained through use of the temperature-time shift relationship for the propellant. This data conversion is necessary in grain failure analysis, as discussed in Section 2.2. The procedure is as follows (Reference, Figure 1-11):

- (a) With curves for the $\log a_T$ shift factor versus temperature and ultimate properties versus temperature for the propellant (Figures 1-7 and 1-10); take the ratio of the reference (experimental) strain rate to the strain rate of interest, $\dot{\epsilon}_r$, defining $\log a_{Tr}$:

$$\log a_{Tr} = \log \frac{\dot{\epsilon}_{\text{experimental}}}{\dot{\epsilon}_r}$$

- (b) At a given temperature T_1 , add $\log a_{Tr}$ to the $\log a_T$ curve at T_1 ;
- (c) Proceed horizontally from the point $a_T + a_{Tr}$ (point 1 in Figure 1-11) left to the propellant $\log a_T$ curve intercepting it to define a temperature T_2 ;
- (d) The ultimate properties at the new strain rate are defined as equal to those at temperature T_2 as shown;
- (e) The shifted curves are then constructed point by point following steps (a) through (d) above.

The steps given above are applied similarly in shifting the σ_m data to obtain the curves as shown in Figure 1-10.

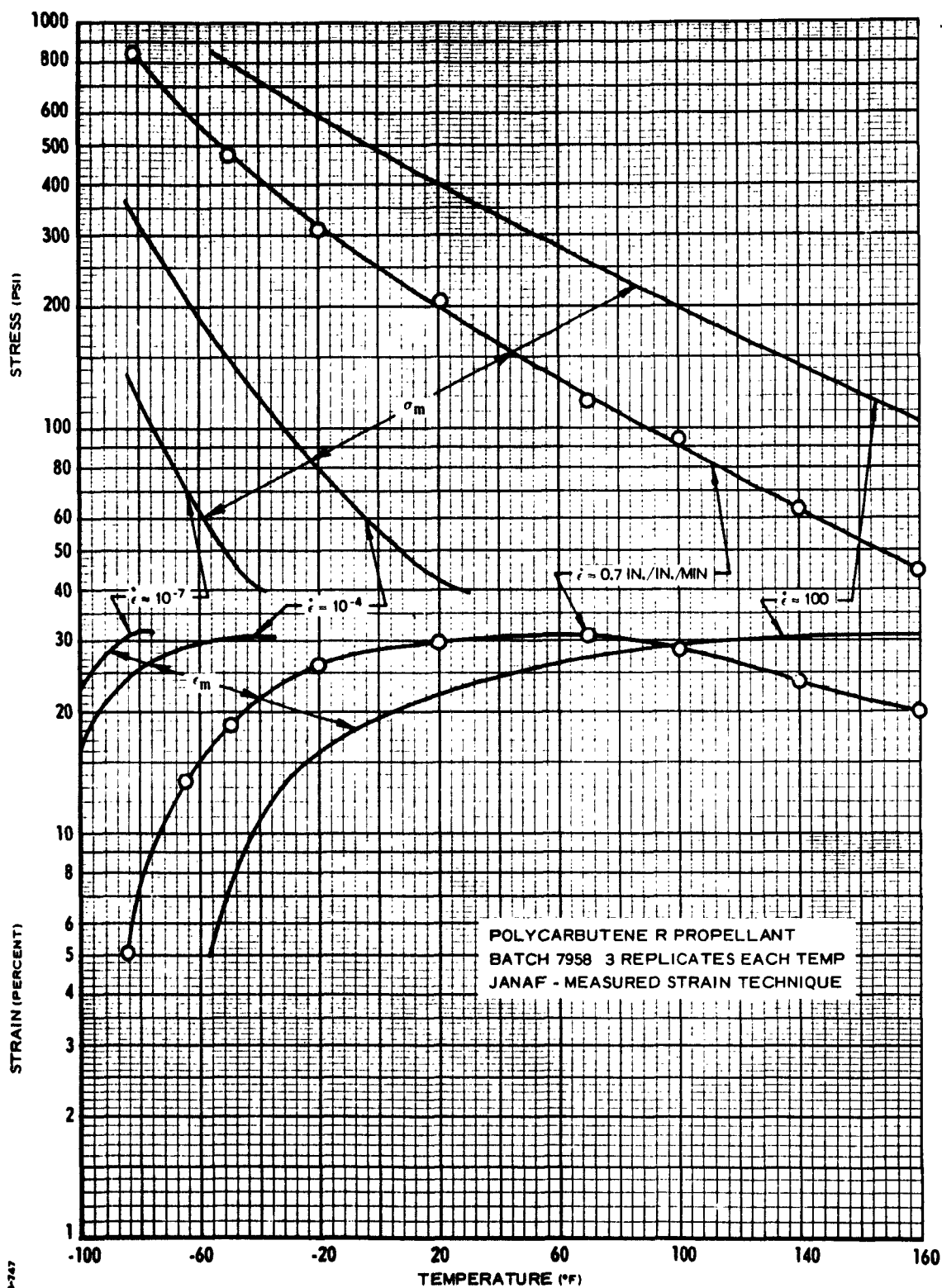


Figure 1-10 Constant Crosshead Rate Properties, Polycarbonate-R
Propellant Batch 7958, JANAF Measured Strain Technique
1-19

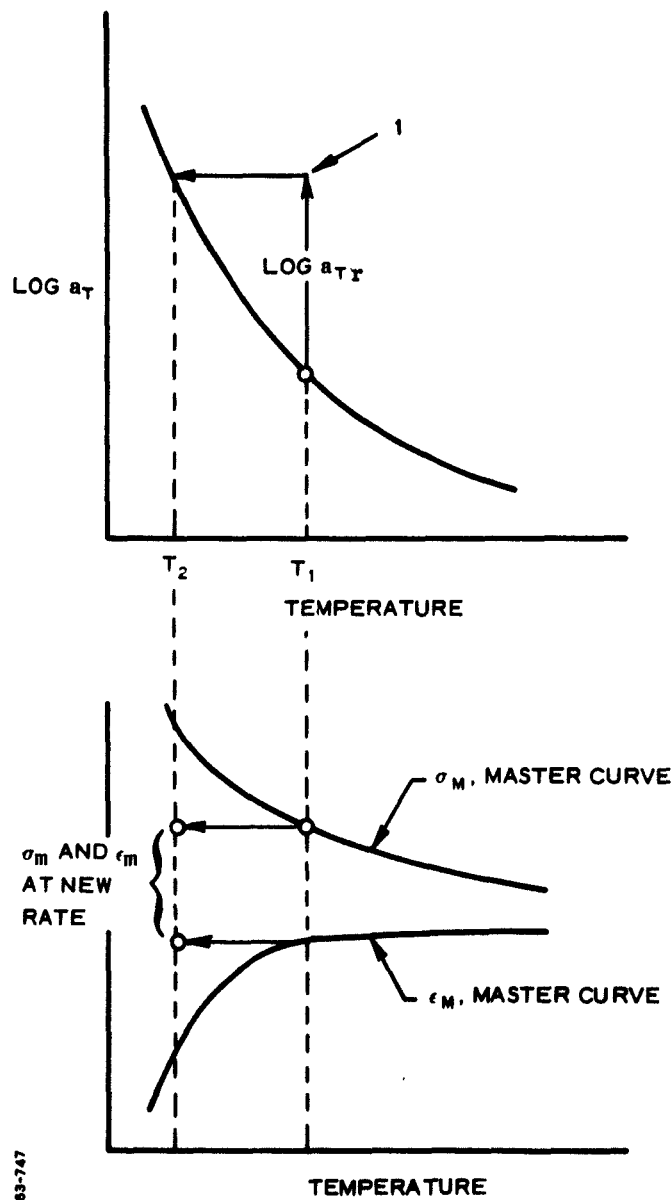


Figure 1-11 Time-Temperature Data Conversion Procedure

1.3 CONSTANT LOAD ULTIMATE PROPERTIES (Reference Section 3.3)

Purpose: Determination of the relaxation of load sustaining capability of a propellant with time and temperature.

Test Equipment: Instron Universal Tester with load cycling controls and temperature conditioning chamber, or equivalent apparatus.

Test Specimen: Machined JANAF "dumbbell" or machined tab-end specimen. Either specimen is acceptable for this test.

Test Method: A specimen is fixed in the grips of the tester and elongated at a constant crosshead displacement speed to a preselected load level, where the load level control of the tester has been set. The load level is maintained until the specimen either fails or the test is terminated. While any initial crosshead speed may be used in this test, a two-inch per minute speed is standard. Defining t_L as the time at which the preselected load level is first attained, tests are made at successively lower load levels such that failures are observed at times in excess of $10 t_L$.

Replicate tests in which the time to failure varies between $10 t_L$ and about $1000 T_L$ are made, defining a curve as in Figure 1-12:

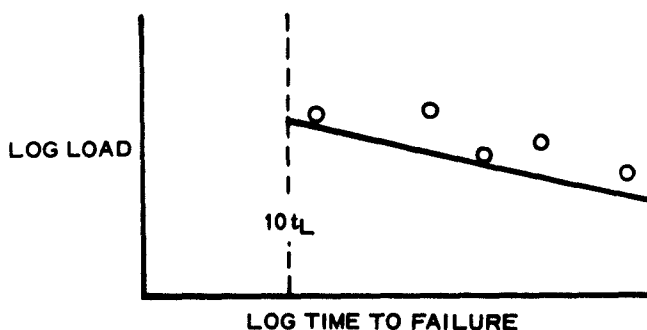


Figure 1-12 Constant Load Data

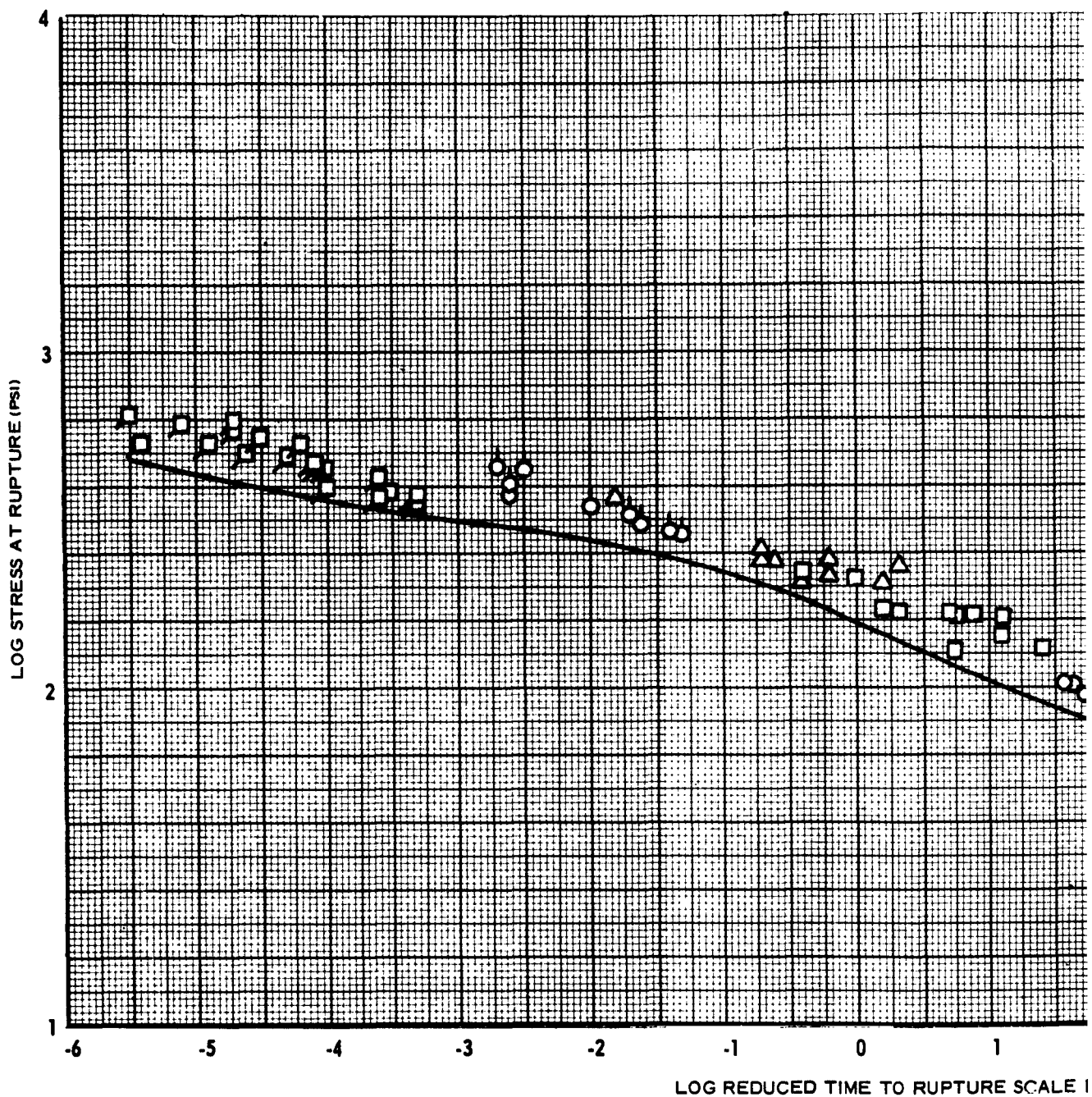
The procedure is repeated at various temperatures.

Data Reduction: As indicated above, the product data of the test are points defining a curve of force versus time to failure. The force readings are reduced to obtain stress σ_r by

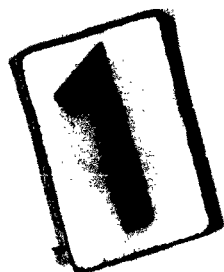
$$\sigma_r = \frac{F_r}{A_o}$$

where F_r is the force at failure (rupture) and A_o is the unstrained cross-sectional area of the specimen. Data points thus reduced are plotted on logarithmic coordinates and shifted in accord with the shift factor for the propellant (Figure 1-7) to obtain a master curve representation. The shifting procedure is that used for reduction of stress relaxation data (Section 1.1). Typical data are shown in the master curve representation (Figure 1-13).

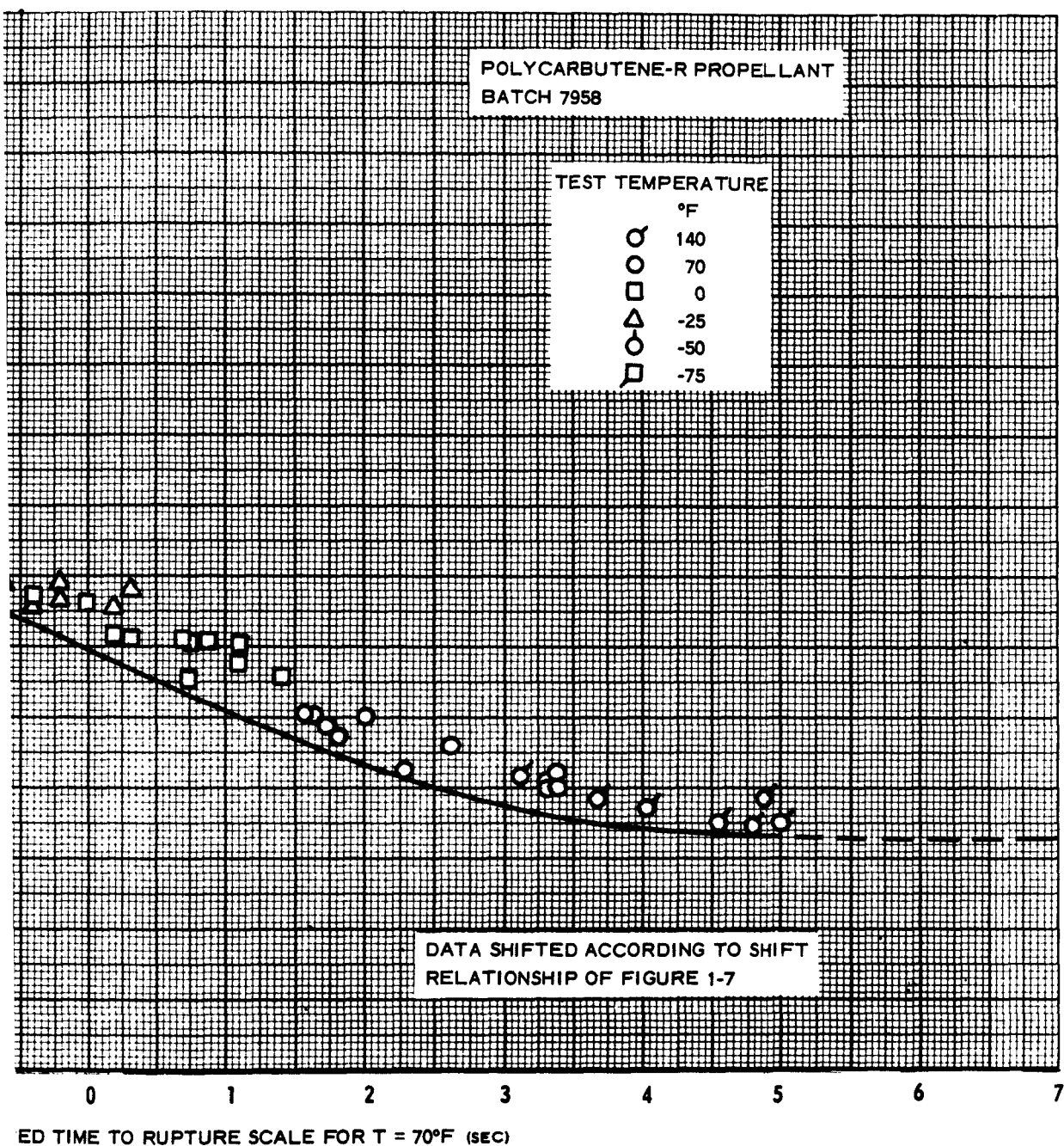
Shifted (and unshifted) data from this test usually show relatively large scatter. Since the data are of use as a failure criterion, the lower scatter limit (stress-wise) is identified as the curve of interest.



69-747



Master Curve for Constant Load Strength versus



2

Figure 1-13

1.4 CONSTANT STRAIN ULTIMATE PROPERTIES (Reference Section 3.4)

Purpose: Determination of the constant strain level below which the time to failure in uniaxial tension approaches infinity.

Test Equipment: Instron Universal Tester with temperature conditioning chamber or equivalent.

Test Specimen: Machined tab-end specimen (Figure 1-1, Section 1.1) or machined JANAF "dumbbell" with provision for strain measurement in the gage section (Reference: Appendix A). The tab-end specimen is preferred. The common availability of JANAF specimens, however, dictates their continued use for this test.

Test Method: The specimen is fixed in the grips of the tester and extended to a preselected strain level at a constant crosshead speed. While any X-head speed may be selected, two inches per minute is a useful laboratory standard. The sample is held at the preselected strain level and the time to failure observed. The test is repeated for various strain levels to define a strain versus time-to-failure (or visible specimen cracking) relationship.

Tests as above are carried out at various temperatures.

Data Treatment: Data for this test method are frequently difficult to treat. It has been observed that with quality PBAA, Polysulfide, and Nitroplastisol propellants the strain that can be supported almost indefinitely without failure is within one or two percent (of strain) of the strain at nominal maximum stress, ϵ_m , as measured in the constant strain rate test when the same straining rate is used in both tests. (Reference: Section 1.2 and 3.4) In such instances, the constant strain test becomes correlative to the constant strain rate test and extensive definition of the time-to-failure relationships is not required. As a practical matter, the usual test observation is that at or above the strain level ϵ_m , specimens fail within a few seconds; at one or two percent below, failure is not observed, in many cases after two or three months. In evaluation of a family of propellants known to exhibit this behavior (on the basis of extensive investigation), thirty-minute duration constant strain screening tests are sufficient to single out important propellant deviations. When such deviations are observed, (i.e., rapidly decaying constant strain resistance to failure) the propellant is usually poor and reference to more detailed consideration is required (Section 3.4).

1.5 PROPELLANT - LINER - SUBSTRATE BONDING ULTIMATE PROPERTIES (Reference Section 3.5)

Purpose: To determine the ultimate strength of the propellant-to-liner-to-substrate (insulation or case) bond.

Test Equipment: Instron Universal Tester with temperature conditioning chamber and load cycling attachment, or equivalent.

Test Specimen: The bond-in-tension specimen is used (Figure 1-14). Propellant is cast through the pipe onto the lined (or otherwise prepared) anvil surface and cured as in the motor application. Materials used in preparation of the anvil surface are those used in the motor application of interest and are applied in the same manner as in the motor. Conveniently, the Teflon spacer has an inside diameter of 1.13 inches (to give a bonded cross-sectional area A_0 of 1 in.²) and a height of 3/16 inch.

Test Method 1: The bond jig assembly is fixed in the jaws of the tester and the anvil and pipe sections are pulled apart at a crosshead speed one-tenth of that used in uniaxial tests of the propellant. The recommended rates are 0.2 and 2 inches per minute. The bond specimen is pulled to failure and the force required for failure observed. The test is repeated at various temperatures.

Data: The force at failure of the specimen is recorded; for the recommended spacer dimension, the force at failure is by definition the unit failure stress.

The type, as to location, of failure of the specimen is recorded:

- (1) Cohesive in propellant
- (2) Cohesive in liner
- (3) Cohesive in substrate
- (4) Interfacial
 - (4a) Liner-propellant
 - (4b) Liner-substrate
 - (4c) Substrate-case

When the failure character is mixed, the estimated percentages are recorded [e.g., 60/40 (1)/(4a)].

In reduction of this type of data for use in analysis, a limit condition is used for routine purposes. Tests in which over 90 percent of the failures are found to be clearly cohesive in the propellant (Figure 1-15) show the propellant to be the strength-limiting component, and propellant data as obtained in the more precise tests (Sections 1.2, 1.3) are used as the governing failure criteria. In this case, the strength as measured in the bond test agrees reasonably well with the uniaxial constant strain rate data except at low temperatures. Typical bond test data are shown in Figure 1-16.

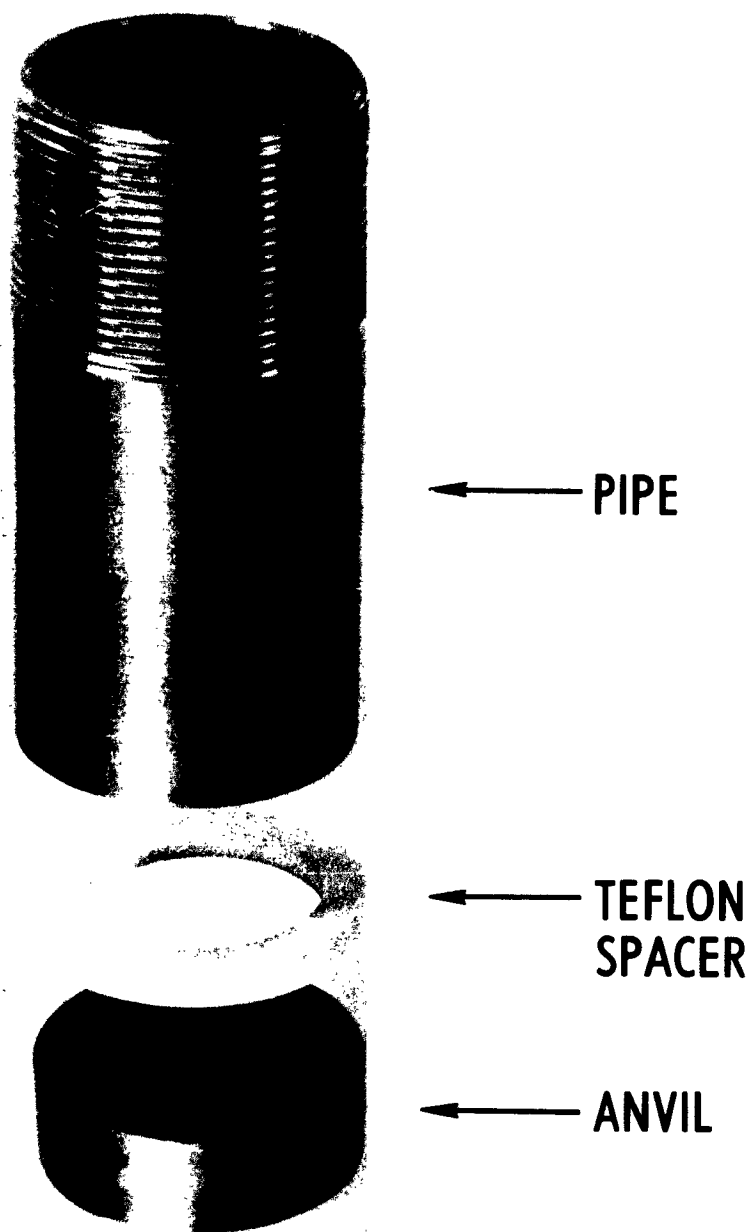


Figure 1-14 Bond in Tension Specimen

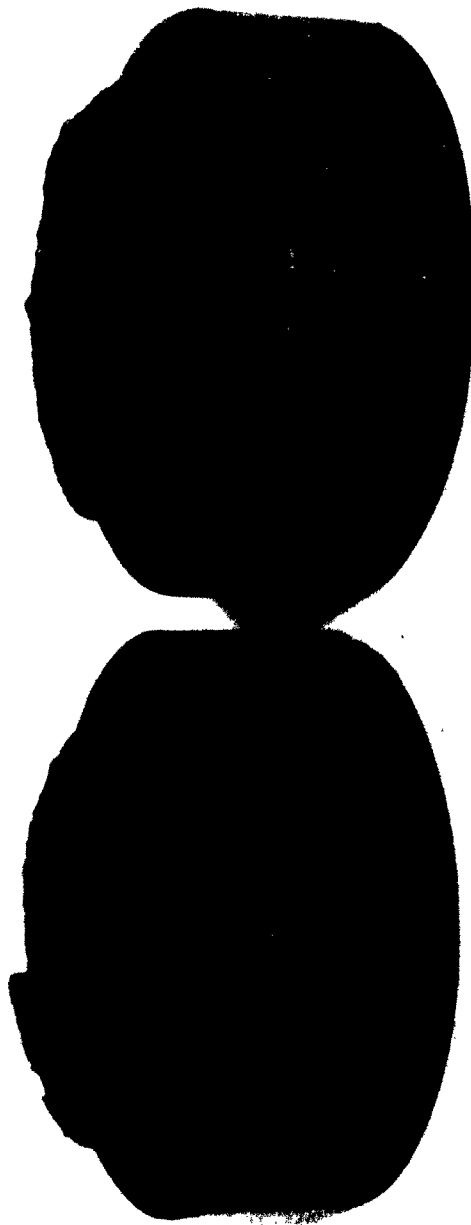
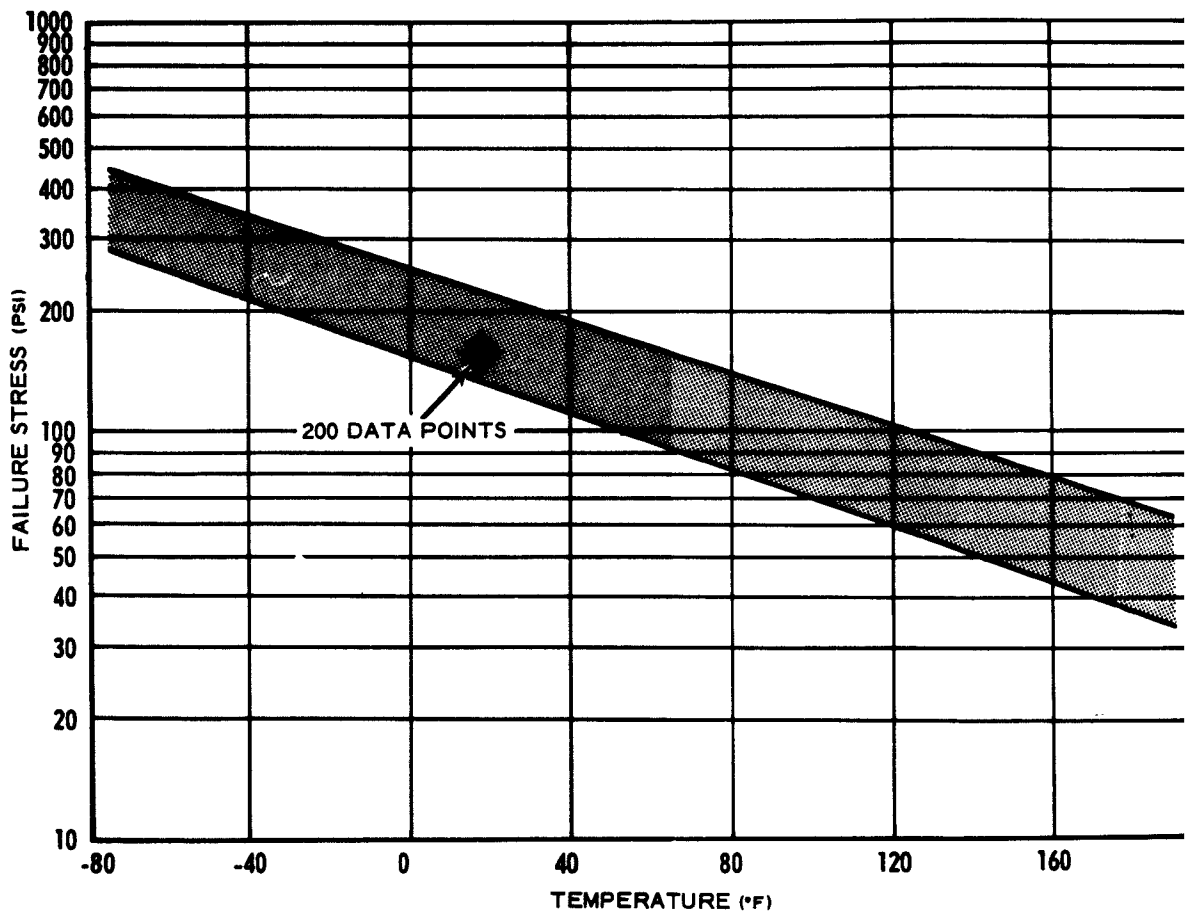
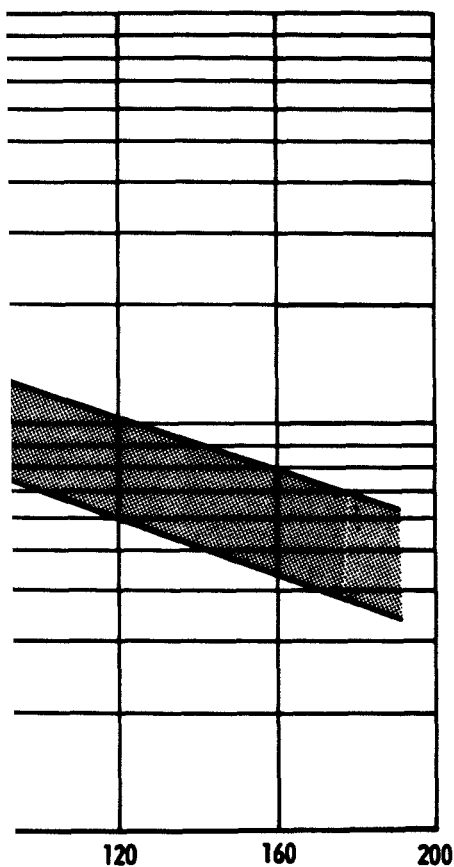


Figure 1-15 Bond Test Specimen Showing Cohesive Propellant Failure

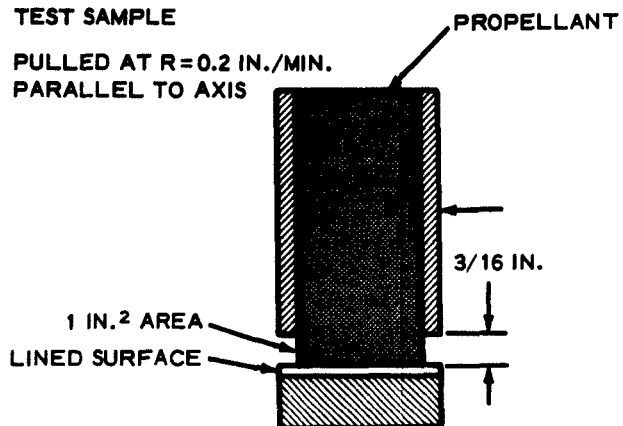


Constant Rate Liner/Propellant/Substrate Bond Data, Po





TEST SAMPLE
PULLED AT $R=0.2$ IN./MIN.
PARALLEL TO AXIS



DATA COMPOSITE FOR:

1. LINER CURE TIME
2. LINER POST CURE
3. LINER SUBSTRATES
4. PROPELLANT - LINER - SUBSTRATE COMBINED AGING
5. MULTIPLE COATS OF LINER
6. VACUUM AGING OF LINER
7. CONTAMINATED LINER SURFACES

92% OF ALL SPECIMENS FAILED
COHESIVELY IN PROPELLANT

2

lant/Substrate Bond Data, Polycarbutene-R Propellant

Figure 1-16

When failure is dominantly interfacial in the liner, or in a substrate, a material or process development problem is indicated. In general, suitable liners and lining techniques yield case bonds superior in strength to propellants. When this is not the case, grain analysis and resolution of the associated problems is decidedly not a routine engineering job.

Test Method 2: The bond jig is fixed in the jaws of the tester and pulled to a preselected load level at a crosshead speed one-tenth of that used in uniaxial tensile tests of the propellant (Section 1.2, 1.3). The preselected load level is maintained until failure is observed. The tests are repeated for various temperatures and load levels.

Data: The treatment of data for this test method are as above for load specification and failure type description. In general, the decay of load sustaining capability for propellant cohesive failure with time correlates to the propellant strength as measured in uniaxial tension (Section 1.3). It may be observed that failure localization at an interface or in a liner will occur under constant load conditions (Method 2) and not under constant rate conditions (Method 1). The analysis of the data in any case proceeds on the basis of the limit considerations delineated in discussion of Method 1.

1.6 REDUCED LINEAR COEFFICIENT OF THERMAL EXPANSION (Reference Section 3.6)

Purpose: Determination of the reduced propellant linear coefficient of thermal expansion.

Test Equipment: Quartz tube dilatometer, associated temperature conditioning and measurement apparatus, and electronic recorders (Figure 1-17), or equivalent apparatus. Reference reports LPC 556-F-1, LPC 578-F-1.

Test Specimen: Cast or machined propellant cylinder of 3/8-inch diameter by 1 to 2 inches in length (l_1) or rectangular equivalent.

Test Procedure: The change in length is measured with temperature of the specimen under cooling (heating) rates of 60°F/hour or less. For a given sample of propellant, cooling and heating cycles are repeated until the identical specimen length versus temperature variation is observed on successive heating and cooling cycles. Details of the test procedures may be found in the previously cited references. Samples are desiccated and maintained in a desiccated environment during the test.

Data: The change in length per unit length, $\bar{\alpha}_p = \Delta l / l_1$, is plotted versus temperature, taking $\Delta l = 0$ and l_1 at a reference temperature T_1 . T_1 is selected to be the zero strain temperature for a motor cast with the subject propellant. Typical values for T_1 are cure temperature plus 15°F for PBAA propellants and cure temperature plus 22°F for Nitroplastisol propellants. Data for Polycarbutene propellant are shown in Figure 1-18 referenced to $T_1 = 155^\circ\text{F}$.

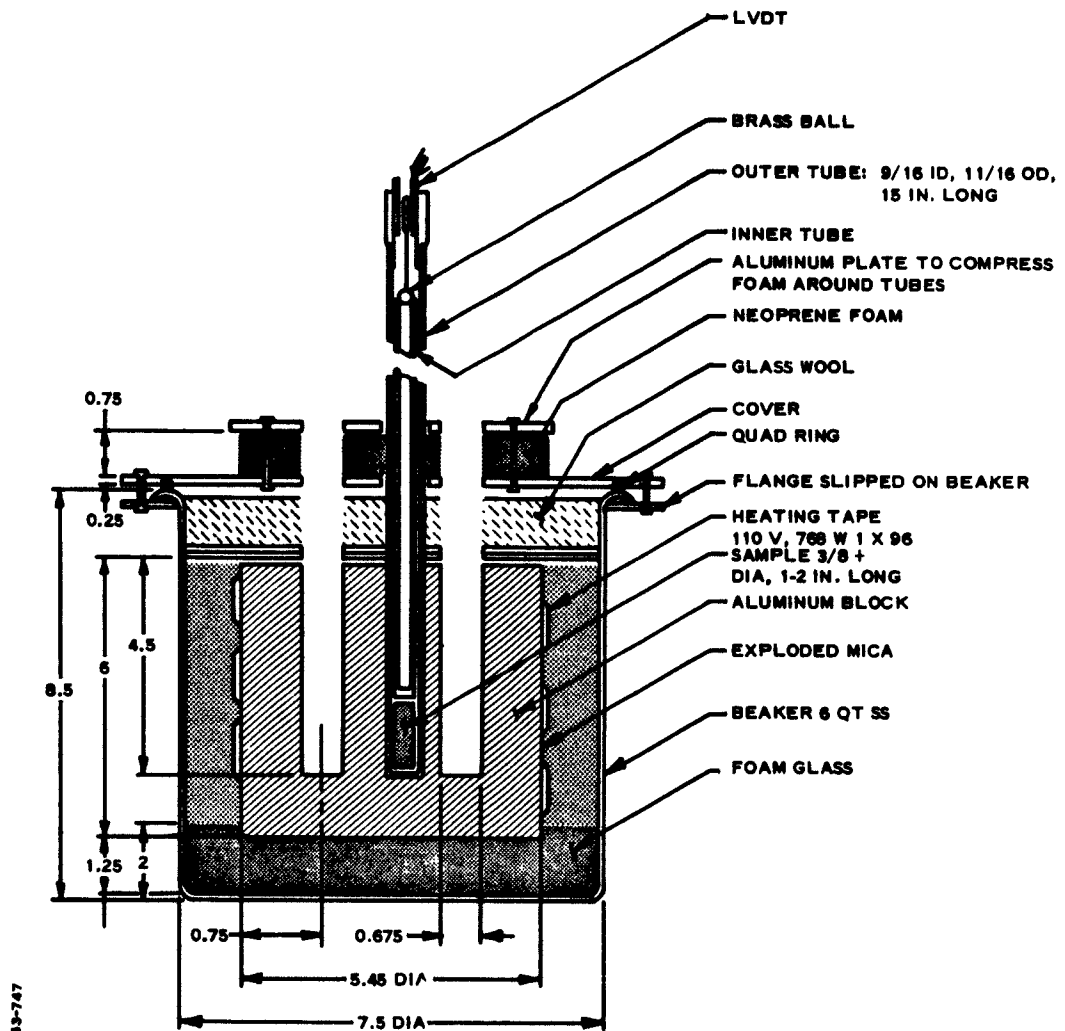
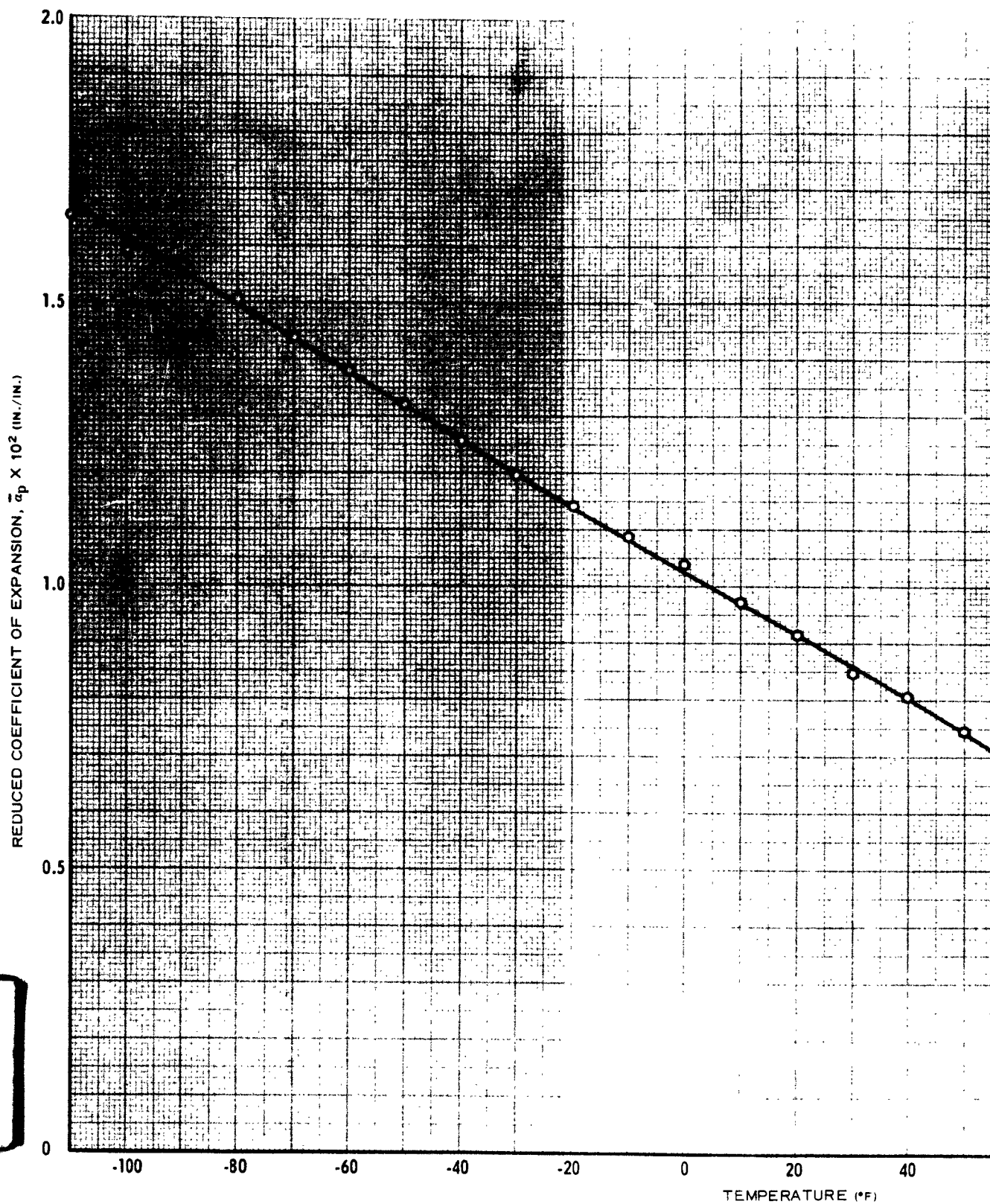
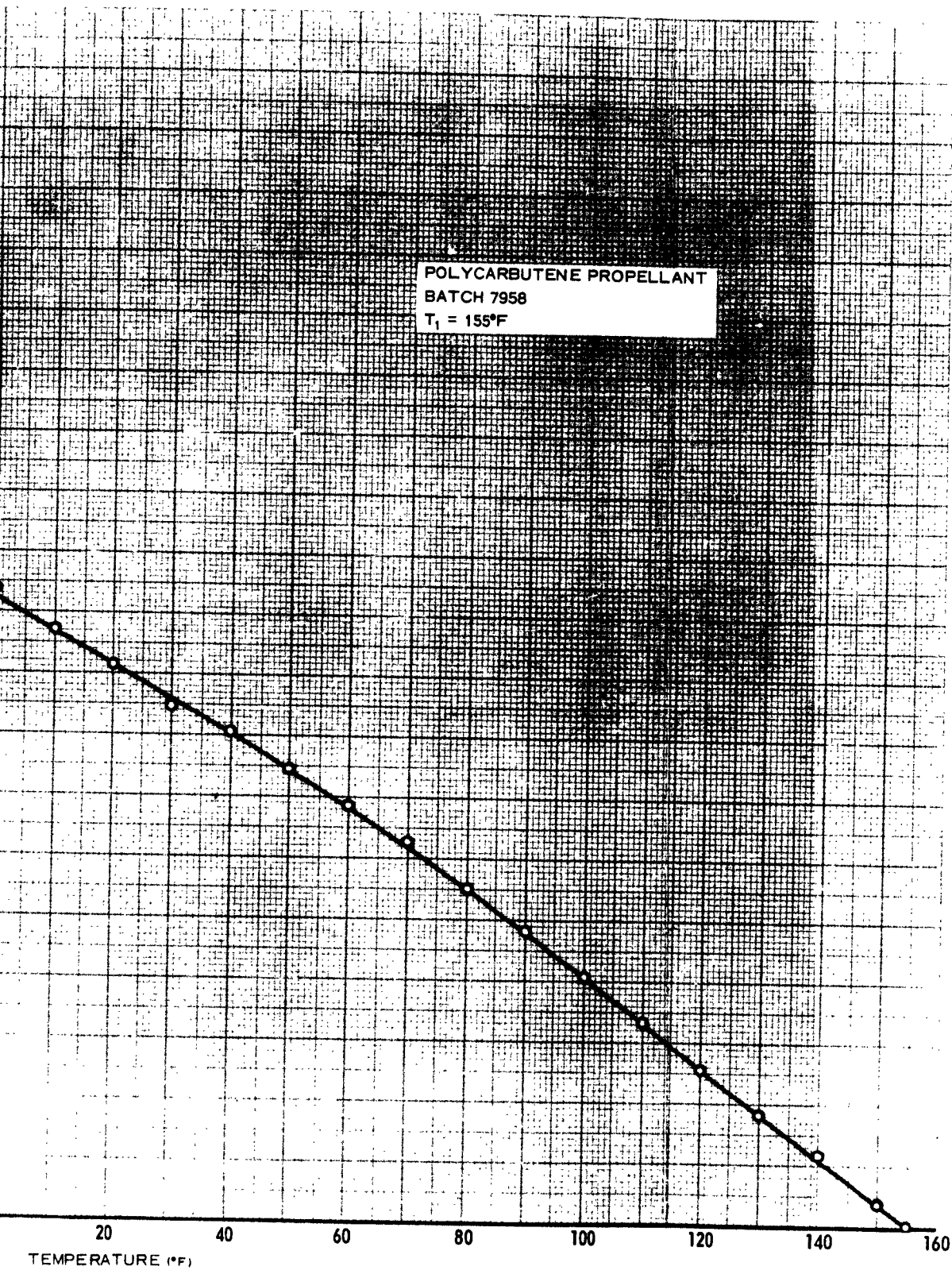


Figure 1-17 Quartz Tube Dilatometer



Reduced Propellant Linear Coefficient of Thermal Expansion



2

Coefficient of Thermal Expansion versus Temperature

Figure 1-18

Section 2

ENGINEERING METHODS FOR GRAIN STRUCTURAL ANALYSIS

CONTENTS

	Page
2. ENGINEERING METHODS FOR GRAIN STRUCTURAL ANALYSIS.	2-2
2.1 THERMAL STRAIN ANALYSIS - PROBLEM 1	2-3
2.2 THERMAL STRAIN FAILURE ANALYSIS - PROBLEM 1A	2-7
2.3 GRAIN SLUMP DEFLECTIONS - PROBLEM 2.	2-9
2.4 GRAIN PRESSURIZATION - PROBLEM 3	2-16
2.5 PRESSURIZATION STRAIN FAILURE ANALYSIS - PROBLEM 3A	2-18

TABLES

2-1 THERMAL STRAIN ANALYSIS - PROBLEM 1	2-4
2-2 COMPUTATION SHEET-GRAIN SLUMP DEFLECTIONS - FREE-FREE GRAIN - PROBLEM 2A.	2-10
2-3 COMPUTATION SHEET-GRAIN SLUMP DEFLECTIONS - FIXED-FREE GRAIN - PROBLEM 2B	2-11
2-4 GRAIN PRESSURIZATION STRAINS - PROBLEM 3	2-17
2-5 PRESSURIZATION FAILURE ANALYSIS - PROBLEM 3A	2-19

FIGURES

2-1 Thermal Strain Failure Analysis, Problem 1A	2-8
2-2 Grain Storage Slump Deflection versus Time at 70°F, Problem 2A.	2-13
2-3 Grain Storage Slump Deflections versus Time at 150°F, Problem 2B.	2-14
2-4 Storage and Pressurization Failure Strain Analysis XSM-EX Motor, Problem 3A	2-20

Section 2

ENGINEERING METHODS FOR GRAIN STRUCTURAL ANALYSIS

In preparing to analyze a solid propellant rocket grain, it is necessary as well as expedient to establish the assumptions under which the analysis will be conducted. Notwithstanding certain obvious deficiencies, particularly in connection with failure theory, the medium is considered as isotropic, homogeneous, and continuous. The practical objections to these assumptions are based upon the fact that the viscoelastic elastomer (consisting of the order of 30 percent by volume) is merely a binder in which various considerably harder particles are imbedded. Thus, a homogeneous medium does not exist--nor does an isotropic medium. Nevertheless, it is assumed that on the average macroscale there does exist an equivalent medium of this type. For most analyses this approximation is satisfactory, although the assumption can be seriously in error in fracture or tearing, where the origin of failure begins on the microscale. Next, the assumption of continuity is not always fulfilled because it implies that there is always a bond between the various solid filler elements and the elastomeric binder. The pullaway effect is well established, wherein excessive tensile stress will cause the filler-binder adhesion to part. Nevertheless, to conduct present analyses it is customary and, at least temporarily, necessary to assume an isotropic, homogeneous continuum.

The second assumption is that the strains will be sufficiently small to allow use of infinitesimal deformation theory. For the loads and geometries used in present motors, strains of 30 percent may be computed from infinitesimal theory, which certainly pushes the limit of validity for this assumption. Alternately, even without viscoelastic effects, finite strain analysis is far from simple. Considering the widespread knowledge of infinitesimal deformation theory and the relative ease of application, it is considered appropriate to begin at this point.

As a third assumption, it is appropriate to neglect inertia forces due to straining, during ordinary viscoelastic deformations. The inertial forces are usually highly damped and exponentially decaying, although in certain cases--such as possible stress wave propagation through the grain due to burning phenomena--this particular assumption ultimately may have to be re-evaluated.

The following subsections present engineering methods for grain structural analysis for the situations of primary interest in preliminary grain design evaluation. As applicable, the propellant physical data of Section 1 are used in determination of grain strains or deflections and grain failure conditions. The problem format has been selected to simplify rapid desk calculator or slide-rule calculations.

The analyses presented in this section are of basic importance both in preliminary and final design evaluations. Background discussion and additional grain structural design analysis information are presented in Section 4.

2.1 THERMAL STRAIN ANALYSIS - PROBLEM 1 (Reference Section 4.1)

Purpose: To calculate the maximum equilibrium thermal hoop strain $\epsilon_{\theta}^{c,s}(a)$ at the port in finite length case-bonded circular and star port rocket grains.

Governing Equation:

$$X_3 = \underbrace{\frac{3}{2}}_{2.12} \underbrace{\overline{P}}_{2.13} \left[\underbrace{\frac{1 + \nu_c}{1 + \nu_p}}_{2.14} \underbrace{\alpha_c}_{2.15} \underbrace{\Delta T}_{2.16} \right] \lambda^2 - \underbrace{\overline{\alpha}_p}_{2.16} ;$$

Notes: 2.12 2.13 2.14 2.15 2.16

$$\epsilon_{\theta}^c(a) = \frac{X_3}{1 + \ln(1 + X_3)}$$

2.11

$$\epsilon_{\theta}^s(a) = \epsilon_{\theta}^c(a) K_i$$

2.17

$\epsilon_{\theta}^c(a)$ = Maximum hoop strain at the midpoint of a circular port, finite length grain

$\epsilon_{\theta}^s(a)$ = Maximum hoop strain at the midpoint of a star perforated, finite length grain

X_3 = Maximum hoop strain at the midpoint of a circular port finite length grain, infinitesimal deformations

λ = b/a = grain O. D. / I. D.

\overline{P} = Parr end effect correction for finite length grains

K_i = Star valley stress concentration factor

$\overline{\alpha}_p$ = Propellant reduced linear coefficient of thermal expansion

ν_c = Case Poisson's ratio

ν_p = Propellant Poisson's ratio, taken as $1/2$

α_c = Case linear coefficient of thermal expansion

ΔT = Temperature increment from grain zero strain temperature

TABLE 2-1

PREPARED BY LC PAGE 1 OF 1
 CHECKED BY [Signature] DATE 6-16-63
 APPROVED BY [Signature] REPORT NO. 578-F-3

THERMAL STRAIN ANALYSIS PROBLEM-1

 K_i = STAR VALLEY STRESS CONCENTRATION FACTOR

 $C_2 = 3/2 \bar{P}$, \bar{P} = PARR CORRECTION FOR FINITE LENGTH GRAINS

NOTE 2.16

 NOTE 2.12
 GRAIN LENGTH TO DIAMETER L/D = 3
 $\bar{P} = 0.97$
 $C_2 = 3/2 \bar{P} = 1.45$

NOTE 2.11

NOTE 2.17

 $K_i = 1.50$

\ominus	a_p	$=$	X_2	\otimes	$C_2 = X_3$	\otimes	$\frac{1}{1 + \ln(1 + X_3)}$	$=$	$\epsilon_{\theta}^C(a)$ CIRC PORT	\otimes	$K_i = \epsilon_{\theta}^B(a)$ STAR PORT	$\ln(1 + X_3)$
-----------	-------	-----	-------	-----------	-------------	-----------	------------------------------	-----	---------------------------------------	-----------	---	----------------

5^{-2}					1.62×10^{-2}		0.985		1.60%		3.02%	0.016
					3.19		0.970		3.09		5.84	0.031
					4.46		0.958		4.26		8.05	0.044
					5.78		0.949		5.48		10.35	0.056
					6.84		0.939		6.42		12.14	0.066
					6.11		0.929		7.53		14.22	0.078
					8.56		0.925		7.91		14.95	0.082

50
00

$$K_i = \frac{H(\lambda^2 - 1)}{2\lambda^2} = \frac{(5.05)^2 - 1}{8} = 1.89$$

01. Star
05 (Fig D-7)

2

\ln = Napierian logarithm

Superscript s = star grain

Superscript c = circular port grain

The procedures used in solving this equation are illustrated on the calculation sheet, Table 2-1, as annotated below.

NOTES:

2.11 This operation corrects for the finite deflection of the port by an approximation technique that yields an accuracy of approximately 1 percent in the calculated strain values at strains up to 25 percent.

2.12 The term

$$\frac{3}{2} \bar{P} = C_2$$

includes the end condition correction factor \bar{P} which is the ratio of strain in a finite length grain to that in an infinite length grain. \bar{P} is obtained from Reference Figures D-1 and D-2 (Appendix D) for a grain length L and diameter $D = 2b$ and of O. D. to I. D. ratio $\lambda = b/a$. In a grain head bonded at one end, obtain \bar{P} equivalently by doubling the actual grain length.

2.13 $\bar{\alpha}_p$, the reduced thermal coefficient is equal to the change in length per unit length in the propellant (unconstrained) for the temperature increment ΔT as referenced to the temperature T_1 , the zero strain temperature of the grain (see Note 2.15). Values for $\bar{\alpha}_p$ are entered directly on the calculation sheet, Table 2-1, from Figure 1-18, Section 1.6 for the temperature at which strain is to be calculated.

2.14 The term

$$\frac{1 + \nu_c}{1 + \nu_p} \alpha_c = \frac{1 + \nu_c}{1.5} \alpha_c = C_1$$

compensates for the effect of the thermal contraction of the case. For a steel case, a typical value of C_1 is 5.05×10^{-6} in./in./°F.

2.15 All calculations are referenced to the motor zero strain temperature T_1 . The zero strain temperature is approximately the temperature at which the grain inside diameter is equal to the mandrel outside diameter. Typical values for T_1 are:

PBAA, Polycarbutene: Cure temperature + 15°F = T_1

Nitroplasticols: Cure temperature + 22°F = T_1

ΔT is the grain temperature increment from T_1 .

2.16 Inclusion of the subtractive term $\bar{\alpha}_p$ in the solution allows prediction of the observed strains in a grain. To reference the grain strain calculation to the same base as the failure data (Section 1.2), omit the subtraction in the computation as indicated on the calculation sheet (i.e., the observed strains, actual port diameter to mandrel diameter, are less than the stress producing strains by the amount mentioned above).

2.17 The star valley stress concentration factor K_i accounts for the strain field perturbation at the star valley of a grain. For a circular port grain $K_i = 1$. K_i is found through the following relationship:

$$K_i = H \frac{(\lambda^2 - 1)}{2\lambda^2}$$

$$\lambda = b/a = \text{grain } \frac{\text{O. D.}}{\text{I. D.}}$$

from Reference Figures D-3 through D-8, for various star grains. The data are from Fourny and Parmerter, 1961, with the permission of the authors. Figure D-3 specifies the geometric nomenclature. The value of K_i obtained from these figures is valid only for star valley shapes in which the sides of the star are approximately parallel and the bottom of the star valley is an arc of a circle in cross-section. Complex star shapes require photoelastic determination of the stress concentration factor.

2.2 THERMAL STRAIN FAILURE ANALYSIS- PROBLEM 1A (Reference Section 4.2)

Purpose: To predict the low temperature storage limit for circular or star port case-bonded rocket grains.

Propellant Data: Strain at nominal maximum stress ϵ_m as determined in accordance with Section 1.2; also, reference Section 1.4.

Procedure: Determine the approximate thermal equilibrium time t_{eq} of the subject motor (about one day for a 1-foot motor, about three days for a 3-foot diameter, about three weeks for a 10-foot motor, uninsulated). Taking the strain (from calculations in Problem 1) in the region of the lowest temperature of interest, define the mean strain rate as

$$\frac{\epsilon_{\theta}^{c,s}(a)}{t_{eq}} = R_y$$

and determine the propellant ϵ_m versus temperature by the procedure of Section 1.2 and plot on Figure 2-1 for the strain rate R_y . Superimpose on Figure 2-1, the strain versus temperature requirements as obtained in Problem 1. The intercept of the two curves defined indicates the probable cracking temperature of the grain to within about $\pm 10^\circ\text{F}$ for the worst condition of monotonic cooling (i.e., the fastest rate possible by normal conditioning-box environments). A minimum safety factor of 1.5 (strain capability \div strain requirements) at the low temperature cycling limit of the grain is recommended for motors to be subjected to extended storage, cycling, vibration, thermal shock, etc.¹ Sustained thermal cycling of a motor usually will cause failure by web cracking at temperatures higher than those predicted above but within the limits imposed by the recommended safety factor (Section 4.2).

¹ Superposition of pressurization strains and thermal strains for pressurization failure analysis is discussed in Section 2.5.

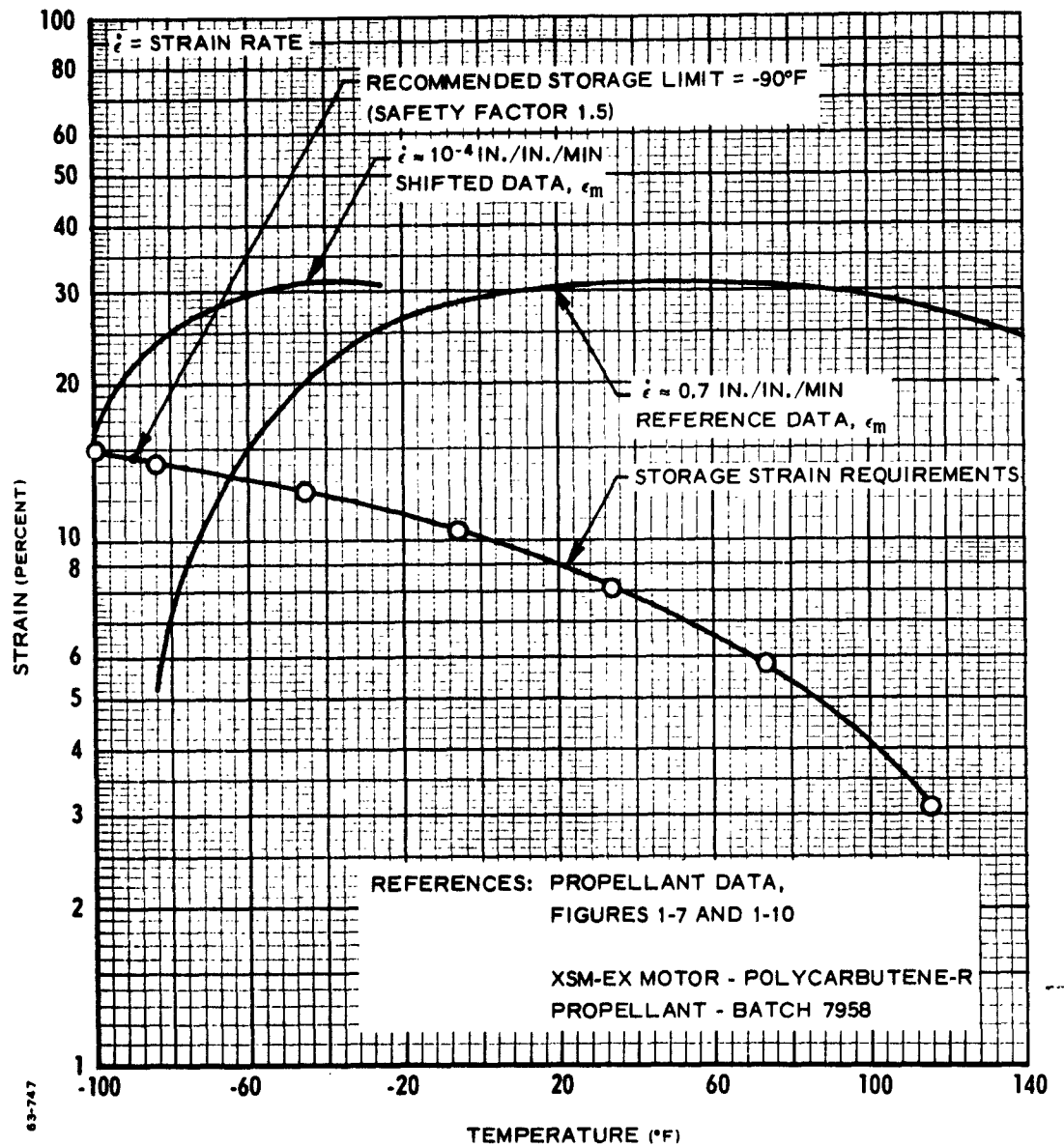


Figure 2-1 Thermal Strain Failure Analysis, Problem 1A

2.3 GRAIN SLUMP DEFLECTIONS - PROBLEM 2:

Purpose: Calculation of grain slump deflections versus time from acceleration imposed coaxial with the propellant grain. Circular port grains enclosed in rigid cases with free-free and free-fixed end conditions are considered (Details 9, 10, 11, Tables 2-2 and 2-3).

Governing Equation:

$$U_{r,z} = (\overset{*}{P}) \frac{\rho \, n_g \, b^2}{E(\tau)}$$

U = Deflection; Sub r: radial, Sub z: axial

$$\overset{*}{P} = \begin{cases} B, & \text{Constant for solution for maximum axial} \\ & \text{deflection of free-free grain (Figure D-10)} \\ C, & \text{Constant for solution for maximum radial} \\ & \text{deflection of free-free grain (Figure D-11)} \\ D, & \text{Constant for solution for maximum axial} \\ & \text{deflection of free-fixed grain (Figure D-12)} \\ F, & \text{Constant for solution for radial deflection} \\ & \text{at free end of fixed-free grain (Figure D-13)} \\ G, & \text{Constant for solution for radial deflection} \\ & \text{at fixed end of fixed-free grain (Figure D-14)} \end{cases}$$

ρ Propellant density

n_g Acceleration in gravities

$2b$ Grain outer diameter

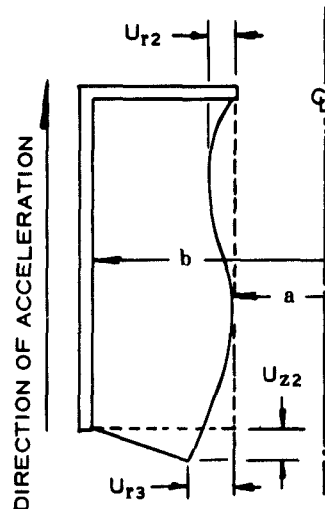
$E(\tau)$ Propellant master stress relaxation modulus

Solution: The deflections are calculated as functions of time using the stress relaxation modulus $E(\tau)$ appropriate to the temperature of interest from Figure 1-7, Section 1.1. The calculations for the various deflections are illustrated by Tables 2-2, 2-3 and Figures 2-2, 2-3. The numerical factors $\overset{*}{P} = B, C, D, F, G$ are scaled from Figures D-10 through D-14 for the motor I.D./O.D. ratio $1/\lambda = a/b$ and grain length to diameter L/D ratios.

For grains with irregular ends (i.e., non-planar), the values of the $\overset{*}{P}$ for the grain based on the L/D for the bonded cylindrical length and the port length are determined and the larger of the two values for $\overset{*}{P}$ used in calculation.

PREPARED BY LCPAGE 1 OF 2CHECKED BY MBDATE 6-16-63APPROVED BY [Signature]REPORT NO. 578-F-3

COMPUTATION SHEET - GRAIN SLUMP DEFLECTIONS - FIXED-FREE GRAIN - PROB 2B

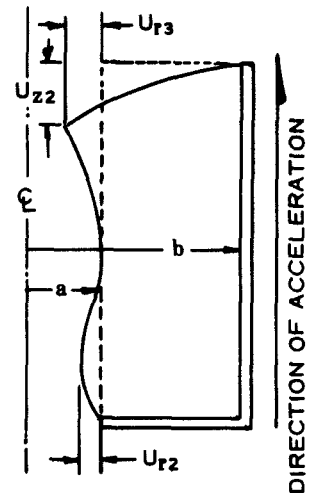


Detail 10

$$U_{z2} = D \frac{\rho n g b^2}{E(r)}$$

$$U_{r3} = F \frac{\rho n g b^2}{E(r)}$$

$$U_{r2} = G \frac{\rho n g b^2}{E(r)}$$



Detail 11

$$1/\lambda = a/b = \frac{25''}{50''} = 0.5$$

$$\frac{\text{GRAIN LENGTH}}{\text{GRAIN DIAMETER}} = \frac{L}{2b} = \frac{200''}{100''} = 2$$

$$\text{FROM REF FIG 2-12, } D = 0.365$$

$$\rho = \text{PROP DENSITY} = 0.063 \text{ (LB/IN.}^3\text{)}$$

$$\text{FROM REF FIG 2-13, } F = 0.092$$

$$b^2 = 2500 \text{ (IN.}^2\text{)}$$

$$\text{FROM REF FIG 2-14, } G = 0.185$$

$$ng = 1 \text{ (GRAVITIES)}$$

$$X_3 = D \rho n g b^2 = 57.5$$

$$\text{LOG } X_3 = 1.759$$

$$X_4 = F \rho n g b^2 = 14.5$$

$$\text{LOG } X_4 = 1.162$$

$$X_5 = G \rho n g b^2 = 29.1$$

$$\text{LOG } X_5 = 1.464$$

$$\text{LOG } E(r) \text{ FROM Figure 1-7}$$

TABLE 2-3(cont'd)

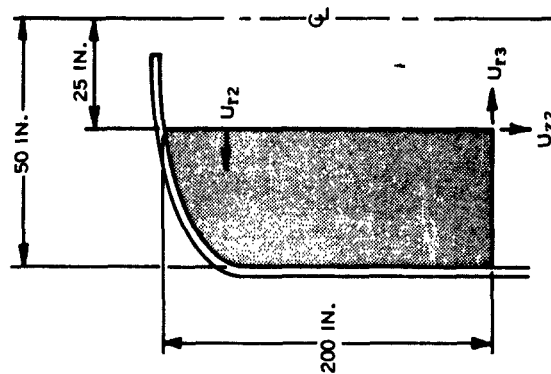
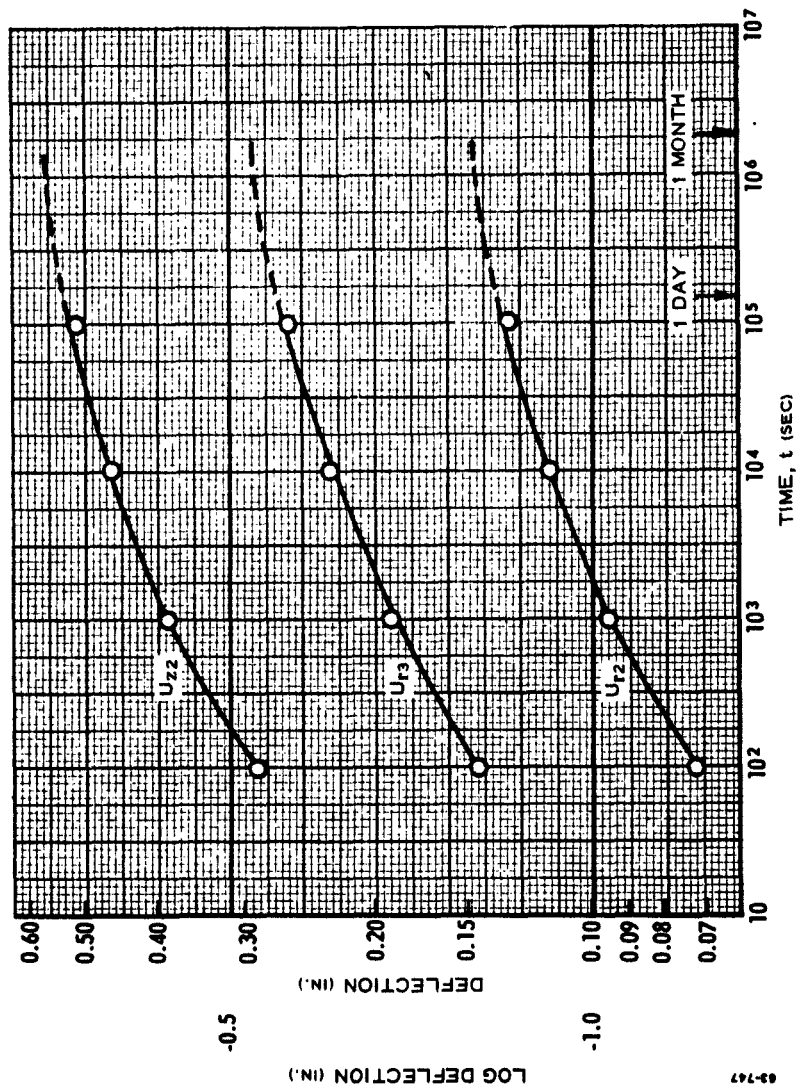
PREPARED BY LC
CHECKED BY MB
APPROVED BY [Signature]

PAGE 2 OF 2
DATE 6-16-63
REPORT NO. 578-F-3

COMPUTATION SHEET - GRAIN SLUMP DEFLECTIONS - FIXED-FREE GRAIN - PROB 2B (CONT)

TEMPERATURE
150 °F

[illegible]



NOTE: DEFLECTIONS ARE IDENTICAL BUT IN OPPOSITE DIRECTIONS FOR SEGMENT IN INVERTED POSITION

Figure 2-3 Grain Storage Slump Deflections versus Time at 150°F, Problem 2B
Reference Table 2-3

The method of solution assumes a step function application of the constant acceleration g at zero time. For storage slumps zero time may be taken when the motor casting hardware is removed. For launch acceleration, zero time is taken as ignition time and the previous storage deflections are added to obtain total deflections.

The method of solution also assumes that the reciprocal of the relaxation modulus $E(\tau)$ is equal to the creep compliance $D(\tau)$. This is an engineering approximation of acceptable accuracy as discussed in Section 3.1.

2.4 GRAIN PRESSURIZATION - PROBLEM 3 (Reference Section 4.4)

Purpose: Calculation of the limit strains at the port(s) in circular and star port grains case-bonded in elastic cases.¹

Governing Equations:

2.4.1 Grains with Free Ends (metal case):

$$\epsilon_{\theta p}(a) = \frac{3.4 b \lambda^2 p_i}{h E_c (3 + \lambda^2)} K_i$$

$\lambda = b/a =$ grain O. D. / I. D. ratio

$2b =$ grain O. D.

$h =$ case thickness (in.)

$E_c =$ case elastic modulus (psi)

$K_i =$ Star valley stress concentration factor (Reference Section 2.17 and Figures D-3 - D-8).

$p_i =$ motor operating pressure

2.4.2 Grains with Bonded Ends (metal case):

$$\epsilon'_{\theta p}(a) = \frac{b \lambda^2 (0.91) p_i}{h E_c} K_i = 0.27 (3 + \lambda^2) \epsilon_{\theta p}(a)$$

(Terminology as for 2.4.1)

The above calculations yield limits for the maximum tensile strain at the port in a star or circularly perforated grain with the appropriate end fixations. For grains with one fixed and one free end, the strains $\epsilon'_{\theta p}(a)$ and $\epsilon_{\theta p}(a)$ indicate, respectively, upper and lower limits for the maximum strain. Propellant compressibility is not taken into account in the above solutions, but is ordinarily of negligible importance in moderately designed grains (<65% web fraction, operating pressure <1000 psi). Methods for calculating strain components arising from propellant compressibility are discussed in Section 4.4.

Typical strain values are illustrated in Table 2-4.

¹ In conventional steel case designs of web fractions up to 60 - 80 percent, pressurization stresses are compressive only. This subject is discussed in Section 4.4 in greater detail.

PREPARED BY LC
 CHECKED BY [Signature]
 APPROVED BY [Signature]

PAGE 1 OF 1
 DATE 6-16-63
 REPORT NO. 578-F-3

Grain Pressurization Strains - Problem 3

XSM - EX Motor

$$\begin{aligned} 2b &= 12.00'' & P_i &= 1000 \text{ psi} & \frac{b}{h} E_c &= \frac{6}{0.09} \times 10^7 \\ 2a &= 6.00'' & K_i &= 1.89 & &= 2.22 \times 10^{-6} \\ h &= 0.09'' & \lambda &= 2 & & \\ E_c &= 3 \times 10^7 \text{ psi} & \lambda^* &= 4 & & \end{aligned}$$

$$\begin{aligned} \epsilon_{ap}(u) &= \frac{3.4 \lambda^* \frac{b}{h} E_c P_i K_i}{3 + \lambda^*} \\ &= \frac{(3.4)(4)(2.22 \times 10^{-6})(10^3)(1.89)}{7} \end{aligned}$$

$$\epsilon_{ap}(u) = 8.15 \times 10^{-3} = 0.82\% \text{ grain ends free}$$

$$\begin{aligned} \epsilon'_{ap}(u) &= 0.27(3 + \lambda^*) \epsilon_{ap}(u) \\ &= (0.27)(7) 0.82 \end{aligned}$$

$$\epsilon'_{ap}(u) = 1.55\% \text{ grain ends bonded}$$

2.5 PRESSURIZATION STRAIN FAILURE ANALYSIS - PROBLEM 3A

Purpose: To predict the low temperature firing limit for circular or star port case bonded grains.

Propellant Data: Strain at nominal maximum stress, ϵ_m , as determined in accordance with Section 1.2.

Procedure: The limit strain of pertinence as determined from Section 2.4 is calculated. The time to full pressurization of the motor, t_p , is determined and the approximate mean pressurization strain rate R_p

$$R_p = \frac{\epsilon_{\theta p}(a)}{t_p} \text{ or } \frac{\epsilon'_{\theta p}(a)}{t_p}$$

determined. The propellant strain at maximum stress appropriate to the strain rate R_p is plotted versus temperature in accordance with the procedures for time temperature shifting (Section 1.2). The low temperature firing limit is determined as the temperature at which the thermal strain $\epsilon_{\theta}^{c,s}(a)$ (Section 2.1) and the pressurization strain $\epsilon_{\theta p}(a)$ or $\epsilon'_{\theta p}(a)$ add viscoelastically to equal the available strain capability of the propellant. The superscripts c and s indicate circular and star port grains, as before. The addition is performed as follows:

$$\frac{\epsilon_{\theta}^{c,s}(a)}{\epsilon_m(R_y)} + \frac{\epsilon_{\theta p}(a)}{\epsilon_m(R_p)} = 1$$

where $\epsilon_m(R_y)$ is the strain capability of the propellant at the maximum cooling rate (Reference Section 2.2) and $\epsilon_m(R_p)$ is the strain capability of the propellant at the pressurization strain rate, both versus temperature. Illustrative calculations are presented in Table 2-5 and Figure 2-4.

It should be noted that the above definition of the firing limit assumes a cumulative damage criterion. In practice, a minimum firing safety factor of 1.5 as determined by the above procedure has been found to be conservative and is recommended. The subject is further discussed in Section 4.5.

PREPARED BY LCPAGE 1 OF 1CHECKED BY CGDATE 6-16-63APPROVED BY [Signature]REPORT NO. 578-F-3

Presturization strain Failure Analysis - Problem 3A

XSM-EX Motor - grain ends bonded
 $t_p = 155$ milliseconds

$$R_p = \frac{\epsilon'_p(\omega)}{t_p}$$

$$R_p = \frac{155 \times 10^{-3}}{155 \times 10^{-3}} \times 60 = 6.0 \text{ in/in/min}$$

Factor of Safety - F.S.

$$\frac{1}{F.S.} = \frac{\epsilon'_p(\omega)}{\epsilon'_m(R)} + \frac{\epsilon'_p(\omega)}{\epsilon'_m(R)}$$

$$T = -60^\circ F$$

$$\frac{13.4}{30} + \frac{1.05}{9.2} = 0.647; F.S. = 1.55$$

$$T = -70^\circ F$$

$$\frac{14}{28} + \frac{1.05}{5.8} = 0.82; F.S. = 1.22$$

$$T = -75^\circ F$$

$$\frac{14}{29} + \frac{1.05}{4.3} = 0.95; F.S. = 1.05$$

Ref: Figure 1-10
Table 2-1
Table 2-4
Figure 2-4

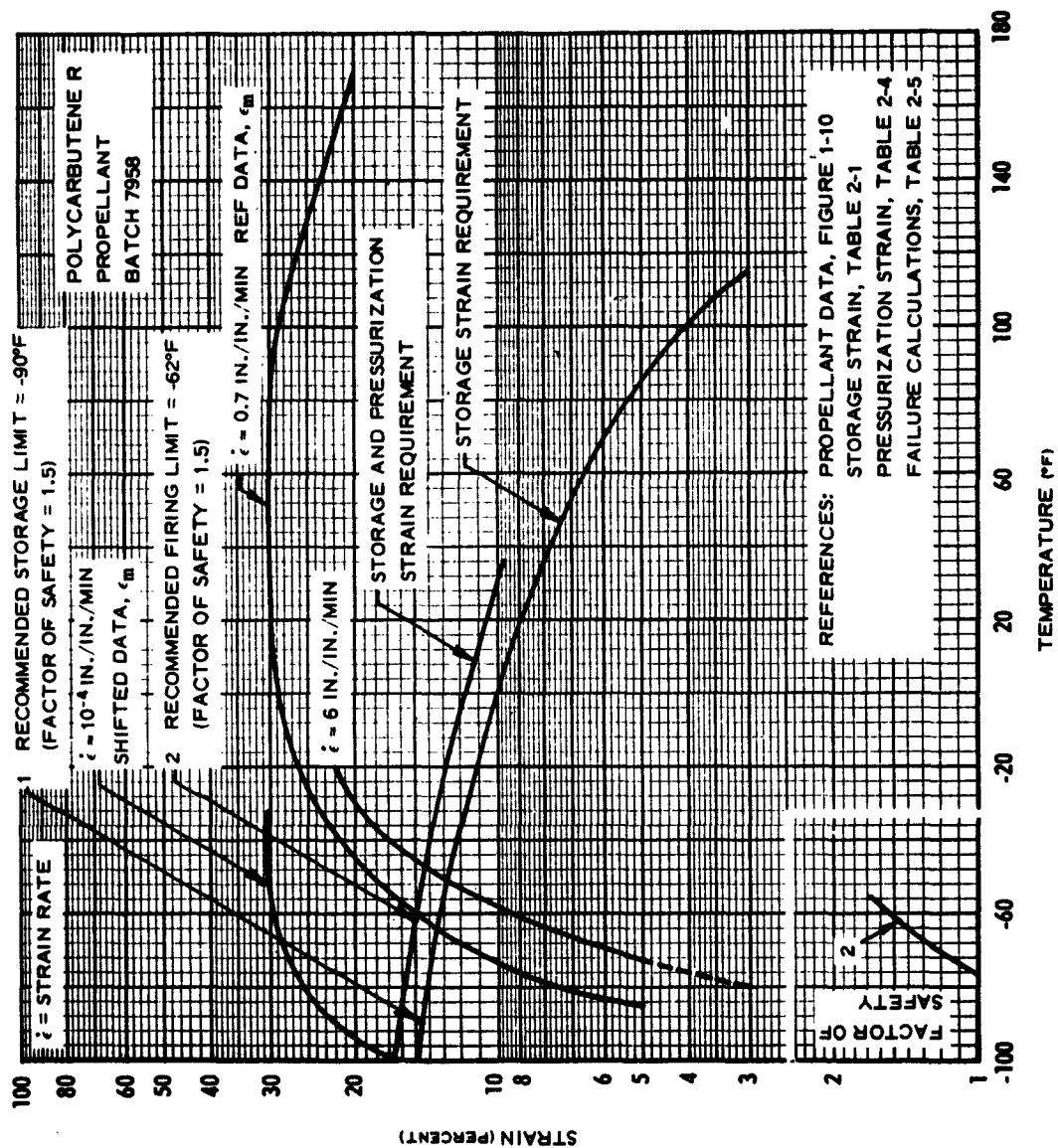


Figure 2-4 Storage and Pressurization Failure Strain Analysis XSM-EX Motor, Problem 3A

Section 3

BACKGROUND AND MATHEMATICAL PROCEDURES

CONTENTS

	Page
3 BACKGROUND AND MATHEMATICAL PROCEDURES	3-2
3.1 PROPELLANT VISCOELASTIC PROPERTIES	3-3
3.1.1 Operational Concept for Stress-Strain Relations	3-3
3.1.2 Linear Viscoelastic Representation	3-7
3.1.3 The Stress Relaxation Modulus	3-9
3.1.4 Temperature-Time Reduced Variable Treatment.	3-19
3.1.5 Creep Compliance	3-19
3.2 CONSTANT CROSSHEAD RATE FAILURE PROPERTIES	3-21
3.3 CONSTANT LOAD PROPERTIES	3-22
3.4 CONSTANT STRAIN PROPERTIES	3-23
3.5 PROPELLANT-LINER-SUBSTRATE BOND PROPERTIES	3-23
3.6 REDUCED LINEAR COEFFICIENT OF EXPANSION	3-24
3.7 BIAXIAL TESTING OF TOXIC OR RARE MATERIALS	3-25
3.7.1 The Diametral Test	3-25
3.8 ANALOG MOTOR TESTS	3-30

TABLE

		Page
3-1	PRONY SERIES COEFFICIENTS MASTER RELAXATION MODULUS AT 70°F	3-18

FIGURES

3-1	Typical Propellant Behavior (a) Relaxation Test, (b) Creep Test	3-4
3-2	Creep Compliance for Stress-Strain Law	3-4
3-3	Stress-Strain Relationships for Step Function Strain, Stress Relaxation Test	3-12
3-4	Stress Relaxation Data	3-13
3-5	Stress Relaxation Data	3-17
3-6	Diametral Compression Test	3-26
3-7	Comparison of Uniaxial and Biaxial Failure Stresses and Strains	3-29
3-8	Four and Seven-Inch Diameter Analog Motors	3-31
3-9	Analog Motor Experimental Set-up	3-33
3-10	Port Measurement of Analog Motor Grains	3-34
3-11	Borescope Inspection of Analog Motor Grains	3-35

Section 3

BACKGROUND AND MATHEMATICAL PROCEDURES

The success of an engineering structural analysis results from application of sophisticated theoretical concepts and from use of accurate physical data for the materials of construction. The physical data are of two essential kinds: data that define the relationship between force and deformation, and data that provide criteria for prediction of structural failure in given force-deformation fields. In direct, but more restrictive definition: the material stress-strain law and failure criteria. As previously indicated, the stress-strain relationship for solid propellants must intrinsically include time and temperature as essential defining parameters. This requirement is true also for definition of propellant failure criteria.

Section 3.1 of the handbook describes the methods of linear viscoelasticity and temperature-time reduced variables as specifically applicable to propellants. Because of its relative novelty in engineering analysis, considerable background in this area is included. Engineering methods for mathematical viscoelastic properties identification are described and numerical examples presented.

Sections 3.2 through 3.6 provide background information pertinent to the engineering techniques described in Section 1.2 through 1.6. Section 3.7 describes and discusses the biaxial diametral test technique which is useful both in obtaining failure criteria information and in application as an economical primary test method for physical screening of toxic or rare propellant formulations. Section 3.8 describes the analog test technique as applied to strain evaluation of propellants in subscale motors.

3.1 PROPELLANT VISCOELASTIC PROPERTIES

To predict the response of viscoelastic materials to applied stress, it is necessary to know the elastic and viscous parameters of the material as a function of time, rate, and temperature. In principle these parameters may all be combined into a generalized stress-strain law such that the strain (stress) may be calculated or deduced for an applied stress (strain) as a function of these parameters. When it is justified to assume this behavior is of linear form, based upon experimental evidence, this association between stress and strain can be viewed as a transfer function having the property which, when multiplied by a linear functional of strain (stress), generates the associated linear functional of stress (strain). The more familiar behavior of metals is considered first.

3.1.1 Operational Concept for Stress-Strain Relations

When a uniaxial steel tensile specimen at a moderate temperature is stretched, it is observed that the instantaneous strain is very nearly proportional to the applied stress up to the yield point; and that if the bar is unloaded the same law is followed. Consequently, the material obeys Hooke's law in tension up to the yield point and

$$\sigma = E\epsilon \quad (3-1)$$

in which stress σ , and strain ϵ , are based on the original specimen dimensions as in the usual engineering sense. The proportionality constant, E , which represents the slope of the stress-strain curve, is called Young's modulus or the tensile modulus. This law can be written also in the inverse form

$$D\sigma = \epsilon \quad (3-2)$$

The proportionality constant D is then commonly referred to as the tensile compliance. It has been found experimentally that the above law holds for many materials, particularly metals, as long as the strains are small.

It is evident that if a material which obeys Hooke's law is held at a constant strain, the stress also remains unchanged with time. However, when a viscoelastic tensile specimen at room temperature is stretched and held at a constant strain ϵ_0 (stress relaxation test), the stress $\sigma(t)$ necessary to maintain this elongation decays with time. In other words, the tensile relaxation modulus, $E(t) = \sigma(t)/\epsilon_0$, decreases. This situation is illustrated in Figure 3-1(a), behavior at constant stress is shown in Figure 3-1(b).

In addition to strong time dependence, the mechanical properties are greatly affected by temperature. Below a temperature, T_g , defined as the glass transition temperature, the propellant is essentially glassy and behaves as a brittle body obeying Hooke's law. Above this temperature, however, the response is time dependent and varies considerably with temperature. This

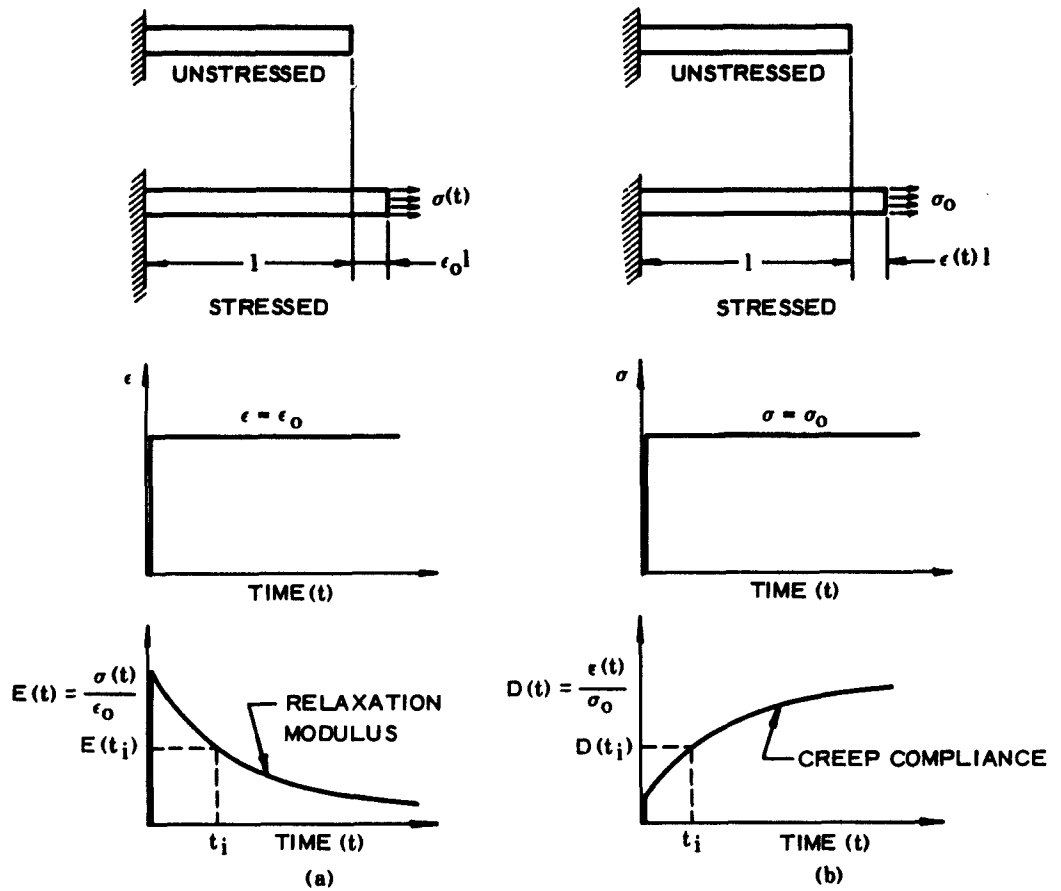


Figure 3-1 Typical Propellant Behavior (a) Relaxation Test, (b) Creep Test

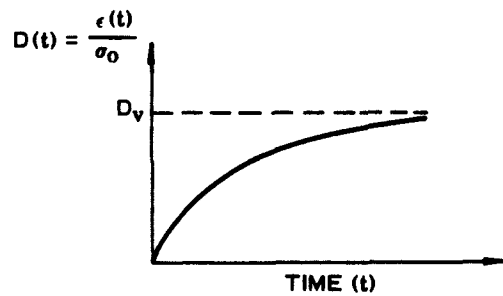


Figure 3-2 Creep Compliance for Stress-Strain Law: $\sigma(t) = [E_v + \eta_v \frac{d}{dt}] \epsilon(t)$

behavior leads to formulation of a general functional relationship between tensile stress and strain which includes both time and temperature dependence for temperatures greater than T_g . However, it has been found for many polymers, particularly plastics and rubbers, that these two variables can be considered separately if the temperature range is not too great. For example, if certain material constants are known at one temperature, it is possible to predict behavior at another temperature by simply shifting the time scale. Since composite propellants are filled rubbers, it is expected that the same rule should hold. Therefore, on this basis only the time-dependent behavior at a fixed temperature will be discussed, but will be followed in later sections by an explanation of the method used to change to a different temperature.

Expanding now the simple stress-strain relation given by (3-1) for a simple elastic behavior to a more general time dependent behavior one can write

$$O_1 [\sigma(t)] = O_2 [\epsilon(t)] \quad (3-3)$$

where O_1 and O_2 represent algebraic and differential operations on $\sigma(t)$ and $\epsilon(t)$. For example, when Hooke's law (3-1) applies, the operators are the simple constants $O_1 = 1$ and $O_2 = E$. It is important to note, however, that these operators are not always linear. Indeed, for large deformations of some metals, a more realistic elastic is, for example

$$\sigma = E(1 - 2\nu\epsilon) \ln(1 + \epsilon) \quad (3-4)$$

where ν is Poisson's ratio. In this instance, O_2 is a non-linear algebraic operator.

A simple time-dependent extension of Hooke's law is to consider stress proportional to both strain and strain rate. For this case, (3-3) becomes

$$\sigma(t) = \eta_v \frac{d\epsilon(t)}{dt} + E_v \epsilon(t) \quad (3-5)$$

in which E_v and η_v are proportionality constants. An important implied property of the differential operator is that it is linear and therefore obeys many of the ordinary rules of algebra, such as association, commutation, and superposition. This allows factoring of (3-5) to yield

$$\sigma(t) = \left[\eta_v \frac{d}{dt} + E_v \right] \epsilon(t) \quad (3-6)$$

and hence identify

$$O_1 = 1; \quad O_2 = \eta_v \frac{d}{dt} + E_v \quad (3-7)$$

If a creep test is considered in which a constant uniaxial stress, σ_0 , is applied to a material following (3-5), the resulting axial strain can be calculated

3.1.2 Linear Viscoelastic Representation

A special generalization of (3-3) is now defined such that O_1 and O_2 are taken to be linear differential operators. In the literature such a stress-strain law is called a linear viscoelastic representation*, and for a simple tensile test is written

$$\left[a_n \frac{\partial^n}{\partial t^n} + \cdots + a_1 \frac{\partial}{\partial t} + a_0 \right] \sigma(t) = \left[b_n \frac{\partial^n}{\partial t^n} + \cdots + b_1 \frac{\partial}{\partial t} + b_0 \right] \epsilon(t) \quad (3-12)$$

or more compactly

$$[P] \sigma(t) = [Q] \epsilon(t) \quad (3-13)$$

where P and Q stand for the bracketed operators O_1 and O_2 respectively. $\frac{\partial^i}{\partial t^i}$ is a linear operator that represents the i th derivative with respect to time, and a_i and b_i are experimental material constants which are obtained by methods to be discussed subsequently.

The relation (3-12) has been verified experimentally for small strains over a wide temperature range for many composite propellants at useful engineering strain levels (LPC-556-F-1).

Before discussing various specializations of (3-12), it should be remarked that the same form of a stress-strain law is found to hold for hydrostatic pressure and volume change, and for shear stress and shear strain in a simple shear test. Thus, the response of an element subjected to hydrostatic pressurization is represented by

$$[P'] \sigma_p(t) = [Q'] \frac{\Delta V(t)}{V_0} \quad (3-14)$$

where $\Delta V(t)/V_0$ is the volume change per unit undeformed volume due to the hydrostatic pressure $\sigma_p(t)$. Similarly, write

$$[P''] \tau(t) = [Q''] \gamma(t) \quad (3-15)$$

* If a time dependent stress produces an associated time dependent strain, then if doubling the magnitude of the stress holding the mode shape of the time variation the same also doubles the strain magnitude without changing the shape of its time dependence, the material is said to be linearly viscoelastic.

in which $\tau(t)$ is a shear stress and $\gamma(t)$ the corresponding shear strain. P'' , Q' , P' , Q are of the general form of P and Q shown in (3-12), but, of course, with different experimental material constants. Equations (3-13), (3-14), and (3-15) are analogous to the elastic stress-strain laws, since for an elastic body undergoing small deformations

$$\begin{aligned} \text{simple uniaxial tension:} \quad & \sigma = E \epsilon; \quad (E = \text{Young's modulus}) \\ \text{hydrostatic pressurization:} \quad & \sigma_p = K \frac{\Delta V}{V_0}; \quad (K = \text{bulk modulus}) \quad (3-16) \\ \text{shear:} \quad & \tau = \mu \gamma; \quad (\mu = \text{shear modulus}) \end{aligned}$$

Similarly for a linear viscoelastic material

$$\begin{aligned} \text{simple uniaxial tension:} \quad & \sigma(t) = \frac{Q}{P} \epsilon(t) \\ \text{hydrostatic pressurization:} \quad & \sigma_p(t) = \frac{Q'}{P'} \frac{\Delta V(t)}{V_0} \quad (3-17) \\ \text{shear:} \quad & \tau(t) = \frac{Q''}{P''} \gamma(t) \end{aligned}$$

where the association of E with Q/P , etc., is obvious.

It may be remarked that a purely mathematical approach to linear theory does not restrict the form of the P , Q operators. However, Biot (1954) has used irreversible thermodynamics to show that the coefficients are restricted in such a way that the ratios Q''/P'' , Q'/P' , and Q/P must be identical with the transfer functions for mechanical models consisting of springs and dashpots*. Since the operator ratios in (3-17) are restricted to be of a definite form, it is often convenient to retain this form rather than multiplying all terms out and separating P and Q . Therefore, $E(t)$, $K(t)$ and $\mu(t)$ will be written in place of Q''/P'' , Q'/P' , Q/P and thus maintain this analogy between the viscoelastic and elastic problems in the notation.

When it comes to actually computing the stresses and displacements in a linear viscoelastic body, use will be made of this analogy by working out an associated elastic solution in terms of the associated operator form of the material representation.

It can be shown that when a three-dimensional elastic body is isotropic and homogeneous there can exist no more than two independent elastic constants (Sokolnikoff, 1956). In their natural form, they are the bulk modulus, K , governing the stress-strain proportionality for (hydrostatic) dilatation acting

* Mathematical analogies for spring and dashpot treatments are included in, for example, LPC 556-F-1, LPC 578-F-1.

alone, and the shear modulus, μ , governing distortion alone. Similarly, as a result of geometric symmetry, only two independent operator relations can exist for an isotropic, homogeneous, linear viscoelastic material. Specifically, from (3-16) and (3-17)

$$\mu \longrightarrow \mu(t) \quad (3-18)$$

$$K \longrightarrow K(t) \quad (3-19)$$

Engineering analysts frequently find it convenient to solve elastic problems in terms of Young's modulus and Poisson's ratio which are related to K and μ , and the viscoelastic associations by

$$E = \frac{9\mu K}{3K + \mu} \longrightarrow \frac{9\mu(t) K(t)}{3K(t) + \mu(t)} = E(t) \quad (3-20)$$

$$\nu = \frac{3K - 2\mu}{6K + 2\mu} \longrightarrow \frac{3K(t) - 2\mu(t)}{6K(t) + 2\mu(t)} = \nu(t) \quad (3-21)$$

In rubber elasticity it has been conventional to note that the ratio of the bulk and shear moduli is very large, leading to the simplification

$$E \cong 3\mu, E(t) \cong 3\mu(t) \quad (3-22)$$

$$\nu \cong 1/2, \nu(t) \cong 1/2 \quad (3-23)$$

In the class of problems to be treated in this handbook, it has been found that the above simplifications are adequate for engineering treatment of well consolidated solid propellants in moderately designed solid propellant motors. In experimental determination of propellant properties, hence, the measurement of $E(t)$ or $\mu(t)$ is the present problem.

3.1.3 The Stress Relaxation Modulus

The viscoelastic stress relaxation modulus $E(t)$ defines a relationship between the time-dependent stress $\sigma(t)$ resulting from an instantaneous straining to a constant strain level ϵ_0 and the viscoelastic properties of the material:

$$E(t) = \frac{\sigma(t)}{\epsilon_0}$$

Numerically, the relaxation modulus is obtained in reduction of data in which stress decay after imposition of strain on a sample is observed. Experimental techniques for accomplishing the tests and reduction of the data therefrom are described in Section 1.1 and will not be given in detail here. The

objective in the following examples will be to illustrate the resolution of the numerical data to mathematical form in terms of the propellant stress-strain law. This resolution of data to generalized form is an essential step in providing the mathematical specification of material properties required in solution of many stress analysis problems. Two forms of the stress-strain law will be treated: the linear differential operator form

$$\begin{aligned}
 P \sigma(t) &= Q \epsilon(t) \\
 P &= \sum_{i=0}^n a_i \frac{\partial^i}{\partial t^i} \\
 Q &= \sum_{i=0}^n b_i \frac{\partial^i}{\partial t^i}
 \end{aligned} \tag{3-24}$$

where $\epsilon(t)$ is time-dependent strain, and the coefficients a_i, b_i are the generalized material properties; and the integral form

$$\sigma(t) = \left[E_e + \int_0^{\infty} \frac{H(\tau)}{\frac{\partial}{\partial t} + \frac{1}{\tau}} \cdot \frac{\partial \tau}{\tau} \cdot \frac{\partial}{\partial t} \right] \epsilon(t) \tag{3-25}$$

where the function $H(\tau)$ and E_e are the generalized material properties. Without treating the methods of solution of these equations in detail, noting that this information is given in LPC 556-F-1, LPC 578-F-1, and GALCIT SM-61-5, the solutions for the relaxation modulus are, for the operational specification,

$$E(t) = \frac{\sigma(t)}{\epsilon_0} = A_0 + A_1 e^{-\alpha_1 t} + A_2 e^{-\alpha_2 t} + \cdots + A_n e^{-\alpha_n t} \tag{3-26}$$

and, in the case of the modified power law approximation, for the integral specification

$$E(t) = \frac{\sigma(t)}{\epsilon_0} = C_{\infty} + C_1 t^{-n}$$

$$t > t_x \tag{3-27}$$

The immediate objective is, then, to obtain numerical values for the constants A_1, α_1 , or C_1, C_{∞} , and n from test data.

(a) The Differential Operator Solution

Assume a step-function uniaxial strain applied to a viscoelastic bar of propellant. Mathematically,

$$\epsilon(t) = \begin{cases} 0, & t = 0 \\ \epsilon_0, & t > 0 \end{cases}$$

and as shown in Figure 3-3. For times greater than zero, stress decay shown in Figure 3-3 may be specified by the following Prony series, which is a solution of the differential operator equation (Equation 3-24):

$$\frac{\sigma(t)}{\epsilon_0} = A_0 + A_1 e^{-\alpha_1 t} + A_2 e^{-\alpha_2 t} + \dots + A_n e^{-\alpha_n t}. \quad (3-28)$$

Proceeding from experimental relaxation data to calculation of the coefficients of a series of decaying exponential terms can be accomplished by graphical term stripping techniques (Tobolsky, 1956). The technique is based upon the observation that after some undetermined time all terms in the series, except those with the smallest coefficients, have become insignificant. Once this time has been determined, the low-order term may be determined and subtracted from the data. The procedure is repeated until all the terms have been extracted.

The collocation method (Schapery, 1962; Brisbane, 1962) may be also utilized. In this method the constants α_i are assumed and the corresponding set of constants A_i are found from a set of simultaneous linear equations. If the constants α_i are properly chosen, the resulting set of linear equations can be solved readily by desk calculations.

An example illustrates the collocation method. Data points taken from a typical stress-relaxation curve (Figure 3-4) at one decade time intervals are:

<u>Time (seconds)</u>	<u>Modulus (psi)</u>
1	635
10	475
100	345
1000	265

"n" of Equation (3-28) is set equal to four (one per decade of time plus 1) and the value of A_0 is found to be 200 psi. Equation (3-28) now reduces to

$$\sum_{i=1}^4 A_i e^{-\alpha_i t} - A_0 = \frac{\sigma(t)}{\epsilon_0} - 200. \quad (3-29)$$

If the α_i are now arbitrarily chosen such that

$$\alpha_i = \frac{1}{2t_i}$$

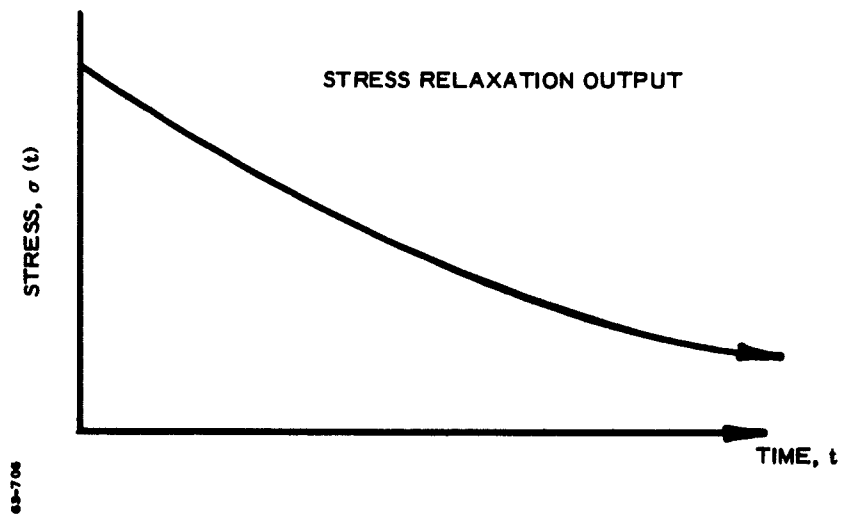
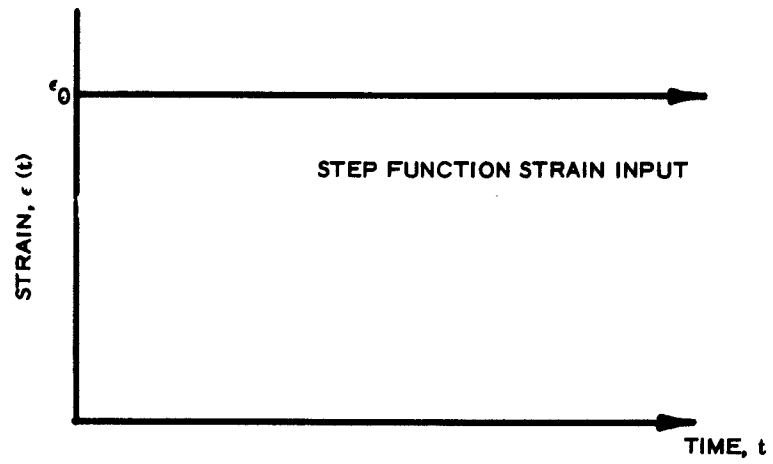


Figure 3-3 Stress-Strain Relationships for Step Function Strain, Stress Relaxation Test

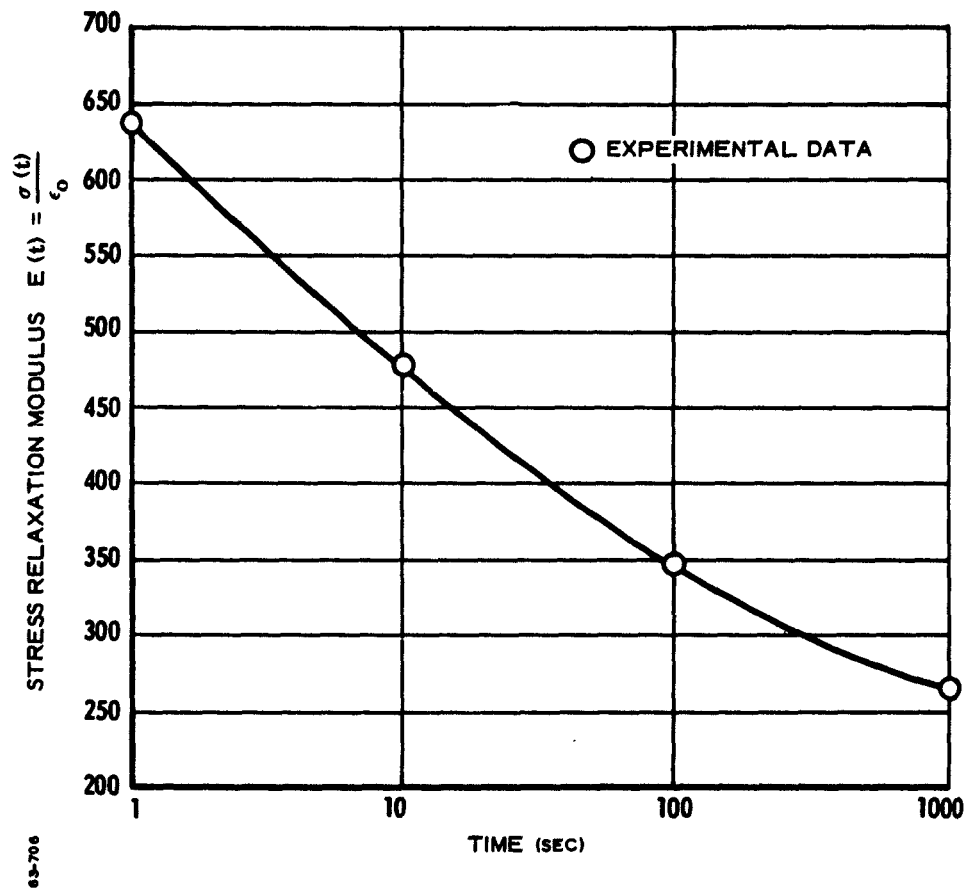


Figure 3-4 Stress Relaxation Data

where t_i is the time at each data point, then

$$\alpha_1 = 0.5$$

$$\alpha_2 = 0.05$$

$$\alpha_3 = 0.005$$

$$\alpha_4 = 0.0005$$

Using these values, Equation (3-29) may be evaluated for the coefficients A_i . The matrix representation of the simultaneous linear equations obtained by writing Equation (3-29) for each data point is

$$\begin{bmatrix} e^{-0.5} & e^{-0.05} & e^{-0.005} & e^{-0.0005} \\ e^{-5} & e^{-0.5} & e^{-0.05} & e^{-0.005} \\ e^{-50} & e^{-5} & e^{-0.5} & e^{-0.05} \\ e^{-500} & e^{-50} & e^{-5} & e^{-0.5} \end{bmatrix} \begin{bmatrix} A_1 \\ A_2 \\ A_3 \\ A_4 \end{bmatrix} = \begin{bmatrix} 435 \\ 285 \\ 145 \\ 65 \end{bmatrix}$$

Evaluating the exponentials,

$$\begin{aligned} e^{-0.005} &\approx 1.000 \\ e^{-0.005} &\approx 1.000 \\ e^{-0.05} &\approx 0.951 \\ e^{-0.5} &\approx 0.607 \\ e^{-5} &\approx 0 \\ e^{-50} &\approx 0 \\ e^{-500} &\approx 0 \end{aligned}$$

the matrix reduced to

$$\begin{bmatrix} 0.607 & 0.951 & 1 & 1 \\ 0 & 0.607 & & \\ 0 & 0 & 0.607 & 0.951 \\ 0 & 0 & 0 & 0.607 \end{bmatrix} \begin{bmatrix} A_1 \\ A_2 \\ A_3 \\ A_4 \end{bmatrix} = \begin{bmatrix} 435 \\ 275 \\ 145 \\ 65 \end{bmatrix}$$

Solving the resultant set of simultaneous linear equations gives the following values for A_i

$$A_1 = 165$$

$$A_2 = 165$$

$$A_3 = 71$$

$$A_4 = 107$$

and the Prony series is

$$E(t) = 200 + 165 e^{-0.5t} + 165 e^{-0.05t} + 71 e^{-0.005t} + 107 e^{-0.0005t} \quad (3-30)$$

which fits the experimental data with an accuracy of 3 percent. The accuracy of the fit can be improved by taking the arbitrary relaxation coefficients α_i at smaller intervals. In studies of propellant data, one exponential per decade of time has been found to yield sufficiently accurate results for grain stress analysis calculations.

Thus, the numerical representation of the stress relaxation modulus is obtained. The above procedure is generalized for consideration of more extensive data time wise by increasing the number of terms of the type

$$A_i e^{-\alpha_i t}$$

in the Prony series. A complete material specification usually requires about 15 to 20 such terms and is, on the practical level, a one-hour desk calculator job. Generalization to the operator equation form requires only algebraic manipulation of the coefficients of Equation (3-30); the relationships are shown in Appendix B.

(b) The Integral Modified Power Law Solution

Assume a step function uniaxial strain is applied to a viscoelastic bar of propellant. It is desired to determine the coefficients C_∞ , C_1 and n of

$$E(t) = \frac{\sigma(t)}{\epsilon_0} = C_\infty + C_1 t^{-n} \quad (3-31)$$

the constant C_∞ , the value of the modulus at $t = \infty$ is, in this instance, zero.

Replotting the data of Figure 3-4 on logarithmic coordinates yields a straight line function (Figure 3-5). The coefficient C_1 is the intercept value at $t = 1$ and the coefficient n is the arithmetic slope of the curve, yielding:

$$E(t) = \frac{\sigma(t)}{\epsilon_0} = 635 t^{-0.170} \quad (3-32)$$

$$1000 > t > 1.$$

It should be noted that the modified power law form used here for illustration is valid only within the time range where the plot of $\log E(t)$ versus $\log t$ is well approximated by a straight line.

(c) General Considerations

The preceding examples serve to illustrate the conversion of numerical viscoelastic data to useful forms of the isothermal stress-strain law for the simplest of conceptual test circumstances, i.e., the step function strain input to a stress relaxation test. In experimental practice, the step function strain input is neither possible nor necessary. Perhaps the present simplest method of viscoelastic characterization is the ramp strain, stress relaxation test, which can be easily and accurately executed using conventional tensile testers such as the Instron. In the ramp test, strain is applied to a tensile specimen at a constant rate until a predetermined strain level is obtained, at which straining is stopped and stress decay with time observed. Rigorously, the appropriate solutions for the ramp relaxation curve must take into account the stress-strain history during the ramp portion of the test for either of the two forms of the stress-strain law discussed. On a practical basis, however, the viscoelastic memory of the propellant can be regarded as a fading one in which the initial ramp strain condition is forgotten by a time approximately 10 times that of the ramp duration. Defining the ramp duration time to be t_1 , the interpretation of the relaxation curve for $t > 10t_1$ is, for engineering purposes, identical to that for the step function strain input as discussed. While there is loss of mathematical rigor in this interpretation, numerical inaccuracy is less than one percent. The preceding example may be interpreted, hence, as applying either to a step function strain input resolved from time zero or a ramp strain input resolved for $t > 10t_1$.

Treatment of viscoelastic data for wider time ranges, such as are obtained from reduced variable representations, proceeds using the methods previously illustrated. For the data shown in Figure 1-7, Section 1.1, the Prony Series coefficients for the 70°F time scale are shown in Table 3-1. The modified power law representation is

$$E(t) = 100 + 616 t^{-0.237} \quad (3-33)$$

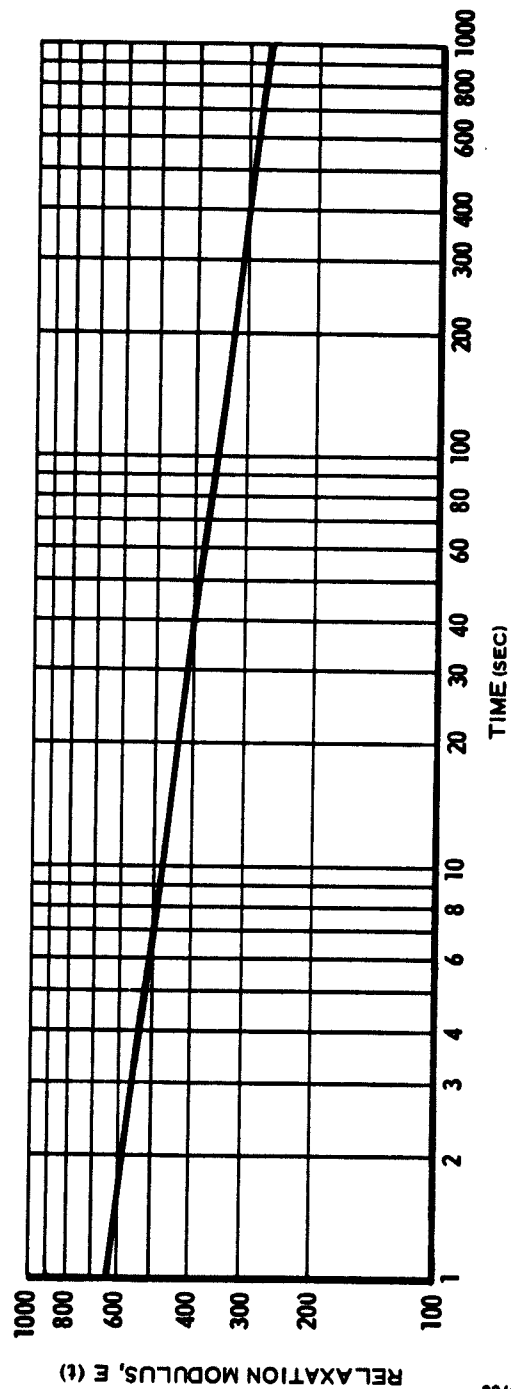


Figure 3-5 Stress Relaxation Data

Table 3-1
PRONY SERIES COEFFICIENTS
MASTER RELAXATION MODULUS AT 70°F

$$E(t) = \sum_{i=0}^n A_i e^{-\alpha_i t}$$

<u>i</u>	<u>α_i</u>	<u>A_i</u>
0	0	1.00×10^2
1	5×10^{-8}	1.98×10^1
2	5×10^{-7}	1.19×10^1
3	5×10^{-6}	3.95×10^1
4	5×10^{-5}	4.25×10^1
5	5×10^{-4}	6.50×10^1
6	5×10^{-3}	9.15×10^1
7	5×10^{-2}	1.69×10^2
8	5×10^{-1}	2.47×10^2
9	5×1	5.71×10^2
10	5×10^1	8.11×10^2
11	5×10^2	1.36×10^3
12	5×10^3	2.56×10^3
13	5×10^4	4.87×10^3
14	5×10^5	8.55×10^3
15	5×10^6	1.40×10^4
16	5×10^7	2.12×10^4

3.1.4 Temperature-Time Reduced Variable Treatment

The essence of the time-temperature reduced variable concept is, for example, that stress relaxation with time t at a given temperature T_s is equivalent to the stress relaxation at a temperature T when measured on a reduced time scale t/a_T . a_T is the temperature-time shift factor. Mathematically, the relationships in terms of the two forms of the relaxation modulus equation are

(a) Differential Operator

$$E(\tau) = \sum_{i=0}^n A_i e^{-\alpha_i \tau / a_T} \quad (3-34)$$

(b) Modified Power Law

$$E(\tau) = C_\infty + C_1 (t/a_T)^{-n} \quad (3-35)$$

where the coefficients A_i , α_i , C_∞ , C_1 and n are those determined at the reference temperature T_s ($a_T = 1$ at T_s). Thus it is seen that changes in temperature correspond physically and mathematically to changes in the time scale of observation.

The reduced variable treatment used in this handbook differs somewhat from the WLF method (Williams, Landel and Ferry, 1955) in that an absolute temperature dependence of the relaxation modulus is ignored. Discussions of this point are available in the above cited reference as well as in LPC 556-F-1 and LPC 578-F-1. In the problems considered in this handbook, the neglect of an absolute temperature dependence of the relaxation modulus results in potential errors in grain stress analysis that are trivial.

3.1.5 Creep Compliance

The stress relaxation modulus

$$E(t) = \frac{\sigma(t)}{\epsilon_0} \quad (3-36)$$

is obtained from solution of the operation Equation (3-13)

$$P\sigma(t) = Q \epsilon(t) \text{ or } \sigma(t) = \frac{Q}{P} \epsilon(t) \quad (3-37)$$

for the strain input condition

$$\epsilon(t) = \epsilon_0 u(t), \quad (3-38)$$

i. e., a step strain input at $t = 0$. The analogous solution for a step stress input, solving for strain is

$$\epsilon(t) = \frac{P}{Q} \sigma(t) \quad (3-39)$$

$$\sigma(t) = \sigma_0 u(t)$$

yielding the expression for the creep compliance $D(t)$

$$D(t) = \frac{\epsilon(t)}{\sigma_0} \quad (3-40)$$

which for the operational solution is

$$D(t) = \sum_{i=0}^n B_i e^{-\beta_i t} \quad (3-41)$$

The Prony Series coefficients B_i , β_i of Equation (3-41) are explicitly related to the coefficients A_i , α_i , of Equation (3-28) through the operators P and Q . Interconversion of these coefficients may be done using the algebraic relationships presented in Appendix B; the subject will not be further pursued in this section.

It is important to notice that while $E(t)$ is not exactly the reciprocal of $D(t)$, to a satisfactory degree of approximation $E(t)$ can be regarded as the reciprocal of $D(t)$. Hence, the creep compliance for the Polycarbuthene-R propellant used as an example in this handbook may be numerically estimated closely enough for engineering calculations by taking the reciprocal of the stress relaxation curve of Figure 1-7, Section 1. The approximation has been used in the solution of grain slump problems in Section 2 of this handbook.

The creep compliance test is a useful adjunct in propellant viscoelastic characterization because of the simplicity with which the test may be executed for extremely long-time test durations. A test procedure for creep compliance measurement has been included as Appendix C to this handbook.

3.2 CONSTANT CROSSHEAD RATE FAILURE PROPERTIES

Constant crosshead rate tensile properties of a propellant are of fundamental importance in both propellant evaluation and motor structural analysis. The test technique is economical and rapid in execution. With some reservations, constant rate properties provide basic failure data for propellants that permit rapid evaluation of new formulations. The constant rate properties are usually the first available to the motor stress analyst when new formulations are under consideration for motor applications. Discussion of the technical aspects of the test method from the point of view of the grain structural analyst is therefore important.

The strain at nominal maximum stress ϵ_m as interpreted from Figure 1-9, Section 1.2, provides a reasonably reliable measure of the useful strain capability of a propellant in motor applications (Jones, 1963). The physical phenomenon most importantly associated with the strain at nominal maximum in composite propellants is the inception of extensive oxidizer-binder dewetting, which produces the change in properties responsible for the abrupt decrease in modulus near ϵ_m .

Extensive motor tests have shown that typical PBAA, PBAN, and Nitroplastisol propellants fail when hoop tensile strains in the motors exceed the ϵ_m as measured in uniaxial tension, regardless of apparent additional elongation to rupture uniaxial tensile capability. Hence, the implication is drawn that while inception of dewetting may not cause immediate rupture under constant rate uniaxial tensile elongation, it does so under the multiaxial conditions and slow rates typical of thermally cooled motors.

The apparently arbitrary interpretation of the value of ϵ_m indicated in Figure 1-9, Section 1.2, has been developed by collation of various types of data. To cite a few, the ϵ_m as interpreted from Figure 1-9 are found to agree with:

- The long term constant strain capability (LPC 556-F-1)
- The strain at failure under long duration constant stress (or load) conditions (LPC 556-F-1)
- The upper strain limit of useful viscoelastic linearity under short duration stress relaxation or creep conditions (LPC 578-F-1)
- The hoop strain at failure in scale and full-scale motor tests (LPC 578-F-1 ; Hart, 1963; Jones, 1963)

The latter item is, of course, the most vital of the types of correlative information. It should be emphasized that these correlations are valid only for comparable conditions of rate and temperature. The methods of data handling and rate-temperature correlation are illustrated in Sections 1.1, 1.2 and 2.1. Before proceeding to discussion of the test method itself, it should be noted that interpretation of all test records for ϵ_m is not possible using the rules indicated in Figure 1-9. Test data of this type require auxiliary investigation,

most conveniently by the constant strain or constant load techniques discussed in Sections 3.3 and 3.4 or in analog motor tests (Section 3.9).

With regard to the mechanics of the test itself, it is of vital importance that a precise test specimen be used. The only generally acceptable method for producing sufficiently precise tensile specimens is by machining, as discussed in Appendix A. Second, an accurate method of strain measurement must be used in tests of JANAF tensile specimens. It has been found that the effective gage length of a JANAF specimen varies with propellant type, temperature, strain rate and strain level (e.g., LPC-531-F, LPC 556-F-1, Duerr, 1961). Either photographic or extensometer (Appendix A) techniques can be used to measure strain in JANAF specimens within 1 percent of strain, the extensometer method being preferred at LPC because of its ease and economy.

In execution of the test it has been found to be important to follow rigorous specimen storage and handling precautions. Following completion of cure, tensile test specimens are exposed to undesiccated conditions for only the time necessary to machine them (about 10 to 25 minutes at R.H. <50 percent), and during the one minute or so required in actual execution of the test in the Instron.

3.3 CONSTANT LOAD PROPERTIES

Constant load propellant strength data provide a measure of the long-term stress capability of a propellant which is useful, for example, in failure analysis for gravitational storage load conditions (Section 4-6). This type of data is also diagnostic for time effects in failure sometimes not observed in the constant rate tests. For example, constant load tests may show a gradual strength decay to near zero after an induction period of a few hours in high temperature tests that may not be evident in constant rate tests under the same temperature and time conditions. Such apparently contradictory data indicate nonlinear effects in a propellant arising, for example, from chemical bond scission in the binder structure under sustained load conditions. The phenomenon, which can result in failure or permanent set in the propellant, generally occurs at temperatures higher than cure temperature after sustained exposure. The end result of the high temperature aging process may be either a completely degraded propellant or an essentially new propellant characterized by a new relaxation spectrum, higher modulus, and reduced low temperature elongation.

3.4 CONSTANT STRAIN PROPERTIES

As indicated in Section 1.4, the constant strain test as commonly employed is diagnostic of propellants with rapidly decaying resistance to failure under sustained extension. In such instances, it is necessary to define the asymptotic level of strain that can be sustained indefinitely without failure. When this level is more than 2 percent strain below the constant rate strain at nominal maximum stress ϵ_m , it supercedes ϵ_m as a failure criterion for the evaluation of low temperature storage and firing limits of a motor.

When ballistic necessity dictates the application of a propellant inherently poor in constant strain properties, it is necessary to evaluate the constant strain asymptote for the effects of temperature and initial strain rate in order to fully define the data needed in the motor strain analysis. Problems in this category require specialized treatment; identification of the existence of the problem, however, is within the scope of standard engineering inquiry.

3.5 PROPELLANT-LINER-SUBSTRATE BOND PROPERTIES

The bond-in-tension apparatus described in Section 1.5 provides the vehicle for only one of a large variety of bond evaluation methods (see the ICRPG Solid Propellant Mechanical Behavior Manual, 1963, for description of additional methods). The bond-in-tension test is preferred as a screening test in ordinary development and quality control work because of its economy in execution and the ease of data interpretation on a limit basis, as discussed in Section 1.5. In general, the limit analysis simply separates excellent bonding properties (cohesive propellant failures) from eminently poor bonding properties (interfacial failures) and isolates inherently weak insulators and liners (cohesive failure in liner or insulation). Where bond strength problems exist, as previously noted, a chemical or process problem requiring solution in the laboratory is indicated. Where optimization of case-bonding strengths to those nearly equal to the observed propellant strength is not possible, extremely difficult failure analysis problems arise; further discussion in this connection is presented in Section 4.

3.6 REDUCED LINEAR COEFFICIENT OF EXPANSION

The propellant coefficient of linear thermal expansion, α_p , is ordinarily a function of temperature well approximated by

$$\alpha_p = C_1 + C_2 T \quad (3-42)$$

where C_1 and C_2 are constants and T is temperature (conveniently T in $^{\circ}\text{F}$ is used to define C_1 as the value of α_p at 0°F). The average value of the thermal coefficient between two temperatures T_1 and T , $\bar{\alpha}_p$, is given by

$$\bar{\alpha}_p = \frac{\Delta l}{l_1} = \frac{1}{T - T_1} \int_{T_1}^T \alpha_p dT. \quad (3-43)$$

where l_1 is the specimen length at T_1 . The solution for thermal strains in a case-bonded motor requires integration of the term α_p , which appears in the elastic small strain solution, or equivalently, direct introduction of the term $\bar{\alpha}_p$ as shown in Section 2.1. The simplest procedure for generation of the thermal coefficient term used in solution for thermal strains in a motor is that shown in Section 1.6. The technique avoids introduction of numerical error through the redundant, successive differentiation and integration of the $\Delta l/l_1$ laboratory measurement. The additional simplification introduced by referencing the $\Delta l/l_1$ relationship to the propellant grain zero strain temperature permits direct correlation of laboratory tensile test data to motor strains in failure analysis.

3.7 BIAXIAL TESTING OF TOXIC OR RARE MATERIALS

Rapid evaluation of the physical properties of toxic or extremely costly propellant formulations results in difficulties in executing tensile tests because of tensile specimen preparation hazards and/or prohibitive cost requirements. The diametral compression biaxial test has been used as a means for ameliorating both difficulties. In the diametral test, a circular disc is compressed along a diameter, producing a vertical compression and a lateral tension, at the center of the disc (Figure 3-6). In extensive tests, it has been found that the lateral tensile stress and strain in the disc agree quite accurately to the uniaxial values σ_m , ϵ_m (Section 1.2, 3.2). The diametral test, hence, has been used as an auxiliary method for screening purposes in development of toxic and expensive formulations. Specimens consisting of pressed discs $\frac{3}{4}$ -inch by $\frac{1}{4}$ -inch in dimension and cast discs $1\frac{1}{2}$ -inch by $\frac{1}{2}$ -inch have been used successfully in this method of evaluation. In both types, no cutting or trimming of the specimen was required and, hence, no propellant waste incurred. In addition, because the physical circumstances of the test facilitate the collection and disposition of all specimen fragments, cumulative contamination of test fixtures with toxic materials can be minimized. The following presents the test procedure used in conducting and analyzing data from the tests.

3.7.1 The Diametral Test

Scope: The following describes the diametral tension - compression biaxial test, presents typical test data, and compares it to uniaxial tensile data.

Test Apparatus: Universal tester equipped with compression platens and load cell, and with temperature conditioning chamber.

Test Specimen: A disc of propellant with a diameter-to-thickness ratio of approximately 3 is preferred. Diameters of 6 inches to $\frac{3}{4}$ -inch have been successfully used. Specimens can be prepared by machining, pressing or casting, but regardless of preparation method, should be circular within 1 percent and opposing planar surfaces should be parallel within 1 percent.

Test Method and Analysis: In the diametral test, a right circular cylinder with a diameter-to-thickness ratio of approximately 3 of the material to be tested is placed between the platens of a compression tester (Figure 3-6). As the platens move together along a diameter of the specimen, the y-axis, a resisting force, F_y , is developed as well as biaxial stresses σ_x and σ_y at the center of the sample.

The stress in line with the compressive force, F_y , is σ_y and given by (Fitzgerald, 1960),

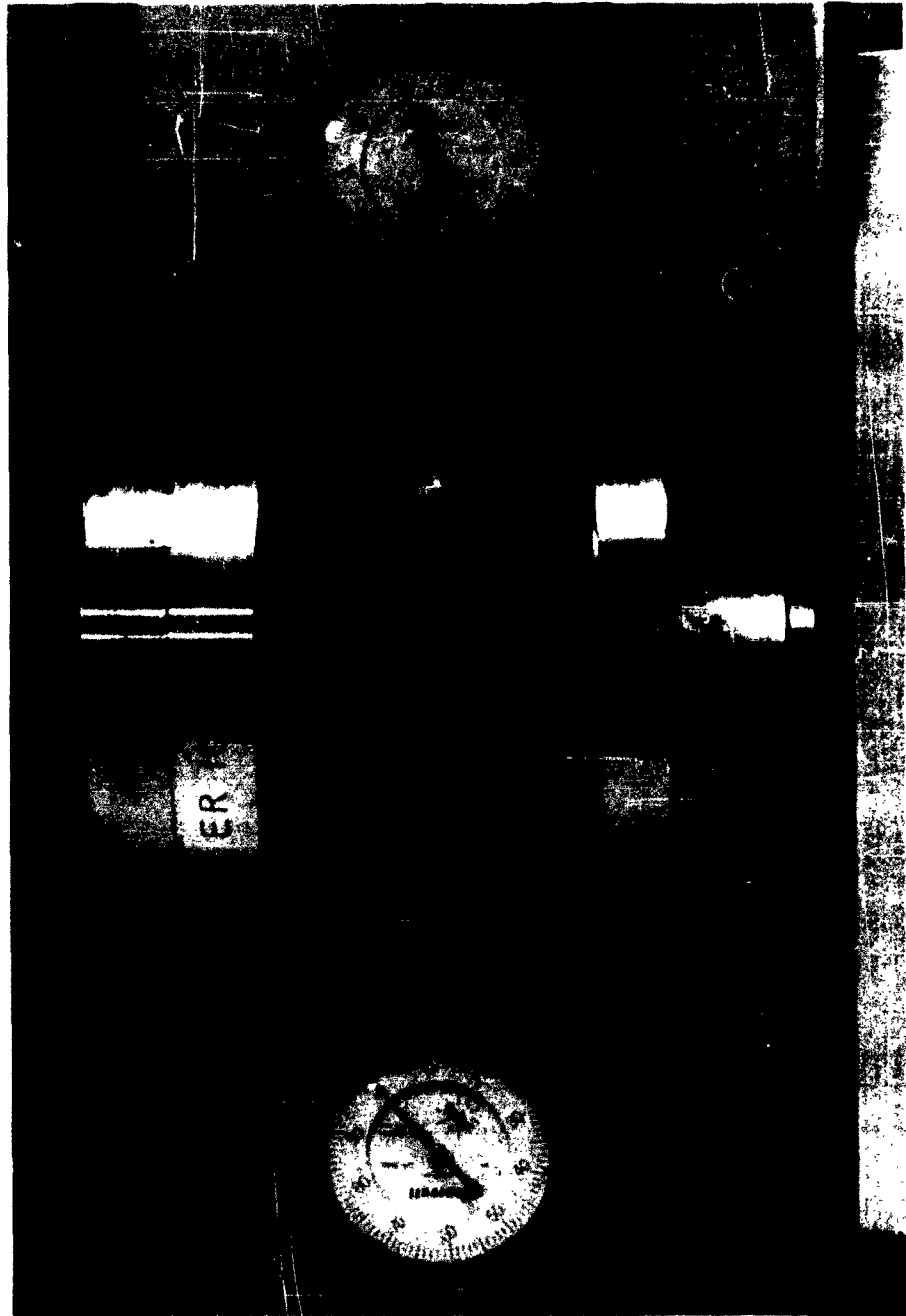


Figure 3-6 Diametral Compression Test

$$\sigma_y = \frac{6 F y}{\pi t d} \quad (3-44)$$

d = sample diameter

t = thickness

the negative sign signifies a compressive stress.

Along the axis normal to the applied force there is developed a tensile stress, σ_x , given by

$$\sigma_x = \frac{2F}{\pi t d} \quad (3-45)$$

the corresponding horizontal strain at the center of the diametral specimen is given by

$$\epsilon_x = \frac{2F y (1 + 3\nu)}{\pi d t E} \quad (3-46)$$

where ν is Poisson's ratio and E the modulus of the material.

Vertical strain at the center of the samples is given by

$$\epsilon_y = - \frac{2F y + (3 + \nu)}{\pi d t E} \quad (3-47)$$

The total deformation along the center horizontal axis $U(x, 0)$ is given by

$$U(x, 0) = \frac{F y}{\pi t E} [(1 - \nu)(2 - \pi) + 2(1 + \nu)] \quad (3-48)$$

The ratio of horizontal strain at the center of the sample to the total horizontal unit deformation is then

$$\frac{\epsilon_x}{U/d} = \frac{2(1 + 3\nu)}{(1 - \nu)(2 - \pi) + (1 + \nu)} \quad (3-49)$$

This ratio of $\frac{\epsilon_x}{U/d}$ is relatively insensitive to Poisson's ratio, varying from 2.058 to 2.11 for values of Poisson's ratio of 0.3 and 0.5, respectively.

The test is carried out at a constant crosshead speed. Measurements of the force F_y and total diameter change \bar{U} are made (Figure 3-6 illustrates one convenient means for measuring \bar{U}) and the stress σ_x and strain ϵ_x at the center of the specimen are calculated for the time at which failure by cracking near the center of the specimen is visually observed.

Biaxial Test Data and Discussion: Data for diametral compression tests of PBAA propellant conducted at -50°F , 100°F , and 130°F are shown in Figure 3-7. Failures at 0°F and lower were characterized by sharp vertical cracks appearing along the vertical axis of the specimens. Samples at 30°F and 70°F failed along lines at 45 degrees to the vertical axis (lines of maximum constant shear) and diametral rupture at 100°F and 130°F occurred along the vertical axis.

Strains were measured photographically at the center of the specimens and also calculated using Equation (3-49) and the total horizontal diameter growth. Strains calculated thus from total diametral deflection were identical within experimental error to the measured strains for all values up to rupture.

Failure stress values calculated for the center of the specimen using

$$\sigma_x(0, y) = \frac{2F}{\pi dt} \quad (3-50)$$

are shown in Figure 3-7 with a failure-stress curve obtained from uniaxial tests. It should be noted that excellent agreement between biaxial failure stresses and uniaxial maximum stresses was obtained even though biaxial stresses were calculated from infinitesimal strain theory. A few percent deviation only was found between uniaxial strain at maximum stress and biaxial strain at failure values.

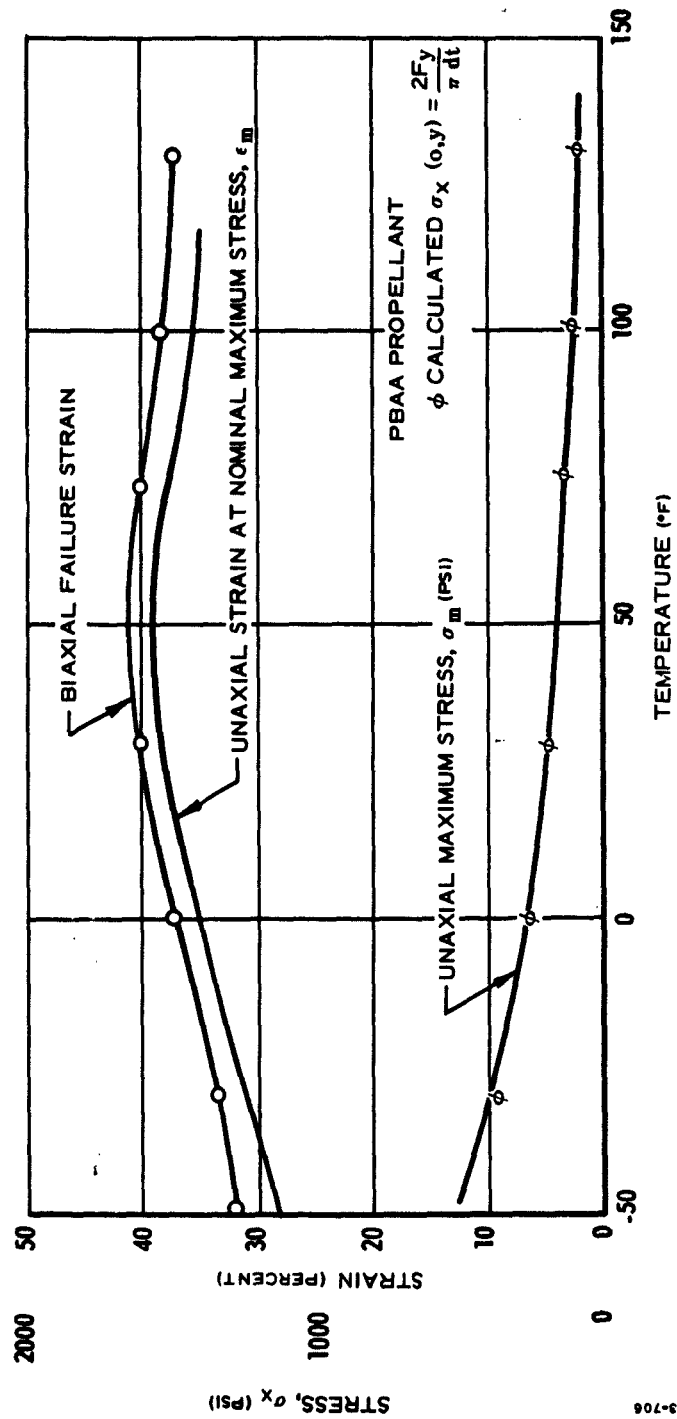


Figure 3-7 Comparison of Uniaxial and Biaxial Failure Stresses and Strains

3.8 ANALOG MOTOR TESTS¹

Analog motors (or strain evaluation cylinders) are circular port, case-bonded motors scaled to duplicate the strain-versus-temperature profile experienced in a flight motor of circular or star-port design. Analog motor sizes ranging from 2-inch diameter to 3-foot diameter have been used in simulation of strains in flight motors ranging from 5-inch to 120-inch diameters. Four- and seven-inch diameter analog sizes (Figure 3-8) have been used extensively at LPC for the following reasons. Four-inch diameter motors are the smallest size in which sufficiently accurate measurements of grain dimensions can be made. While most of the 4- and 7-inch analogs are cast in nonfireable sleeves, casting and ballistic test hardware are available for both sizes of motors. The availability of casting tooling decreases the cost of analog fabrication and the availability of firing tooling facilitates the simultaneous investigation of ballistic and structural behavior under controlled conditions.

Design of scaled circular port grains to simulate star-perforated motors proceeds from consideration of the thermal strain solution presented in Section 2.1. The pertinent equations are:

$$\epsilon_{\theta}^c = \frac{x_3}{1 + \lambda x_3 (1 + x_3)} \quad (3-51)$$

$$x_3 = [(\bar{\alpha}_p - \Delta T \frac{(1+\nu_c)}{1.5} \alpha_c) \lambda^2 - \bar{\alpha}_p] \frac{3}{2} \bar{P} \quad (3-52)$$

$$\epsilon_{\theta}^s = \epsilon_{\theta}^c K_i \quad (3-53)$$

where

ϵ_{θ}^c = hoop strain at port, circular port

$\bar{\alpha}_p$ = reduced thermal coefficient of grain propellant

ΔT = temperature increment below zero strain temperature (Section 2.1)

ν_c = case Poisson's ratio

α_c = case thermal expansion coefficient

λ = b/a = grain O. D. / I. D. ratio

\bar{P} = Parr end condition correction for finite length grains (Section 2.1)

K_i = star valley stress concentration factor (Section 2.1)

¹Analog test techniques are also discussed in detail in LPC-578-F-1, and in the ICRPG Solid Propellant Mechanical Behavior Manual, Section 4.8. Also see: Ignatowski, 1963.

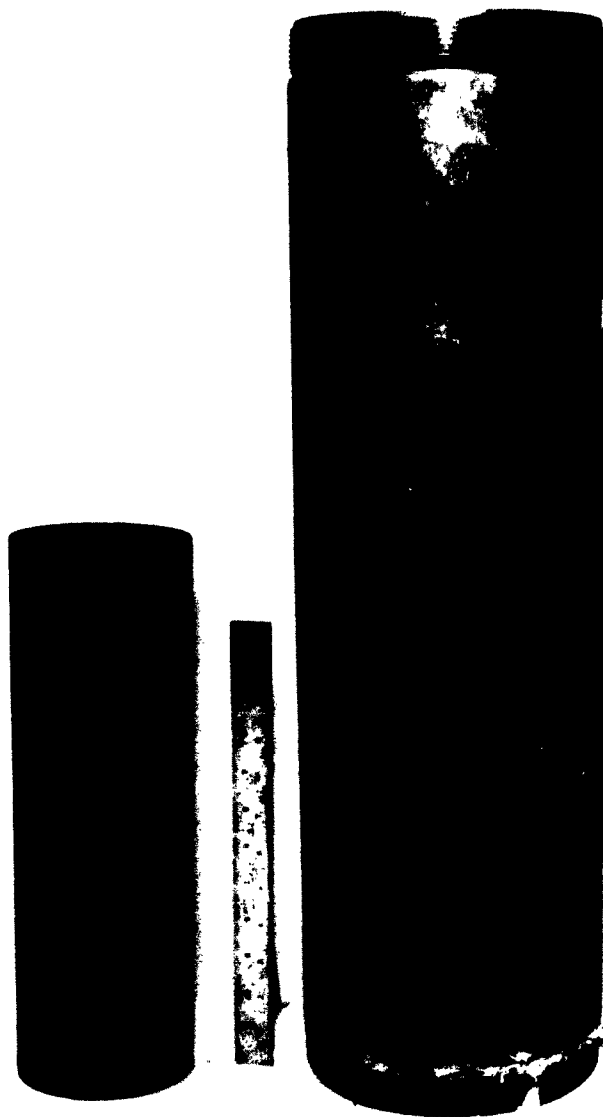


Figure 3-8 Four and Seven-Inch Diameter Analog Motors

A circular port grain scales linearly to analog sizes by keeping equal values of λ and length to diameter (equal \bar{P}). In scaling of star grains for circular port analog strain simulation, the values of \bar{P} and/or λ for the circular port analog grain are increased to compensate for the K_1 term for the star grain. \bar{P} increases with grain length to diameter ratio and decreases with increasing λ ; hence, some juggling of these values is necessary to arrive at the dimensional requirements for the analog design. Generally, it is convenient to take the available lengths of analog motor and scale λ appropriately to obtain the required strain simulation.

Parenthetically, it should be noted that analog scaling, keeping \bar{P} for the analog equal to \bar{P} of the simulated motor, is rigorously more desirable since the biaxial stresses in the analog will more closely simulate those of the simulated motor. With the exception of motors having $\bar{P} \geq 0.99$, the stress biaxiality does not appear to be particularly significant. When \bar{P} for a motor is equal to or in excess of 0.99, scaling of the analog simulation motor to maintain \bar{P} of the analog equal to or in excess of 0.99 is advisable.

Analog motors are conventionally tested by controlled thermal cycling, introducing heat flow only through the case wall and maintaining the grain under desiccated conditions. A typical experimental arrangement is shown in Figure 3-9. When simulation of behavior of the large motor conditions is desired, the analog cooling (heating) rates are controlled such that the strain-time variation at the port of the analog reproduces that observed for the large motor. The resulting low temperature cracking observations in the analog will generally prove to be slightly conservative (on the high side) with respect to the full-scale motor.

When analog motors are used as vehicles for supplemental laboratory characterization of propellants per se, shock cycling, extended storage at low temperature, etc., may be used and the data correlated through strain rate and temperature correlation where the rate and temperature of the port (at the midpoint of the grain) are the parameters of interest.

In tests of the analog motors, the usual observations are the grain port diameter at the grain midpoint (Figure 3-10) visual inspection of the grain, and temperature measurements. The strain at the grain midpoint is that predicted by Equations 3-51 and 3-52 and is given experimentally by

$$\epsilon_{\theta}^c = \frac{\Delta d}{d_1} \quad (3-54)$$

where d_1 is the port diameter at the zero strain temperature (or the mandrel O.D.) and Δd is the change in port diameter with respect to that temperature. Visual inspection of analog grains with the unassisted eye is inadvisable since the incipient fissuring of grains that usually precedes crack propagation is quite difficult to see. Borescope observation is usually a necessity (Figure 3-11). Thermocouple grain and case temperature measurement then completes the required set of experimental data necessary for correlation of rate and temperature behavior of the analogs.

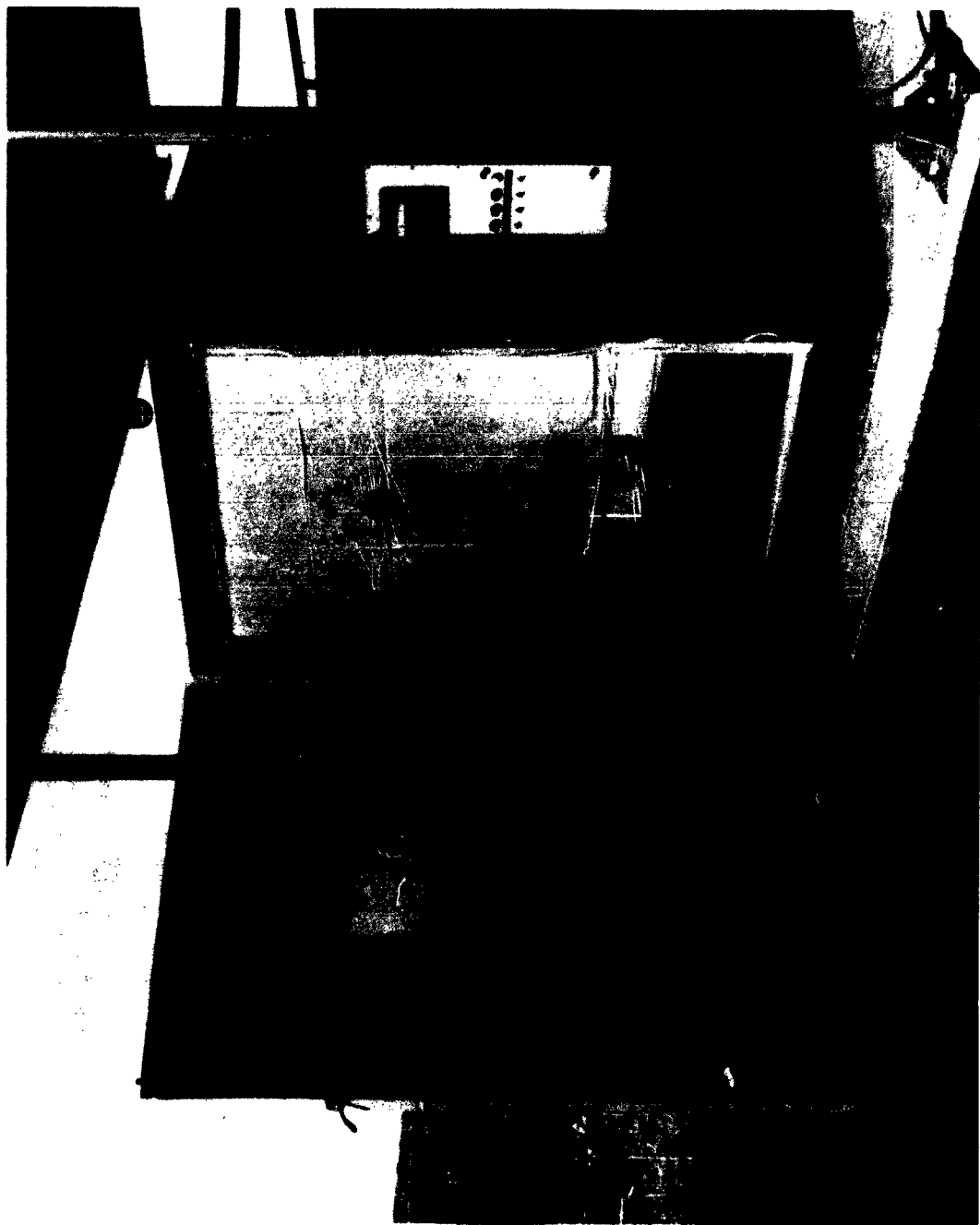


Figure 3-9 Analog Motor Experimental Set-Up



Figure 3-10 Port Measurement of Analog Motor Grains



Figure 3-11 Borecope Inspection of Analog Motor Grains

It should be noted that the zero strain temperature T_1 appears to be influenced somewhat by analog size, particularly for analogs smaller than 4 by 14 inches cast with rubber-base propellants. A method for independent determination of T_1 is discussed in LPC 556-F-1.

In summary, analog testing can be regarded as second only to full-scale evaluations. Examples of the results of analog motor tests are discussed in LPC 578-F-1 of this report and by Jones, 1963.

Section 4

GRAIN STRUCTURAL ANALYSIS METHODS DISCUSSION, ALTERNATE METHODS, AND LIMIT DESIGN CONSIDERATIONS

CONTENTS

	Page
4. GRAIN STRUCTURAL ANALYSIS METHODS DISCUSSION, ALTERNATE METHODS, AND LIMIT DESIGN CONSIDERATIONS	4-2
4.1 THERMAL STRAIN ANALYSIS	4-2
4.2 THERMAL STRAIN FAILURE ANALYSIS	4-4
4.3 GRAIN SLUMP DEFLECTIONS	4-6
4.4 GRAIN PRESSURIZATION	4-8
4.5 PRESSURIZATION FAILURE ANALYSIS.	4-9
4.6 STORAGE AND LAUNCH STRESSES	4-10
4.7 GRAIN TERMINATIONS.	4-11
4.8 STAR POINT DEFLECTION DURING HORIZONTAL STORAGE	4-15
4.8.1 Time Dependence of Slump Deflection	4-15

FIGURES

4-1	Grain Case Termination Cracking	4-12
4-2	Grain Termination Crack Depth versus Motor Diameter . .	4-13
4-3	Typical Case-Grain Termination Stress Reliefs.	4-14
4-4	Equivalent Cantilever Beam Approximation to Star Point. .	4-16
4-5	Wedge Star Point Geometry	4-16
4-6	Truncated Star Point Geometry.	4-17

Section 4

GRAIN STRUCTURAL ANALYSIS METHODS DISCUSSION, ALTERNATE METHODS, AND LIMIT DESIGN CONSIDERATIONS

Background discussion and additional information pertinent to the engineering methods described in Section 2 are presented. Limit design analysis techniques for storage and launch grain stresses, grain-case terminations and horizontal star point deflections are described in Sections 4.6, 4.7, and 4.8.

4.1 THERMAL STRAIN ANALYSIS

The thermal strain analysis solution given in Section 2.1 considers a case-bonded circular port grain under plane strain end constraint for a condition of thermal equilibrium. Using data developed by Parr (1962), the influence of finite grain length is accounted for. These data are reproduced in graphical form in Appendix D with the permission of the authors. Using the data of Fourney and Parmerter (1961), the perturbation of the strain field by geometrically regular star port perforations is accounted for. These data also are reproduced in Appendix D with the permission of the authors.

The equivalent iteration technique, which compensates for finite grain port deflection (Reference Note 2.11, Section 2.1), is an empirically developed operation that has been found to be within one percent agreement with precise computer iteration solutions at strain levels up to 25 percent. The neglect of thermally induced shear stresses near the grain-case boundary produces a trivial effect upon the predicted strains. The detailed analysis for the plane strain cylinder is included in Williams, et. al, 1961 (GALCIT SM 61-5); the treatments for end conditions and internal star geometry are presented in the previously referenced publications of Parr, Fourney and Parmerter. Additional details of the thermal strain analysis problem and experimental data are included in LPC 578-F-1 and LPC 556-F-1. Further discussion herein is limited to the key factors that require emphasis in engineering applications.

The given solution predicts the tensile hoop strain at the midpoint of a grain for a propellant of known coefficient of thermal expansion and zero strain temperature T_1 (Section 1.6). Grain hoop strain is ordinarily a maximum at this location and localizes web crack initiation there. Deviations from thermal equilibrium in the grain produce errors in strain prediction: upper and lower limits for the strains can be calculated in such instances by taking equilibrium strain-versus-temperature data for the upper and lower bounds of the grain temperature. The strain at thermal equilibrium at a given temperature will be the upper limit of strain at that temperature.

Referencing the strain calculations to the temperature T_1 is necessary in predicting grain failure, as discussed in Section 4.2. The typical values given for grain zero strain temperatures lead to reasonably accurate grain failure analysis. An experimental technique for independent measurement of T_1 is given in LPC 556-F-1. In the absence of other experimental information, determination of the temperature at which a grain I. D. is equal to the corresponding mandrel O. D. yields a reasonable estimate of the zero strain temperature. It may be observed that long term storage or cycling of a motor produces changes in the grain dimensions in addition to changes caused purely by thermal contraction effects. In general, changes in dimension that tend to reduce the grain port I. D. (as measured at a given temperature) are indicative of incipient failure in the grain, arising possibly from binder-filler dewetting. Increases in port I. D. are indicative of additional propellant cure or, at low temperature, binder crystallization. In the latter instances, the properties of the propellant are also subject to severe alteration and special methods are required in structural analysis of the grain. The zero strain temperature of the grain can be expected to change in these cases, invalidating the grain failure calculations to an unknown extent. In fully cured PBAA, Polysulfide and PBAN formulations such changes are usually of minor extent.

The analysis as given assumes a propellant Poisson's ratio of $1/2$, i. e., the usual assumption of rubber-like incompressibility. While a certain amount of controversy exists with regard to the assumption, the following summarizes pragmatic observations in this regard. Thermally induced grain strains have been accurately predicted in motor sizes ranging from four-inch to three-foot diameters at temperatures between 110° and $+200^{\circ}$ F in more than one hundred motors examined under conditions of rigorously controlled environment (LPC 556-F-1; LPC 578-F-1; Jones, 1963). The Poisson's ratio for the propellants, which ranged up to 86 percent solids loading by weight, was taken as $1/2$. Measured port strain levels ranged up to 25 percent. In all such cases examined, grain measurements indicating apparent values of Poisson's ratio of less than $1/2$ exhibited grain failure, in the majority of cases by web cracking. Strains in sound grains were predicted analytically to within a percent of strain. Hence, the assumption is considered to be accurate for the condition of interest and cannot, by itself, lead to other than conservatively high strain predictions.

The Parr end condition correction \bar{P} was developed using infinitesimal elastic theory and numerical data developed by computer calculation at Rohm and Haas Redstone. Within the assumption of infinitesimal deformations, previously unpublished experimental data at LPC have shown the values of \bar{P} to be exact within the limits of experimental accuracy.

The star valley stress (strain) concentration factor K_i data as developed by Fourney and Parmeter also considered only infinitesimal strain conditions. Generally, thermal cooling produces an increase in the radius of star valley curvature, tending to reduce the stress concentration factor. Values of K_i based on zero strain temperature grain (or mandrel) dimensions lead in any case to slight conservatism in that predicted strains will tend to be high. In

instances where the star valley geometries deviate from a circular arc, estimates of K_i using the data of Fourney and Parmarter are inaccurate. While bounding values may be estimated using minimum and maximum radii for the star valley geometry, it is usually necessary to obtain values for K_i by photo-elastic modeling of the actual grain cross-section. The techniques required in experimental measurement of K_i are specialized in nature; Fourney and Parmarter, 1961, present an up to date discussion of the techniques and pertinent source references.

4.2 THERMAL STRAIN FAILURE ANALYSIS

The method for grain failure prediction presented in Section 2.2 is an engineering approximation to a cumulative strain failure criterion proposed by Williams, et. al, 1961 (GALCIT SM 61-5) and discussed by Jones, 1963. For the particular condition of interest, monotonic cooling to failure, cumulative strain failure calculations agree with the method shown. In spite of the fact that thermal gradient conditions and attendant port hoop strain rates are treated in apparently cavalier fashion, the technique works quite accurately, (LPC 578-F-1; Jones, 1963). The dominating factor in determining low temperature grain cracking is the rapid decrease in propellant strain capability at low temperatures. At temperatures near the glass transition region (approximately -120°F in the example shown in Section 2.1 and 2.2), the properties of the propellant vary about equally for a ten-degree change in temperature or a one order-of-magnitude change in strain rate; hence, the relative unconcern with precision in specifying strain rates in this region. In consideration of the effects of thermal gradients it should be noted that in cooling to a given temperature, the thermal gradient disappears as that temperature is approached. Because of the greater sensitivity of the propellant properties to temperature than to strain rate in the low temperature regime, the final stages of cooling are of greatest significance in determining failure. The physical conditions in a grain approaching thermal equilibrium near its cracking limit dictate a convergence toward the assumed conditions of thermal equilibrium and, thus, a convergence in the accuracy of failure prediction. Errors introduced from this cause tend to lead to prediction of conservatively high grain cracking temperatures. In short, the procedure leads to prediction of minimum safety factors for the worst condition of thermal cooling ordinarily imposed on a motor.

Where more complicated conditions of cooling require analysis, the procedure is as follows. Starting from the zero-time zero strain condition, the temperature, strain and strain rate at the port of a grain are calculated incrementally. In a small temperature increment, the ratio of the incremental strain to the strain capability in the temperature increment and at the mean strain rate is calculated and taken to be the fractional use of the strain capability of the propellant. For conditions of monotonic cooling, then, failure is predicted when the sum of the fractional usage of strain with an increasing

number of temperature increments reaches the value unity. This technique requires considerable precision in all phases of the analysis and is presently regarded to be a matter of concern for specialists in grain analysis.

Comment is required on the correlation of propellant uniaxial failure properties to prediction of motor failure under the multiaxial strain field existing at the port of either circularly or star perforated grains. Laboratory multiaxial failure data suggests that propellant strain capabilities in strong triaxial tensile strain fields are much smaller than in uniaxial tension. Since the thermal strain field in a cooled grain tends to be triaxially tensile, it may be suspected that uniaxial data would predict erroneously low motor-cracking temperature. Noting that intensive research in this connection is currently in progress throughout the propellant industry, the present status of engineering knowledge in this connection is best summarized as follows.

Properly and precisely executed, the simplified engineering analyses presented in this handbook have been demonstrated to be either accurate within the accuracy limits stated or conservative in all instances where either model or flight motors have been cooled to failure at LPC during the past two years. The experience cited includes propellants based on PBAN, Polysulfide, PBAA, and terminally carboxylated binders in motors ranging in size from 4-inch to 120-inch diameters. Proper analysis of the laboratory physical property data is, of course, vital to the analysis (Reference Section 1 and 3).

Referencing the grain strain calculations to the zero strain temperature is essential because the total strain imposed on the propellant regulates the initiation of failure and is indeed the strain measured in the laboratory tensile test. Omission of the calculation step in which the subtractive term $\bar{\alpha}_p$ is neglected (Reference Table 2-1 and Note 2.16), is also essential in correlating failure strains in the grain to the corresponding strains as measured in the laboratory.

4.3 GRAIN SLUMP DEFLECTIONS

The solutions for slump deflections in circular port grains subjected to axial accelerations given in Section 2.3 were extracted from Parr, 1963, with the author's permission. The numerical methods used by Parr in obtaining the dimensionless form of the pertinent solutions are discussed in the above referenced report and in Parr, 1962.

In each of the cases considered by Parr, an elastic solution was obtained relating a deflection U to the imposed acceleration ng , the density of the propellant ρ , the radial dimension of the case b , the propellant (elastic) modulus E , and a numerical constant \bar{P} which is dependent on the grain web fraction, constraint, and length to outside diameter ratio:

$$U = \bar{P} \frac{b^2 \rho n \cdot g}{E}.$$

The motor case was considered to be rigid in all instances. The viscoelastic solution for the time dependent deflection $U(t)$ is obtained, in terms of the differential operator notation (Section 3.1) as

$$U(t) = \frac{P}{Q} [\bar{P} b^2 \rho] n \cdot g(t)$$

where P and Q are linear differential operators and the notation $n \cdot g(t)$ indicates the time dependence of the applied axial acceleration. Rigorously, the solution for a step function acceleration

$$n \cdot g(t) = n \cdot g \quad U(t), \quad \begin{cases} n \cdot g(t) = 0, & t \leq 0 \\ n \cdot g(t) = n \cdot g, & t \geq 0 \end{cases}$$

is

$$U(t) = \bar{P} b^2 \rho n \cdot g \sum_{i=0}^n B_i e^{-\beta_i t},$$

where the notation (Section 3.1 and Appendix B) indicates the compliance form of the propellant viscoelastic stress-strain law. In approximating this solution for engineering calculations the nearly exact relationship between creep compliance $D(t)$ and relaxation modulus $E(t)$, in uniaxial tension,

$$E(t) = \frac{1}{D(t)}$$

was introduced. Hence,

$$U(t) = \dot{P} b^2 \rho n \cdot g D(t)$$

$$\approx \frac{\dot{P} b^2 \rho n \cdot g}{E(t)} ,$$

the latter form of the equation being the one on which the numerical solutions shown in Section 2.3 were based. The solutions thus are approximations that are estimated to be within tolerable engineering limits of accuracy, with respect to the viscoelastic assumptions. The accuracy of the elastic solutions of Parr, insofar as experimental data are available, is also within the limits of engineering accuracy (LPC 556-F-1, Fitzgerald, et. al, 1961).

4.4 GRAIN PRESSURIZATION

The limit solutions for grain pressurization strains were obtained from the Lamé solutions for stresses in a right circular cylinder (for example, see pp. 125-145, GALCIT SM 61-5). The limit solution for end-bonded grains is the plane strain analysis for a case-bonded grain as given in the cited reference for the condition where the modulus of the propellant grain is taken to be zero. The solution considers a radially expanding, longitudinally rigid motor case. In the limit solution given in Section 2.4, the propellant is assumed to be incompressible (i. e., Poisson's ratio is taken as 1/2) and for the case Poisson's ratio is taken as 0.3. The limit solution for the grain with unbonded ends proceeds with the assumptions as given above except that the grain longitudinal stress σ_z is specified as $\sigma_z = -p_i$, where p_i is the motor pressure. In both solutions only the strain at the port, the largest strain, is given.

The grain strains at the port in the cases considered increase from zero toward the limits given in Section 2.4 with a strain-time variation controlled by the viscoelastic properties of the grain and the time history of pressurization. Viscoelastic solutions for the strains are not usually pertinent for moderate web fraction grains in metal cases since the limit solutions show trivial limiting values for the strains. Instances where the pressurization limit strains exceed two or three percent present special analysis and design problems beyond the present scope of this handbook.

The effect of finite compressibility on the pressurization strains, by limit analysis, is given by

$$\epsilon''_{\theta p} = \epsilon'_{\theta p} + \frac{(\lambda^2 - 1)}{2} \frac{p_i}{K}$$

for the plane strain (ends bonded) condition where K is the propellant bulk modulus, p_i the internal pressure and λ the O. D. to I. D. ratio for the grain. Typical values for the contribution of finite grain compressibility to grain pressurization are 0.3 and 1.5 percent for 50 and 75 percent web fraction grains operating at 1000 psi internal pressure for a typical value of $K = 5 \times 10^5$ psi/in.³. Grain hoop strains from compressibility effects are lower for grains with unbonded ends.

In summary, grain pressurization strains in moderately designed, steel-case rocket motors are generally of minor importance, except very near the low temperature storage cracking limit of the grain. In this region and in the instances of high web fraction high pressure operation and/or low modulus casings, highly specialized analytical techniques are required in precise evaluation of grain capabilities.

4.5 PRESSURIZATION FAILURE ANALYSIS

The cumulative damage criterion applied in pressurization failure analysis has not as yet been adequately demonstrated for solid propellants. Hence, its adoption for this purpose is pragmatic in nature in that it is consistent with engineering practice and has not been contradicted by experimental motor firings at LPC. Research in cumulative damage processes is presently in progress at LPC.

Selection of the port hoop strain as the failure-producing phenomenon of direct interest is founded on both theoretical and experimental grounds. Viscoelastic analyses for hoop stresses in dynamically pressurized case-bonded propellant grains show that few if any modern propellants possess transient modulus values sufficiently large to permit the development of hoop tensile stress at the port except, possibly, when the grain temperature is so low that glassy behavior may be expected. In general, grain failure from thermally induced strains will be predicted at higher temperatures in such instances. The hoop stresses in a grain can be expected to be compressive in most instances and therefore cannot produce stress-determined tensile failure. The failure of propellants in a state of tensile strain and hydrostatic compression has been shown to be relatively independent of the superposed hydrostatic field, and in reasonable agreement with the tensile failure strains as measured by standard techniques (Kruse and Mahaffey, 1963).

4.6 STORAGE AND LAUNCH STRESSES

Shear stresses at the propellant-case interfacial area in vertically stored or axially accelerated grains have been a matter of concern, particularly in the vicinity of the top grain termination circumference. In general, the geometric conditions at the termination circumference preclude a precise analytic evaluation of stress conditions there, and it has been expedient to proceed in pragmatic consideration of the problem. Present design practice at LPC requires that the average shear stress $\tau_z(b)$ at the case be $\leq 1/6$ the tensile strength of the propellant, as compared in the appropriate viscoelastic time and temperature envelope. The stress $\tau_z(b)$ is defined as

$$\tau_z(b) = \frac{n \cdot g W}{A}$$

where

$n \cdot g$ = acceleration in gravities

W = total weight of the grain

A = bonded area of the grain

With reservations, the analysis is applied to grains independently of the geometry of the grain end, so long as a stress relief boot or flap terminates the grain at the motor case wall (Ref. Section 4-7). Only unpressurized motors are considered: in pressurized motors the bond stresses are subjected to a superposed compressive stress that compensates for the effects of the acceleration body forces except, possibly, in extremely high-acceleration motors.

The rationale for the design relationship assumes a 1 to 2 relationship between a shear stress and its uniaxial tensile equivalent and accounts for a stress concentration at the termination of 3. The relationship is considered to be conservative, and the fact that it is conservative has been borne out in a limited number of experiments. Research in this connection is presently in progress at LPC.

In illustration of the $\tau_z(b) \leq \sigma/6$ relationship in design evaluation, consider a 50 percent web fraction, 240-inch diameter circular port case-bonded grain with unsupported ends stored with its axis vertical. The shear stress $\tau_z(b)$ is, approximately, $3\frac{1}{2}$ psi and the equivalent tension 21 psi. The propellant-case bond constant load strength (see Section 1.5) required for conservative design for a storage temperature of 70°F would be 21 psi at the maximum anticipated storage time. Similarly, unpressurized and under a launch acceleration of 10 gravities for two minutes, the required minimum constant load bond strength would be 210 psi for two minutes.

This analysis is presented as a reasonable and conservative engineering estimate, not as a necessarily valid means for specifying grain structural safety factors.

4.7 GRAIN TERMINATIONS

One of the most common grain failures is the circumferential cracking that occurs at the grain-case termination location (Figure 4-1). Such cracks typically propagate along the propellant-case interfacial zone, slightly inside the propellant grain, and stop permanently at some distance from the ends of the grain. As applied to specification of the stresses at the termination circumference, elastic analysis predicts infinite stress at this location when a geometric discontinuity exists. The prevalence of the failures experienced when the grain-case termination does include a geometric discontinuity bears out the analysis in that they present prima facie evidence for the existence of high stresses there.

The observed behavior of the failures, i. e., the finite propagation depth, has been predicted for the case of interest in an unpublished analysis by J. E. Fitzgerald based on a published analysis of M. L. Williams. The analysis predicts that the depth of propagation along the interface should vary with motor diameter as indicated in Figure 4-2, which also shows measured crack depths. The specific influence of other motor geometric parameters, such as web fraction, irregular case-end geometry, and motor length-to-diameter ratio is uncertain. The cited information applies generally to motors of approximately 50 percent web fraction, length-to-diameter ratio 1 to 3, and of cylindrical design as indicated in Figure 4-1.

In the relative absence of precise stress and deformation field design information relative to the termination circumference, the obvious engineering approach of stress relief modification of the geometry has been found to be effective. Typical grain terminations modified for stress relief are shown in Figure 4-3. As applicable in the geometries, the stress relief flaps extend to approximately the depths from the ends of the grains where crack propagation would be expected to stop, based on the data of Figure 4-2.

The selection of materials for the flap of "boot" is governed by the necessity for:

- (a) Compliance equal to or greater than that of the propellant at all anticipated use temperatures.
- (b) Tensile strength and elongation greater than that of the propellant at all anticipated use temperatures.
- (c) Insulation capability consistent with the ballistic environment.

In general, most high-quality, silica-filled insulation rubbers are adequate for the purpose. It is vital that the bond of the boot to its usual insulation substrate and the insulation substrate-to-case bond both be strong and continuous.

The use of boot relief at the ends of motors, as shown in the lower examples of Figure 4-3, tends to minimize thermal strain requirements on moderate length grains (Reference Section 2.1, 4.1) and minimize bonding difficulties at the ends of grains of any length.

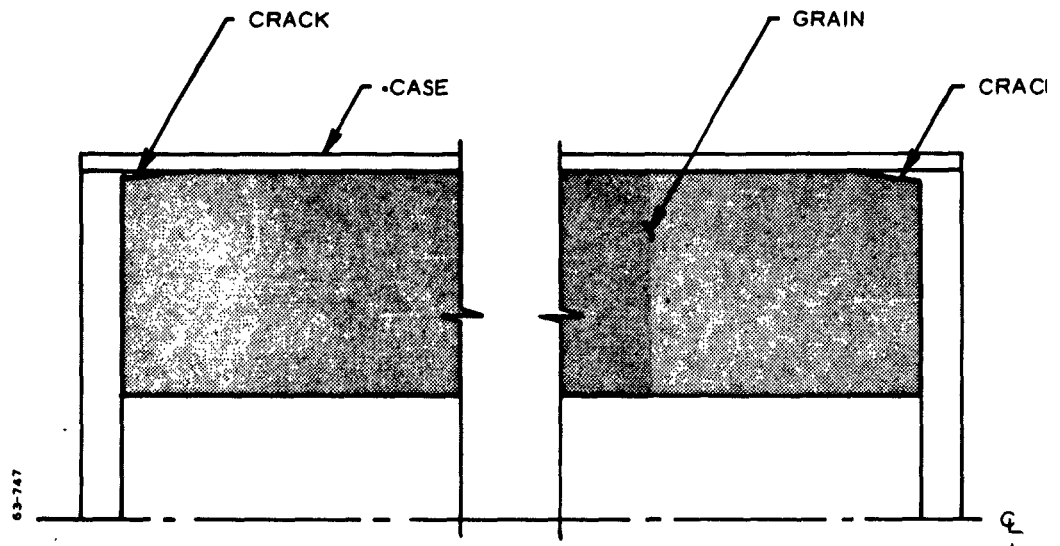


Figure 4-1 Grain Case Termination Cracking

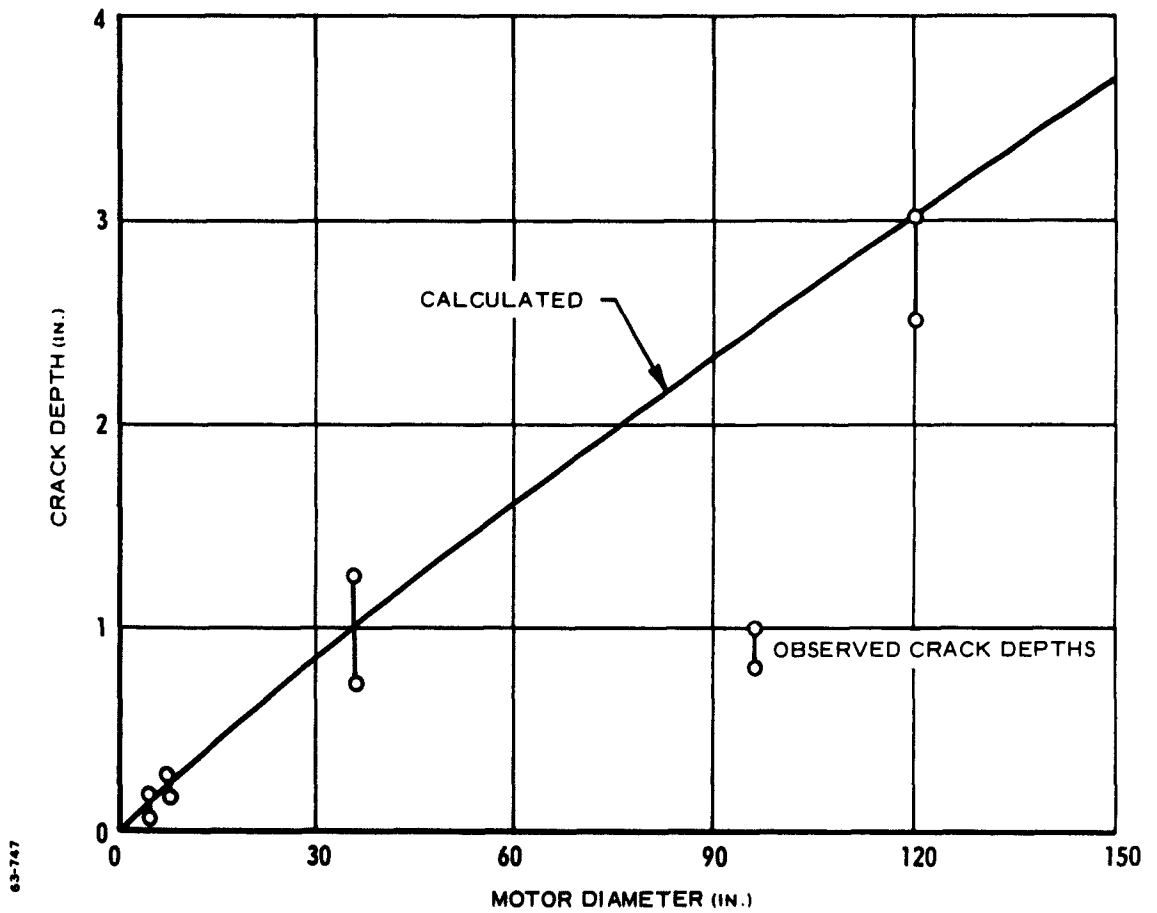


Figure 4-2 Grain Termination Crack Depth versus Motor Diameter

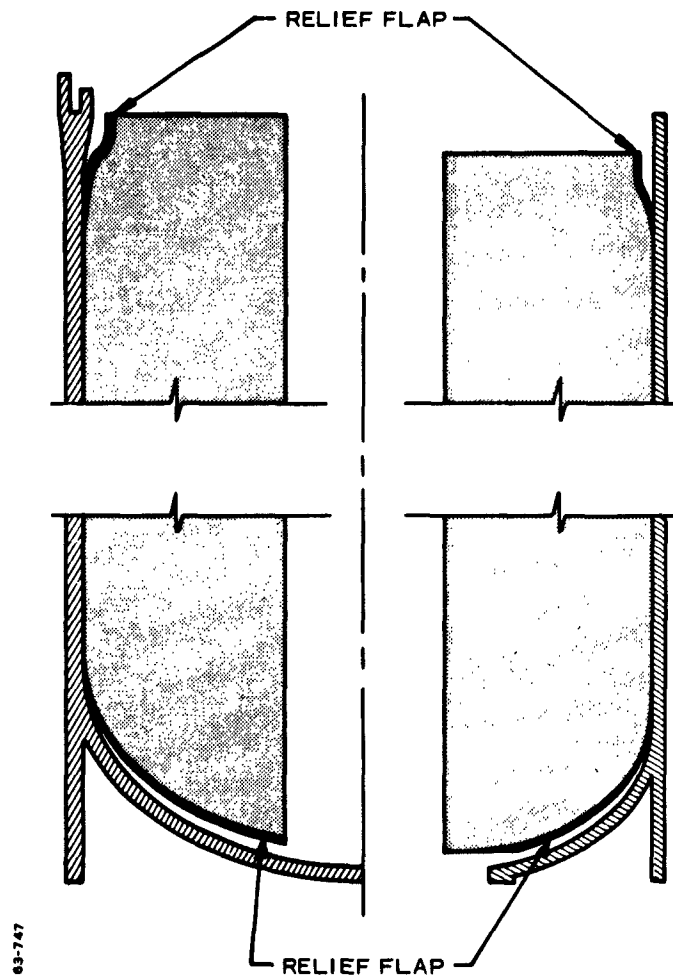


Figure 4-3 Typical Case-Grain Termination Stress Reliefs

4.8 STAR POINT DEFLECTION DURING HORIZONTAL STORAGE

The rigorous analysis for star point slump deflection requires, as a starting point, a solution within the theory of elasticity (Timoshenko and Goodier, 1951). However, under consideration of the appropriate field equations and boundary conditions, useful information can be obtained by employing simple beam analysis for an estimate (Timoshenko, 1956). Although a star point is not supported in a simple manner near the motor case it is expedient to assume that it deflects like a cantilever beam of nonuniform cross section which is supported rigidly at the wall (Figure 4-4). The star point may be approximated geometrically either by a truncated or nontruncated triangular section. If the star point cannot be represented reasonably by such a configuration, the following equations do not apply.

4.8.1 Deflection Expressions

The deflection Y at a star point tip in a motor in horizontal storage (Figure 4-5) can be written as

$$Y = Y_B + Y_S.$$

For the non-truncated triangular beam (Figure 4-5) one obtains for the elastic solution:

$$Y_B = \frac{3}{4} \frac{\rho}{E} \frac{L^4}{H^2}$$

$$Y_S = 1.13 \frac{\rho}{E} L^2$$

where:

ρ = Propellant density (lb/in.³)

E = Propellant modulus (psi)

L, H = As defined in Figure 4-5, in inches.

The star point is assumed to be long with respect to the dimension L .

If the star point is represented by a moderately truncated section (Figure 4-6), the appropriate expressions are, for $h_o/H < 0.1$:

$$Y_B \approx \frac{\rho L^2}{4E} \left\{ \left(\frac{L}{H} \right)^2 + 1.13 \frac{h_o}{H} \right\}$$

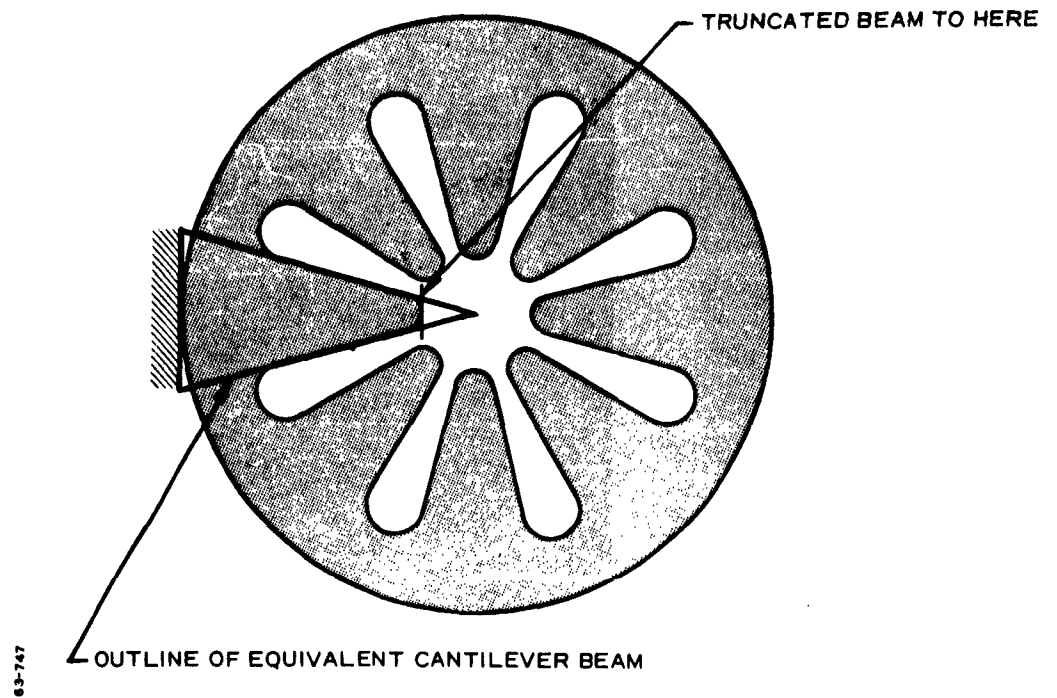


Figure 4-4 Equivalent Cantilever Beam Approximation to Star Point

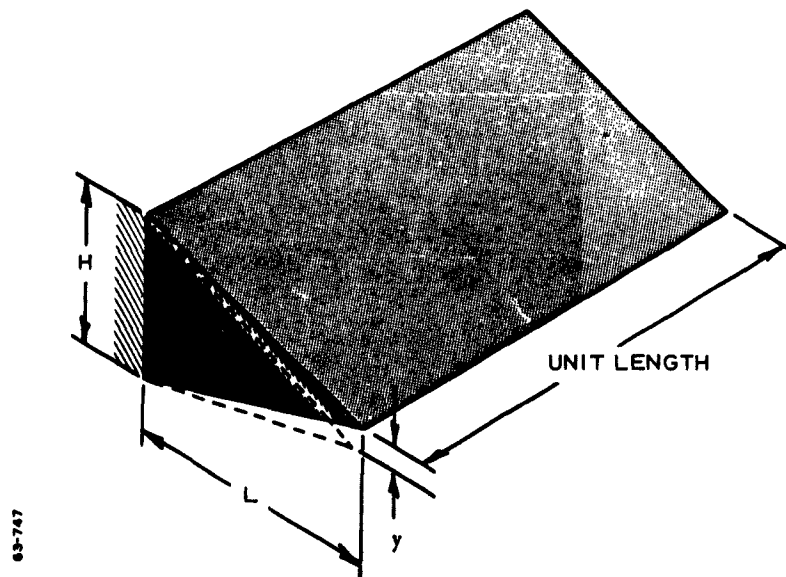


Figure 4-5 Wedge Star Point Geometry

63-747

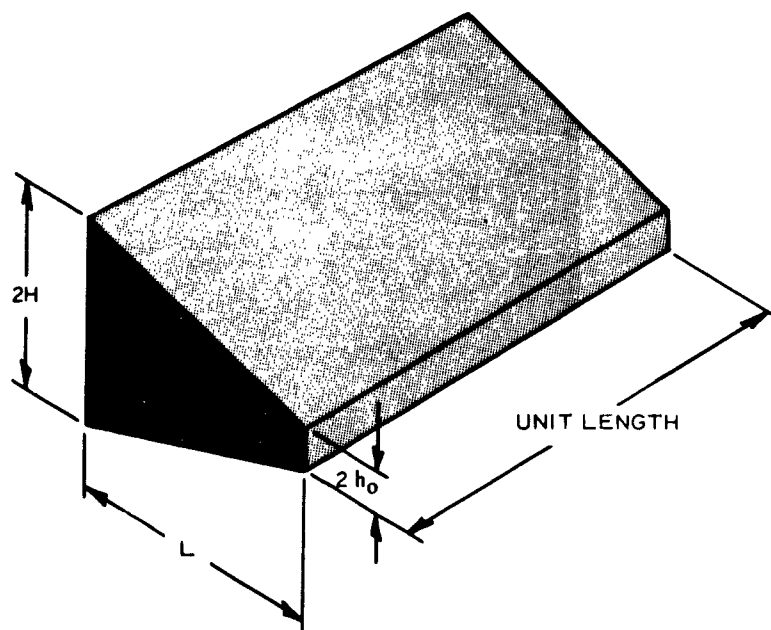


Figure 4-6 Truncated Star Point Geometry

$$Y_S \approx \frac{1.13\rho}{E} \left(\frac{L}{H} \right)^2 \left\{ 1 + 2 \frac{h_o}{H} \right\} .$$

where ρ and E are as defined above and the dimension L , H , and h_o are as shown in Figure 4- 6 .

4.8.2 Time Dependence of Slump Deflection

The time dependent forms of the preceding equation are obtained approximately by replacement of $E(\tau)$ for E , where the numerical values of $E(\tau)$ may be obtained for the appropriate temperatures from Figure 1- 7 , Section 1.1. The solutions given will generally tend to give conservatively large estimates of maximum star point tip deflections.

APPENDIX A

TEST SPECIMEN PREPARATION

CONTENTS

	<u>Page</u>
A-1 TEST SPECIMEN PREPARATION.	A-2
A-1.2 PROPELLANT CUTTING -- GENERAL	A-2
A-1.3 PROPELLANT MILLING -- GENERAL	A-5
A-1.4 PREPARATION OF JANAF TENSILE SPECIMENS	A-9
A-1.5 PREPARATION OF WOODEN TAB END TENSILE SPECIMENS	A-9
A-1.6 PREPARATION OF SPECIMENS FOR BIAXIAL TESTING.	A-15
A-1.7 TENSILE SPECIMEN STRAIN MEASUREMENT.	A-15
A-2 TEST SPECIMEN HANDLING AND STORAGE.	A-19

FIGURES

A-1 Vertical Band Saw Adapted for Remote Operation	A-3
A-2 Remote Control of Propellant Saw.	A-4
A-3 Milling Machine Modified for Propellant Machining	A-6
A-4 Propellant Fly Cutter	A-7
A-5 Propellant Specimens Being Machined in Manual Vise Mill Table Attachment.	A-8
A-6 Tab End Tensile Specimens Being Machined on Vacuum Vise Mill Table Attachment	A-10
A-7 JANAF Specimen Dimensions	A-11
A-8 Tab End Tensile Sample Box Cast with Propellant.	A-12
A-9 Tab End Tensile Specimen	A-13
A-10 JANAF Tab End Hybrid Tensile Specimen	A-14
A-11 Biaxial Test Specimen	A-16
A-12 LPC Plastic Extensometer	A-17
A-13 Typical Instron Test Record	A-18

Section A-1

TEST SPECIMEN PREPARATION

A-1.1 BACKGROUND

The essential purpose in laboratory testing of solid propellants is to determine the physical characteristics of the propellants as they exist in actual rocket motors. It is of critical importance, therefore, that the laboratory test specimens be cut, machined, and handled using techniques that do not degrade the bulk characteristics of the propellant. The practical problem is one of imposing the minimum clamping and handling stresses that permit the production of accurately dimensioned test specimens. A second problem, but not an unimportant one, is that of performing the necessary specimen preparation operations while maintaining a high degree of personnel protection against the possibility of fire or explosion. The following technique is representative of the recommended procedures for preparation of JANAF and bonded tab end tensile specimens.

A-1.2 PROPELLANT CUTTING--GENERAL

Bulk samples of propellant for reduction to test specimen form are customarily received in the form of cylindrical or rectangular blocks ranging in volume size between one quart and one gallon. Modified band saws are used for cutting the bulk samples to various section shapes slightly larger than the size of the desired final test specimen; final sizing and shaping of specimens are done by machining.

A typical saw (in use at LPC) is an industrial two-wheel, vertical band saw (Figure A-1) modified for use in propellant cutting as described below. The conventional electric motor was replaced with an explosion-proof motor; metal blade guides were changed to teflon, a vacuum scavenging port was installed for collection of small cuttings and oxidizer dust, and the existing sample vise was modified for gripping the various sample containers present in propellant sample cutting. Conventional skiptooth bandsaw blades with high-side, rake angle teeth are used in routine cutting.

In cutting propellant, it was found that vacuum scavenging was only partially effective, consequently manual cleanup of propellant fragments between saw cuts is a necessary safety precaution. The sawing procedure followed is one in which the actual saw cut is made using remote control from outside the sawing barricade to actuate the hydraulically operated table feed (Figure A-2).

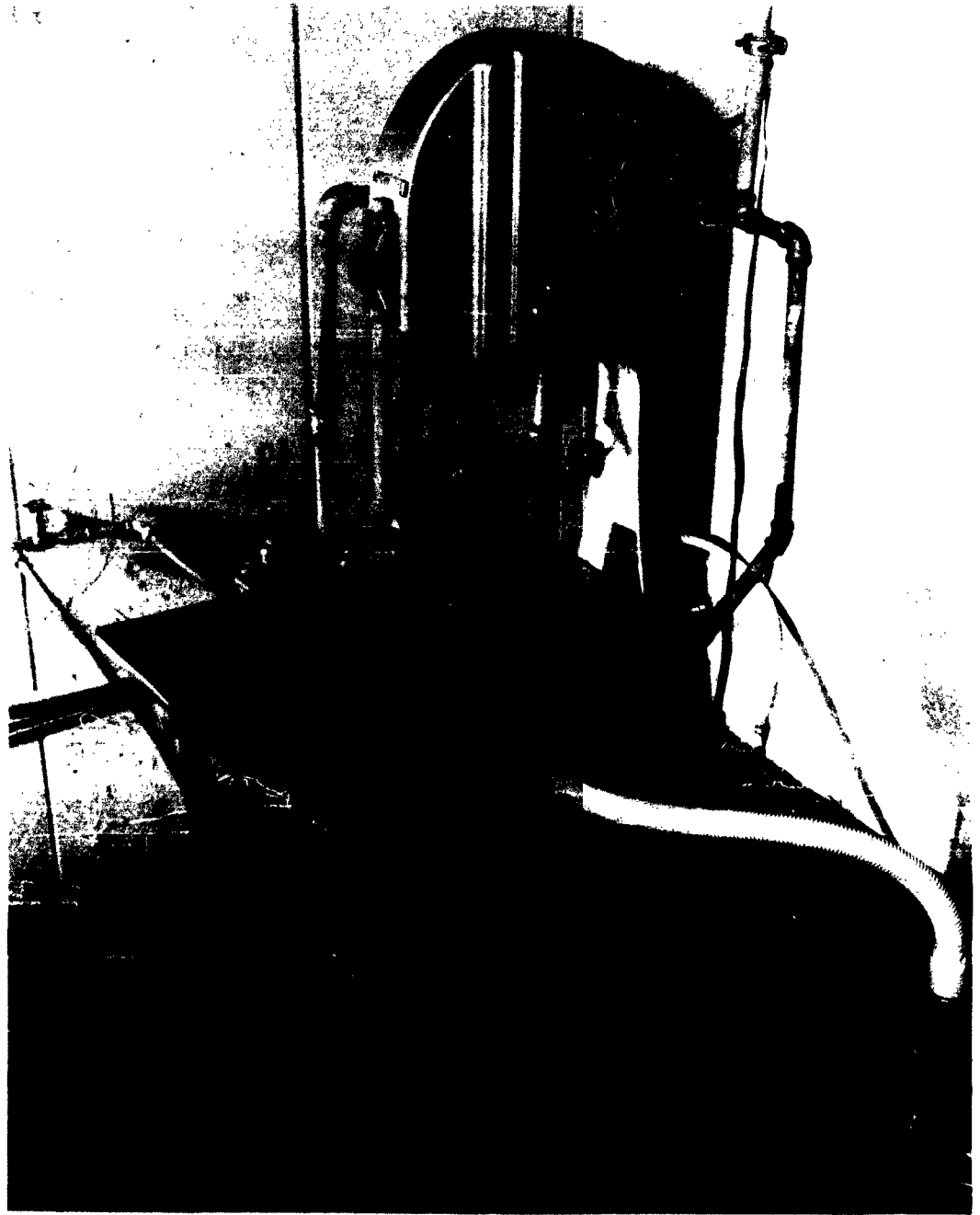


Figure A-1 Vertical Band Saw Adapted for Remote Operation

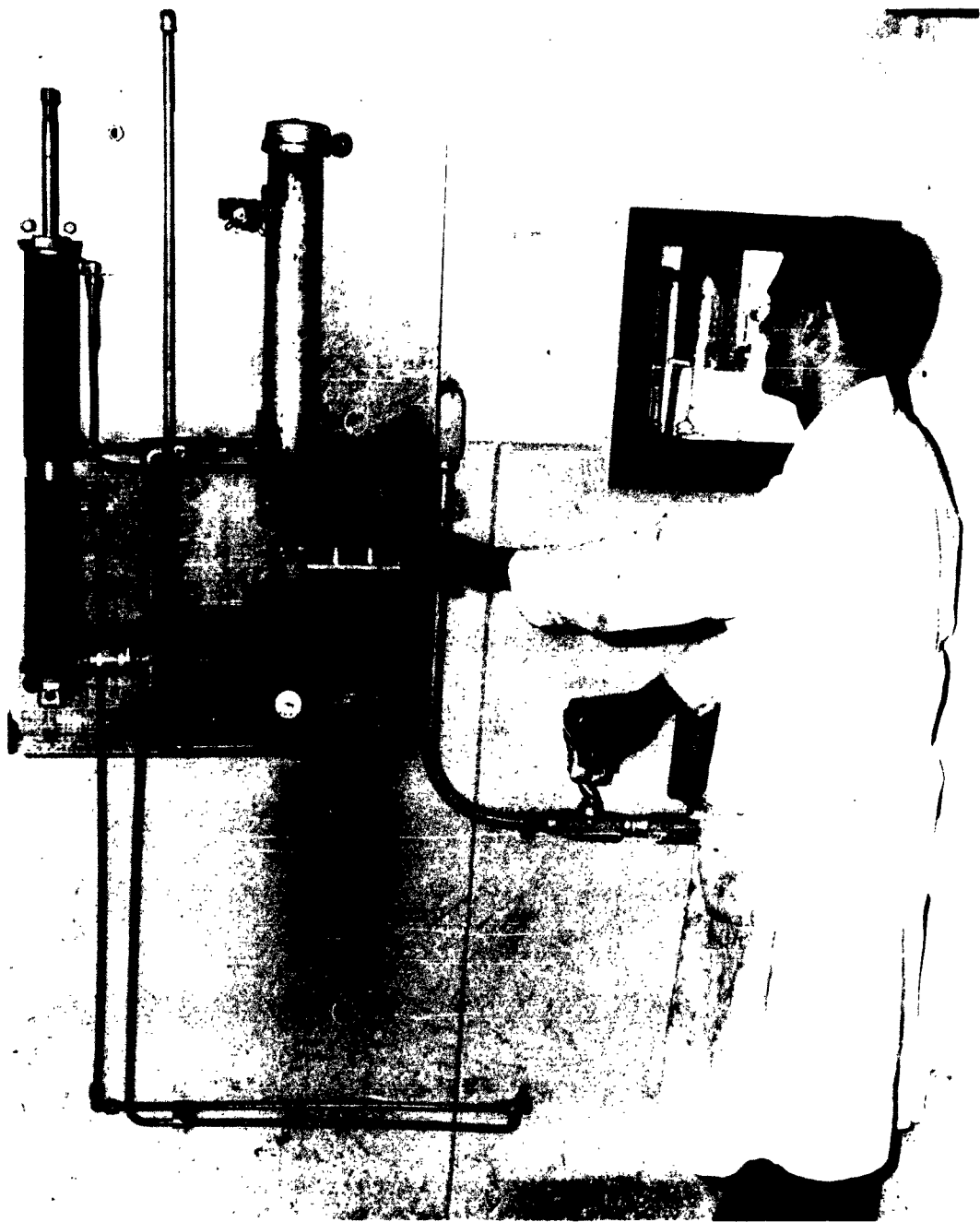


Figure A-2 Remote Control of Propellant Saw

Reduction of a bulk sample takes place by sawing and resawing until blocks, bars, slabs, etc., of the desired rough size are obtained. The modified vise on the saw permits the preparation of blocks and bars with cubic or rectangular dimensions between one-half and seven inches. The vise used in clamping samples for saw cutting is a conventional screw type vise, except for elimination of metal-to-metal contact.

The saw installation is set up with both automatic and manual water drowning provisions. Ordinarily, the saw operator can operate the manual valve faster than the fusible valves at the saw melt when a propellant fire starts. In either case, the water sprays minimize damage to the equipment when fires occur. The vacuum system uses only plastic hose conduit and has an intermediate drowning tank for collection of propellant dust at the saw.

A-1.3 PROPELLANT MILLING--GENERAL

Propellant samples rough cut by sawing are machined to final size using a modified milling machine (Figure A-3). The basic modifications to the commercial model machine are described herein. The standard electric motors for the cutting head and table feed drives are replaced with explosion-proof motors, and the belt drive mechanism in the head of the machine is covered and sealed. A sample holding fixture, complete with dust cover and cutting basket, is fixed to the mill table. Vacuum scavenging arrangements and water drowning heads are included in the installation. The operational features of the drowning system are identical to those of the saw operation previously described. In general, the methods employed with the mill are the same as those used in saw operation. All operations that must be done manually in the mill barricade are designed so that metal-to-metal frictional contact is eliminated in adjustment of the mill between passes and clamping of specimens on the mill table. Manual scavenging of propellant cuttings is necessary between cuts. Operation of the mill during the actual cutting operation is carried out by remote control.

The cutter heads used in all milling operations are of the circular fly cutter type (Figure A-4). These cutters are adjusted variously for cutting the re-entrant section on JANAF tensile specimens or for milling planar surfaces on slab or bar samples. The usual cutter speed used in propellant milling is approximately 900 rpm and the table feed rates are varied between one and ten inches per minute, depending on the milling characteristics of the propellant. The general philosophy applied is that the best specimens are produced by a combination of high cutter speeds and maximum feed rates.

The two basic cuts milled on propellant specimens are the planar surface cut and the re-entrant section cut on a JANAF tensile specimen. A simple, manually operated clamping device is used ordinarily for the shaping of the re-entrant section of the JANAF samples. Bar or slab samples for milling planar surfaces can be clamped by manual vises (Figure A-5); however, this technique has restrictions imposed by difficulties in maintaining tolerances during



Figure A-3 Milling Machine Modified for Propellant Machining

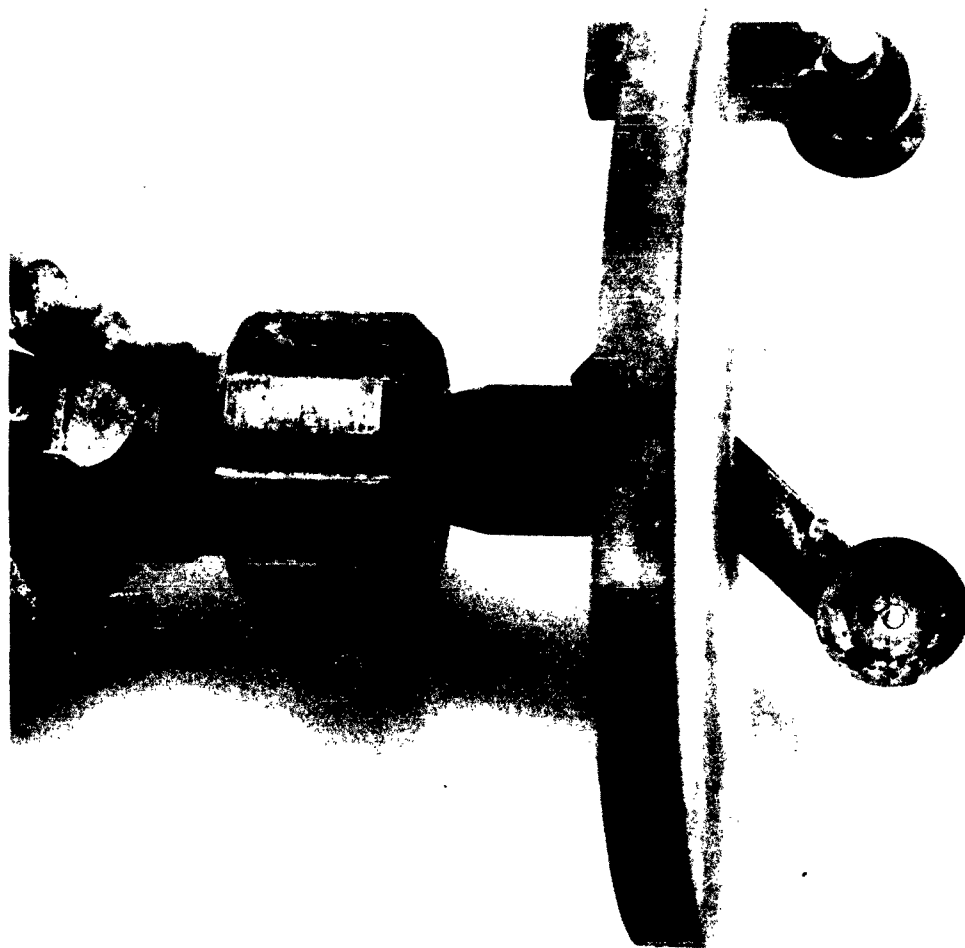


Figure A-4 Propellant Fly Cutter



Figure A-5 Propellant Specimens Being Machined in Manual
Vise Mill Table Attachment

milling, particularly when slabs or long bars are being processed. To overcome this difficulty, a vacuum gripping plate vise may be utilized. A vacuum plate vise in use for milling tab end specimens is shown in Figure A-6. A standard portable vacuum pump maintains satisfactory gripping of specimens.

A-1.4 PREPARATION OF JANAF TENSILE SPECIMENS

JANAF tensile specimens are prepared from rough cut blanks approximately five inches long by five-eighths-inch thick by one and one-eighth-inch wide. The specimens are processed in groups of five through the milling operation, maintaining in the final specimen the tolerances and dimensions shown in Figure A-7. The surface roughness of all milled specimens is considerably below one mil.

In the preparation of JANAF specimens, tolerances of 4 mils are maintained on the re-entrant section of the specimen.

A-1.5 PREPARATION OF WOODEN TAB END TENSILE SPECIMENS

Wooden tab-end specimens are prepared using case-bonding techniques in which the tab segments of the specimens are bonded to the propellant by casting uncured propellant against the treated wooden surface. The wood ends of the containers are cross cut into one-half by six-by-six inch slabs that are used to make box ends spaced five inches apart. Prior to casting propellant, the box is lined with a suitable bonding agent. In practice (PBAA, Polysulfide) the best bonding agent has proven to be the motor case liner material. After lining, the box is vacuum cast with propellant (Figure A-8).

Boxes with cured propellant are sawed into slabs of the desired size, retaining the wooden sides of the box as integral parts of the slabs. The sawed slabs are milled on both surfaces to the desired thickness and sawed into strips. The sawed surfaces of the strips finally are milled to obtain rectangular bars of square cross-section (0.375 or 0.500-inch square), maintaining tolerances of 2 mils. The specimen is illustrated in Figure A-9.

When marginal bonding is obtained, wooden tab-end specimens satisfactory for use in viscoelastic characterization may be prepared in the form of JANAF/tab-end hybrids as shown in Figure A-10. These specimens display a constant gage length behavior to a satisfactory accuracy, but require specialized techniques for machining.



Figure A-6 Tab End Tensile Specimens Being Machined on Vacuum
Vise Mill Table Attachment

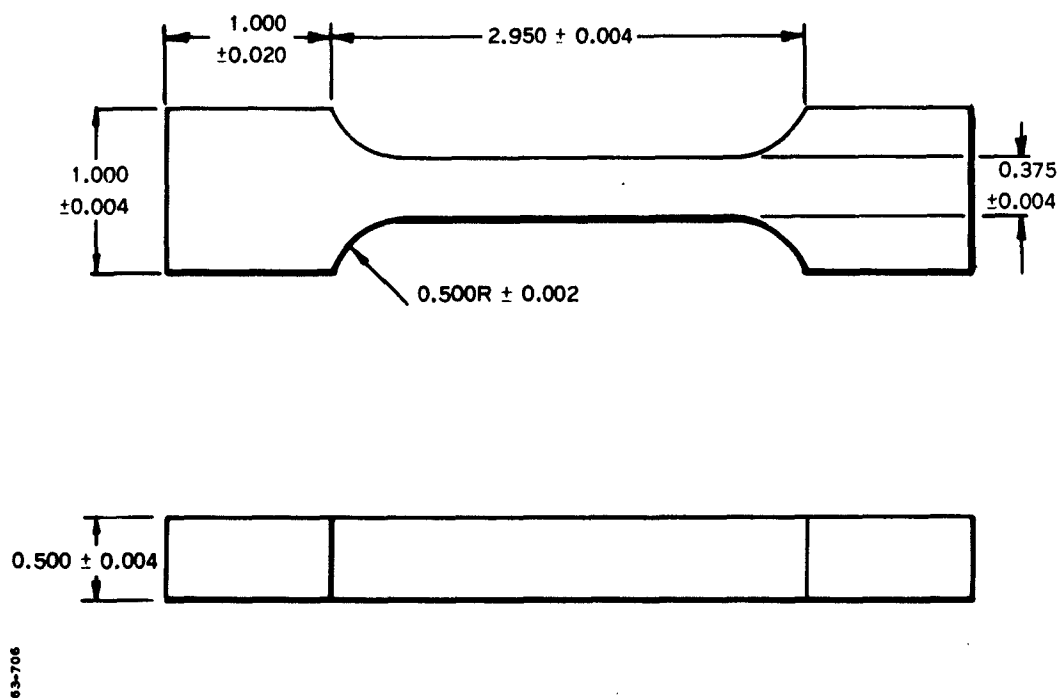


Figure A-7 JANAF Specimen Dimensions

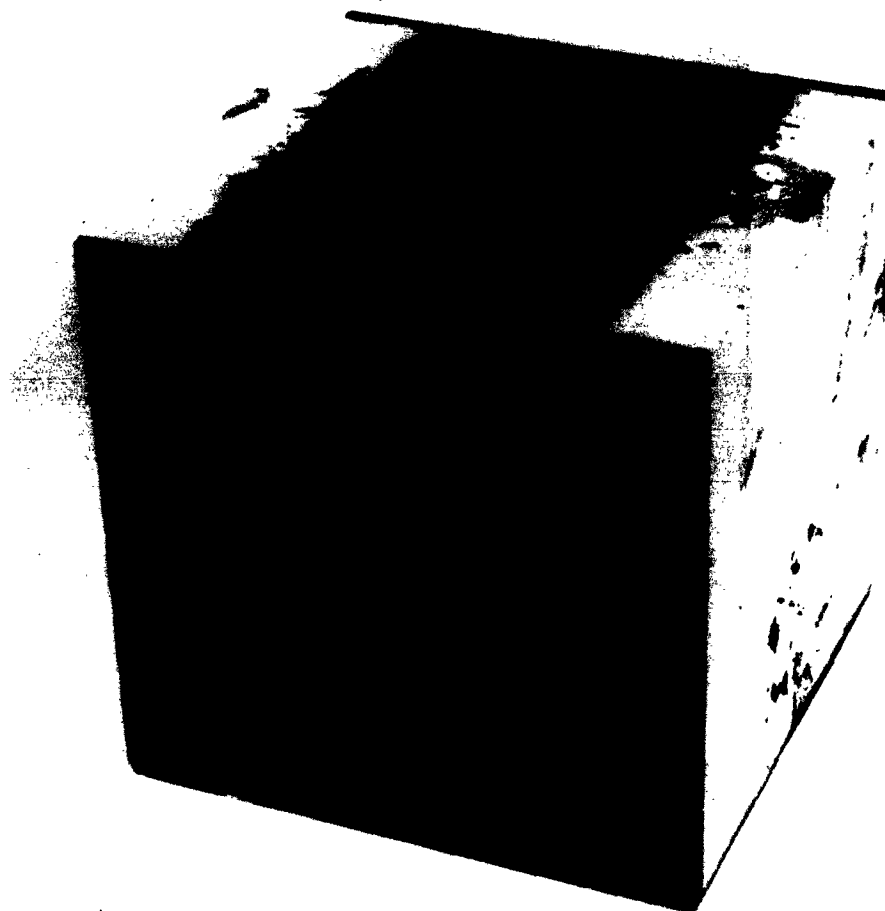


Figure A-8 Tab End Tensile Sample Box Cast with Propellant



Figure A-9 Tab End Tensile Specimen

63-706

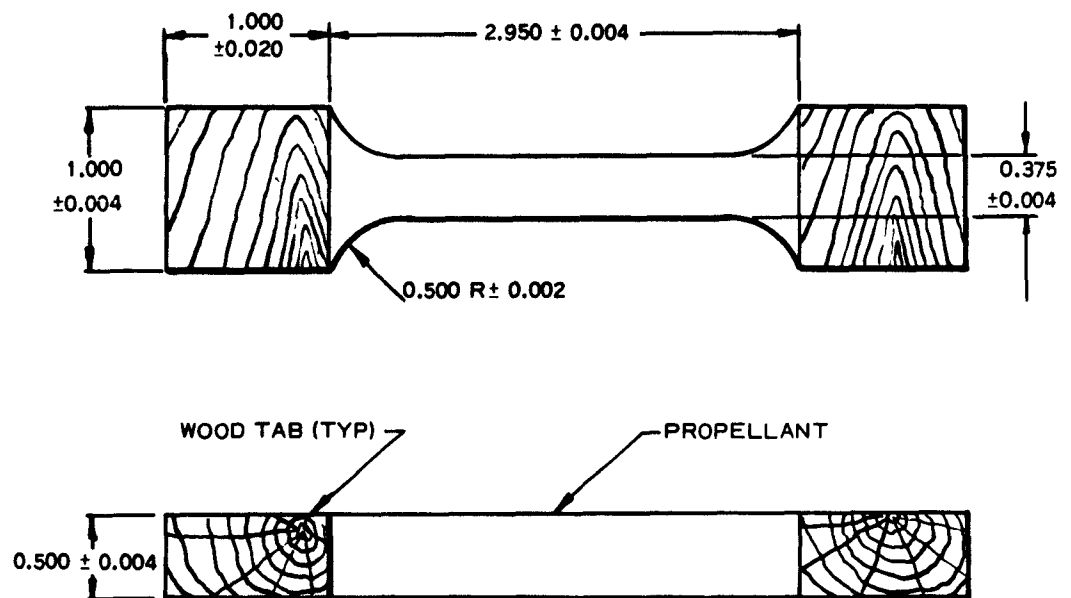


Figure A-10 JANAF Tab End Hybrid Tensile Specimen

A-1.6 PREPARATION OF SPECIMENS FOR BIAXIAL TESTING

Biaxial propellant specimens are prepared by casting long cylinders (in "Seal-rite" containers, for example) of propellant with the desired diameter, then cutting and milling to produce coplanar faces (Figure A-11.) Extremely toxic or expensive materials are cast directly into molds of the desired shape and tested after removal from the mold without further preparation.

A-1.7 TENSILE SPECIMEN STRAIN MEASUREMENT

Two methods of measuring the strain in JANAF specimens are now in use in the solid propellant industry. The first method consists of placing thin lines or bench marks on the central portion of a JANAF specimen and photographically recording their separation during tests. Data reduction for this process is expensive and time consuming. The method in use at LPC (LPC-556-F-1, 1963) utilizes a plastic extensometer fixed directly on the test specimen (Figure 1-8, Section 1). The plastic extensometer consists of a positive film transparency (Figure A-12), which is affixed to a specimen at Point A and in alignment with an indicial bench mark on the unstrained specimen (Point B). As the specimen is stretched, the increase in length can be measured by noting the passage of the specimen bench mark past the indicial marks C on the extensometer. When the spacing of the marks C are as shown (Figure A-12) and the length between the point of attachment of the gage and the specimen bench mark has increased successively to 1.025, 1.05, 1.075, 1.10, 1.15, etc., the corresponding strains will be 2-1/2, 5, 7-1/2, 10, 15, etc., percent. The strain readings are placed directly on the test record by use of the tester "Pip marker", reading the strains visually during the test. A typical test record is shown in Figure A-13. Strain values are then scaled directly from the test record during data reduction.

In practice, the gage is assembled to the propellant samples by cementing a 0.020-inch diameter metal wire to the plastic extensometer at point A, which is subsequently cemented to the propellant with a quick drying adhesive. To keep the free end of the extensometer from curling away from the propellant, a staple is placed loosely over the lower edge of plastic in the flow region of the propellant (Figure 1-8, Section 1).

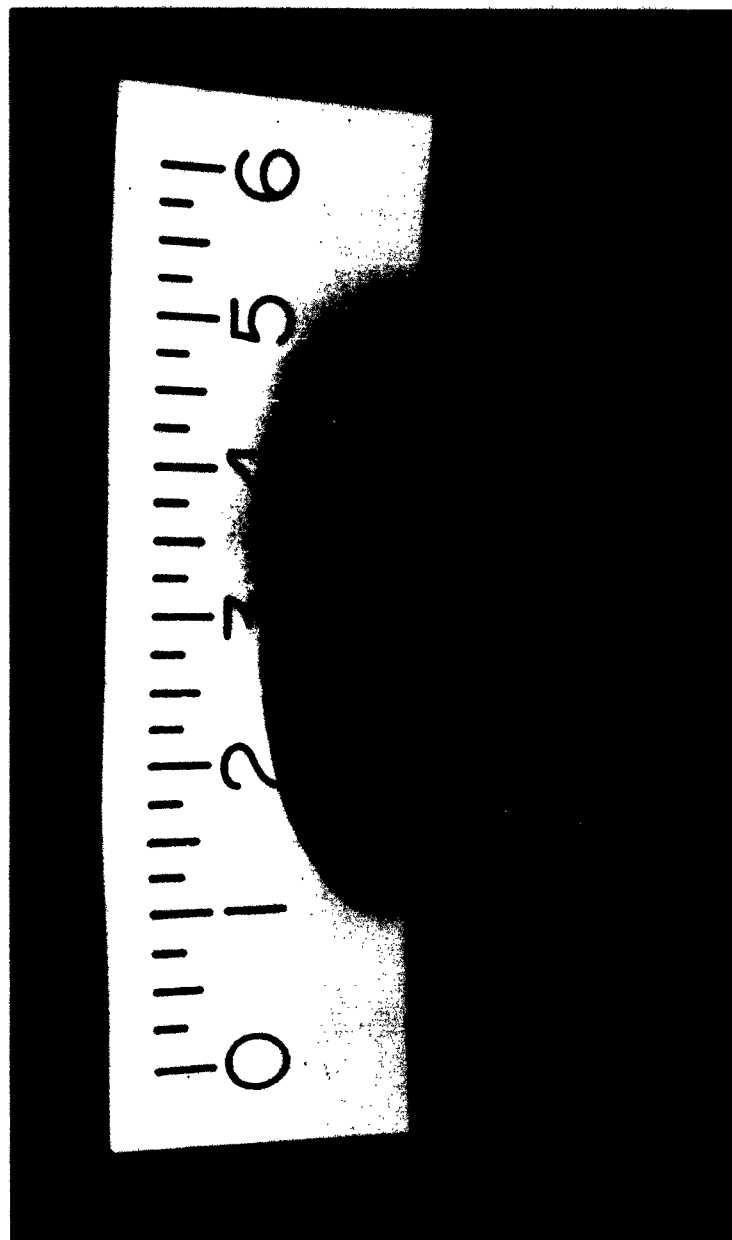


Figure A-11 Biaxial Test Specimen

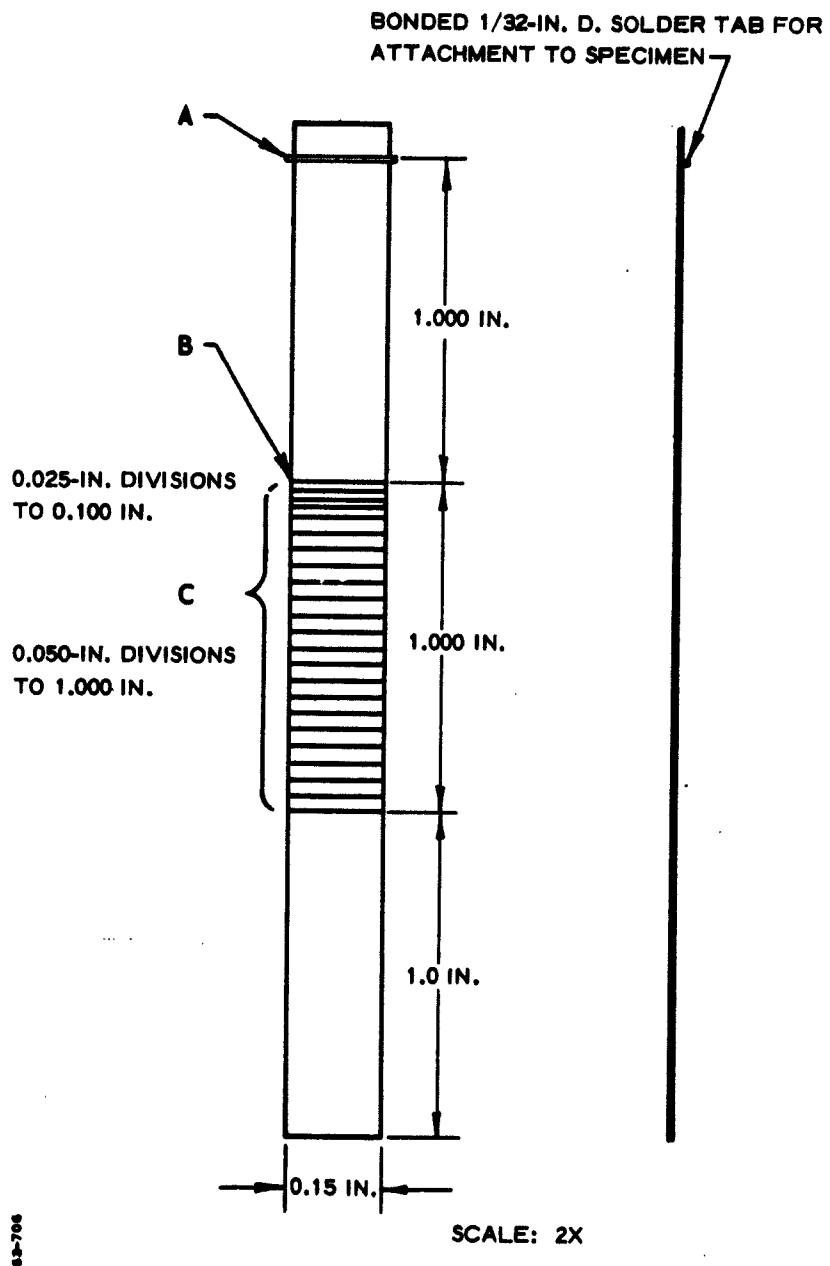


Figure A-12 LPC Plastic Extensometer



A-18

LOCKHEED PROPULSION CO

Section A-2

TEST SPECIMEN HANDLING AND STORAGE

Absorbed moisture is probably the single most important environmental contaminant that must be controlled during handling and storage. Recommended standard procedure in this connection is to store all samples and specimens in plastic bags with laboratory desiccant (e.g., silica gel or "Drierite") from the completion of cure until a specimen is fixed in the tested jaws. Exposure of propellant during propellant sawing and machining is minimized and preferably carried out in an air conditioned and humidity controlled environment (77°F, 50% R.H. or less).

During handling and storage, test specimens are packed flat on planar surfaces (e.g., stiff cardboard) to prevent specimen distortion. Any specimen subjected to accidental flexing should be discarded. Temporary sample or specimen storage is preferably done at moderate temperature (70°F ± 10°F), but is not a strict necessity.

Appendix C
UNIAXIAL TENSILE CREEP COMPLIANCE TEST

CONTENTS

	Page
C-1 Constant Stress Creep Test Apparatus	C-3
C-2 Constant Stress Creep Compliance Apparatus	C-4
C-3 Typical Creep Compliance Data	C-6

Appendix B

OPERATOR EQUATION - PRONY SERIES COEFFICIENTS¹

Standard notation has been adopted in this report for the differential operator equation and the associated Prony Series form. This notation and basic relations between coefficients of the equations are presented herein.

1.0 The basic operator equation is given by

$$P\sigma(t) = Q\epsilon(t) \quad (B-1)$$

where

$$P = \sum_{i=0}^n a_i \frac{\partial^i}{\partial t^i} \quad (B-2)$$

and

$$Q = \sum_{i=0}^n b_i \frac{\partial^i}{\partial t^i} \quad (B-3)$$

2.0 Defining P and Q in terms of the associated transform polynomials gives

$$\bar{P} = \sum_{i=0}^n a_i S^i = a_n \prod_{i=1}^n (S + \alpha_i) \quad (B-4)$$

$$\bar{Q} = \sum_{i=0}^n b_i S^i = b_n \prod_{i=1}^n (S + \beta_i) \quad (B-5)$$

3.0 As used in the text of this report, the partial fraction residuals contained in the Prony Series coefficients for equations of the form

$$\sigma(t) = C_0 + C_{00}t + \sum_{i=1}^n C_i e^{-\alpha_i t} \quad (B-6)$$

or

$$\epsilon(t) = D_0 + D_{00}t + \sum_{i=1}^n D_i e^{-\beta_i t} \quad (B-7)$$

¹ Reference: LPC 556-F-1.

are given by

$$\begin{aligned}
 A_o &= \frac{C_o}{K_1} = \frac{b_o}{a_o} \\
 A_{oo} &= \frac{C_{oo}}{K_2} = \frac{b_1}{a_o} - \frac{a_1 b_o}{a_o^2} \\
 A_i &= \frac{C_i}{K_i} = \frac{\left[\sum_{k=0}^n b_k S^k \right] [S + \alpha_i]}{S \prod_{k=1}^m (S + \alpha_k)} \quad \begin{aligned} S &= -\alpha_i \\ S &\neq 0 \end{aligned}
 \end{aligned} \tag{B-8}$$

or

$$\begin{aligned}
 B_o &= \frac{D_o}{K_4} = \frac{a_o}{b_o} \\
 B_{oo} &= \frac{D_{oo}}{K_5} = \frac{a_1}{b_o} - \frac{b_1 a_o}{b_o^2} \\
 B_i &= \frac{D_i}{K_i} = \frac{\left[\sum_{k=0}^n a_k S^k \right] [S + \beta_i]}{S \prod_{k=1}^n (S + \beta_k)} \quad \begin{aligned} S &= \beta_i \\ \beta_i &\neq 0 \end{aligned}
 \end{aligned} \tag{B-9}$$

where the K_i are arbitrary constants defined by the stress or strain input conditions.

It should be noted that the A residuals are normalized with $a_n = 1$ and the B residuals with $b_n = 1$. The coefficients with subscript "oo" are associated with constant rate stress or strain inputs only (LPC 556-F-1).

4.0 The relationships between the Prony Series coefficients α_i , A_i , or β_i , B_i and the operator coefficients a_i , b_i , are as follows. For strain determined functions, the coefficients α_i are obtained directly and the product

$$\prod_{i=1}^n (S + \alpha_i) \tag{B-10}$$

can be formed. The coefficients a_i of the resulting polynomial are, by definition, the coefficients of the P operator when $a_n = 1$. For stress determined functions, the coefficients β_i are obtained directly and the product

$$\prod_{i=1}^n (S + \beta_i) \quad (B-11)$$

yields the Q operator coefficients with $b_n = 1$.

In the usual case, it is necessary to obtain both the a_i and b_i operator coefficients from either a strain determined or stress determined Prony Series. For strain determined functions, the a_i are obtained from Equation B-10 above. The b_i are obtained as follows.

$$\begin{aligned} b_n &= A_0 + A_1 + A_2 + \cdots + A_n \\ b_{n-1} &= A_0 M_1^n + A_1 M_1^n (\alpha_1=0) + A_2 M_1^n (\alpha_2=0) + \cdots + A_n M_1^n (\alpha_n=0) \\ &\vdots \\ b_1 &= A_0 M_{n-1}^n + A_1 M_{n-1}^n (\alpha_1=0) + A_2 M_{n-1}^n (\alpha_2=0) + \cdots + A_n M_{n-1}^n (\alpha_n=0) \\ b_0 &= A_0 M_n^n \end{aligned} \quad (B-12)$$

where M_r^n is defined as the summation of all possible products of the n α_i coefficients taken r at a time. For example

$$\begin{aligned} b_{n-1} &= A_0 (\alpha_1 + \alpha_2 + \cdots + \alpha_n) + A_1 (\alpha_2 + \alpha_3 + \cdots + \alpha_n) + \\ &\quad A_2 (\alpha_1 + \alpha_3 + \cdots + \alpha_n) + \cdots + A_n (\alpha_1 + \alpha_2 + \cdots + \alpha_{n-1}) \end{aligned} \quad (B-13)$$

For stress determined functions, the b_i are found from Equation B-11 above. The a_i are obtained as follows

$$\begin{aligned} a_n &= B_0 + B_1 + B_2 + \cdots + B_n \\ a_{n-1} &= B_0 M_1^n + B_1 M_1^n (\beta_1=0) + B_2 M_1^n (\beta_2=0) + \cdots + B_n M_1^n (\beta_n=0) \\ &\vdots \\ b_1 &= B_0 M_{n-1}^n + B_1 M_{n-1}^n (\beta_1=0) + B_2 M_{n-1}^n (\beta_2=0) + \cdots + B_n M_{n-1}^n (\beta_n=0) \\ b_0 &= B_0 M_n^n \end{aligned} \quad (B-14)$$

APPENDIX B

OPERATOR EQUATION - PRONY SERIES COEFFICIENTS

Appendix C

UNIAXIAL TENSILE CREEP COMPLIANCE TEST

Scope: A method is described for laboratory measurement of the creep compliance $D(t)$ under constant stress loading using time-temperature reduced variable techniques.

Test Equipment: In general, standard laboratory equipment is adequate. A precision temperature controlled chamber is required with provision for control of humidity in the chamber. A typical experimental set-up is described in connection with description of the test procedure.

Test Specimen: Bonded tab-end tensile specimens as described in Appendix A.

Test Procedure: Creep compliance $D(t)$ under isothermal conditions is determined by observation of the strain versus time $\epsilon(t)$ under constant stress σ_0 loading:

$$D(t) = \frac{\epsilon(t)}{\sigma_0}.$$

Since the cross-sectional area of a tensile specimen decreases on extension, it is necessary to provide a means for continuous decrease of the applied load F on the specimen. This is accomplished, for example, by a compensating spring in series with the creep specimen (Figure C-1).

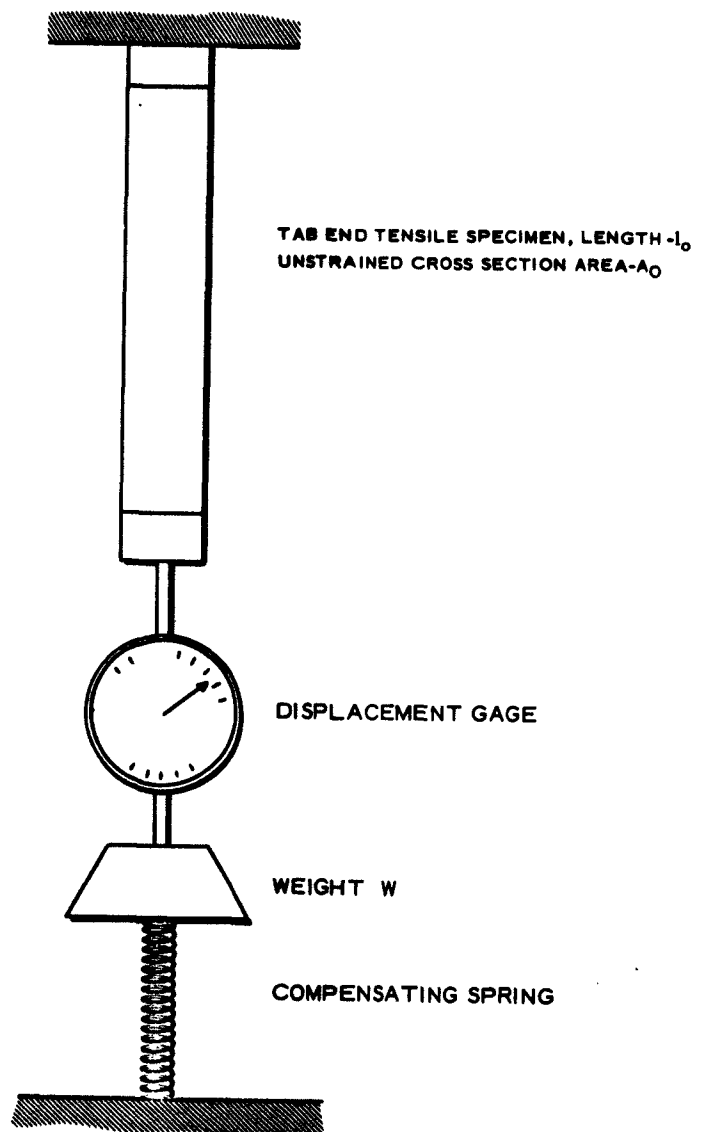
With reference to Figure C-1, a typical test set-up consists of a specimen connected in series through a dial displacement gage (with spring action removed) with a weight connected with an extended spring (Figure C-2). The test is initiated with the specimen under initial load, but with the spring extended to give an initial force F_2 acting on the weight. The spring is selected, in consideration with the weight W (W includes the weight of the connecting elements) to have a spring constant k determined by

$$k = \frac{W}{A_0 l_0} \quad (\text{lb/in.})$$

where

A_0 = unstrain cross-sectional area of the test specimen (in.^2)

l_0 = specimen gage length (in.)



63-706

Figure C-1 Constant Stress Creep Test Apparatus

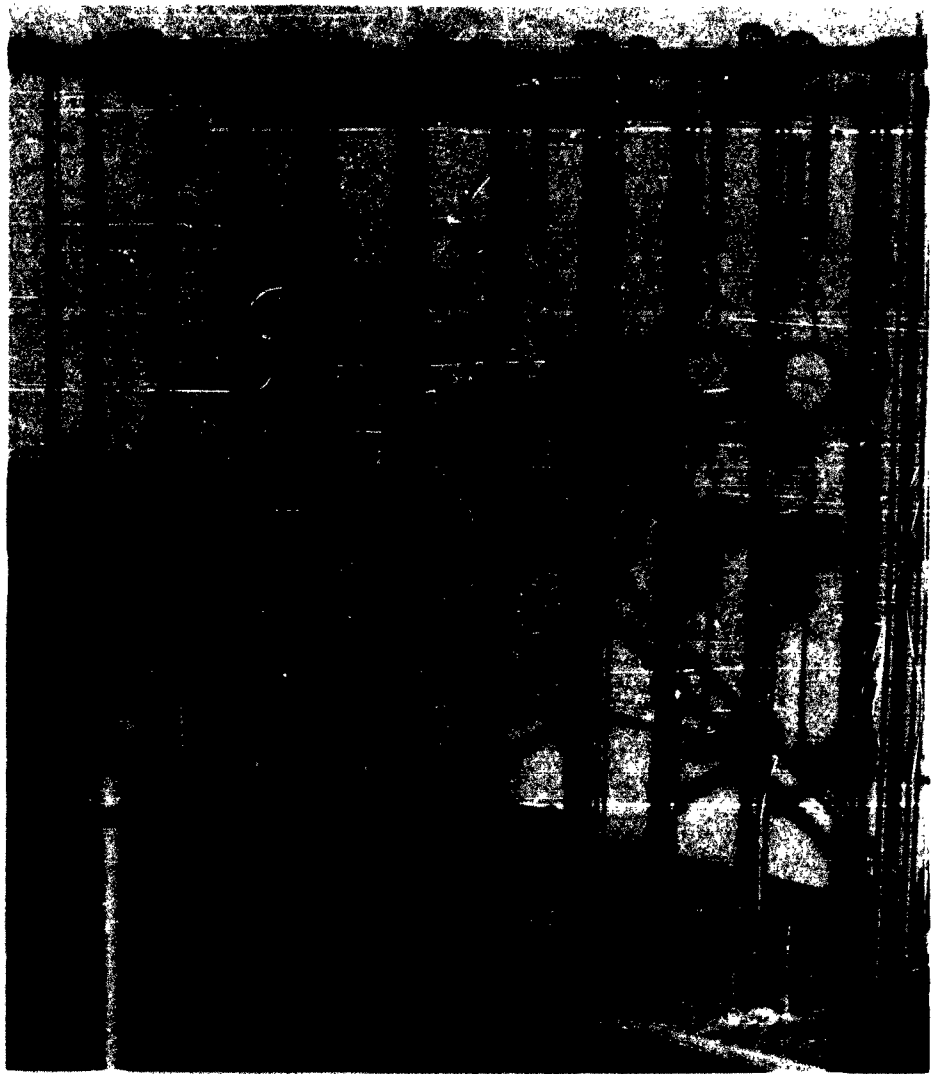


Figure C-2 Constant Stress Creep Compliance Apparatus

Upon release of the weight to act on the specimen, the stress σ_0 acting on the specimen will be

$$\sigma_0 = \frac{W}{A_0} + k \Delta l_s$$

where Δl_s is the initial spring extension. Defining strain in the specimen as

$$\epsilon(t) = \frac{\Delta l(t)}{l_0} \quad (\text{in./in.})$$

where $\Delta l(t)$ is the increase in specimen length with time as measured by the dial gage; the measured creep compliance is then given by

$$D(t) = \frac{\epsilon(t)}{\sigma_0}$$

The test can be initiated by either auxiliary automatic equipment or simply by gently releasing the weight by hand.

Data Reduction: The time necessary for the weight to be fully supported by the specimen, t_1 , is noted and the compliance $D(t)$ under constant temperature conditions is calculated for times in excess of $10 t_1$. Data for various temperatures may be obtained and reduced to master curve form by reduced variable techniques as illustrated in Sections 1.1 and 3.1. Typical creep compliance data at 70°F are illustrated in Figure C-3.

POLYCARBUTENE R PROPELLANT
WOODEN TAB END SAMPLES
TEMPERATURE: 70°F ± 2°F

$\sigma_0 = \bigcirc$ 5 PSI
 $\sigma_0 = \square$ 10 PSI
 $\sigma_0 = \triangle$ 20 PSI

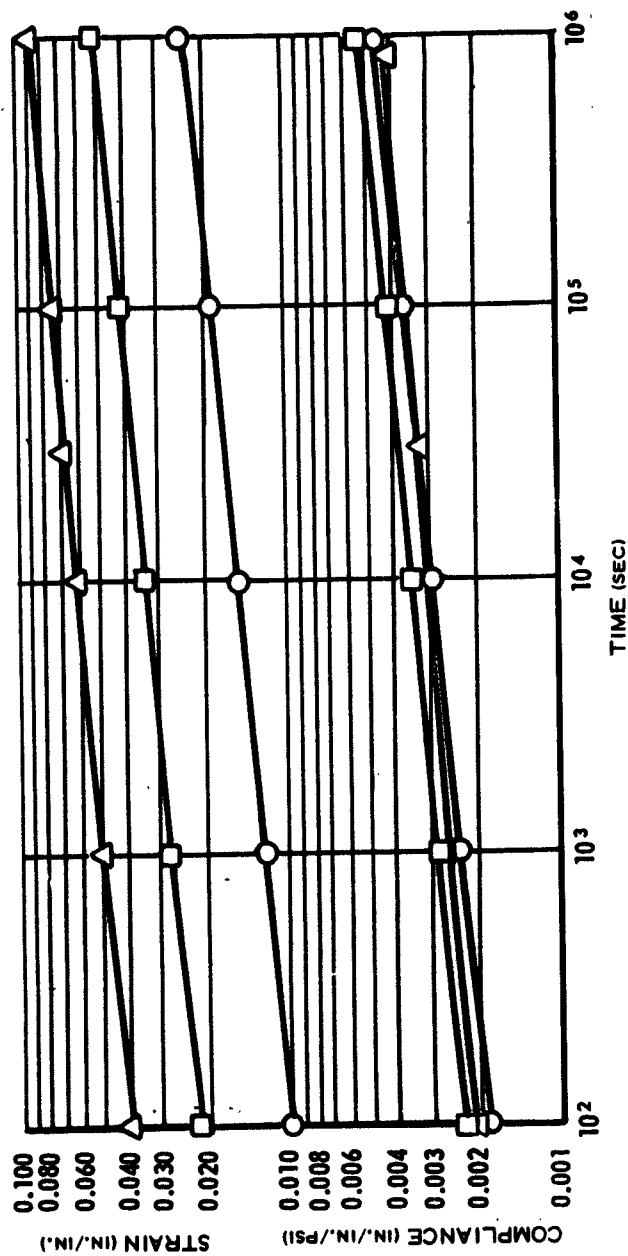


Figure C-3 Typical Creep Compliance Data

Appendix D

REFERENCE FIGURES FOR GRAIN STRAIN

FIGURES

		Page
D-1	Parr-End-Condition Correction Factor for Finite Length Grains, \bar{P} versus L/D	D-2
D-2	Parr End Condition Correction Factor for Finite Length Grains, \bar{P} versus λ	D-3
D-3	Nomenclature for Star Valley Stress Concentration Relationships, Figures D-4 through D-8.	D-4
D-4	Star Valley Stress Concentration Factor H for Three-Slotted Grains	D-5
D-5	Star Valley Stress Concentration Factor H for Four-Slotted Grains	D-6
D-6	Star Valley Stress Concentration Factor H for Five-Slotted Grains	D-7
D-7	Star Valley Stress Concentration Factor H for Six-Slotted Grains	D-8
D-8	Star Valley Stress Concentration Factor H for Eight-Slotted Grains	D-9
D-9	Nomenclature for Grain Slump Relationships, Figures D-10 through D-14	D-10
D-10	Dimensionless Axial Displacement U_{z1} of Free Corner of Free-Free Grain	D-11
D-11	Dimensionless Radial Displacement U_{r1} of Free Corner of Free-Free Grain	D-12
D-12	Dimensionless Axial Displacement U_{z2} of Free Corner of Fixed-Free Grain.	D-13
D-13	Dimensionless Radial Displacement U_{r2} of Free Corner of Fixed-Free Grain.	D-14
D-14	Dimensionless Radial Displacement U_{r2} Near Fixed End of Fixed-Free Grain	D-15

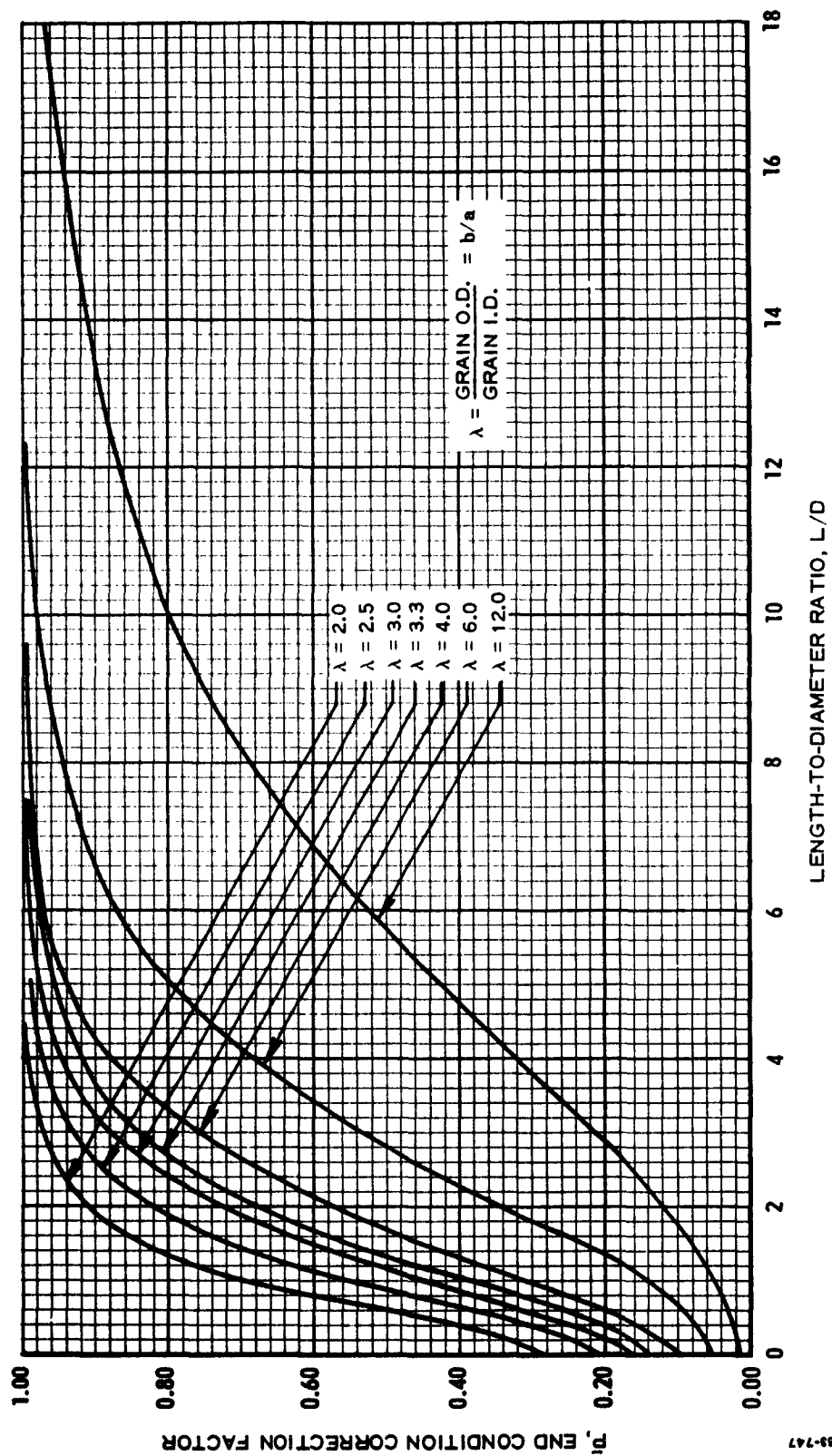


Figure D-1 Parr End Condition Correction Factor for Finite Length Grains, \bar{P} versus L/D

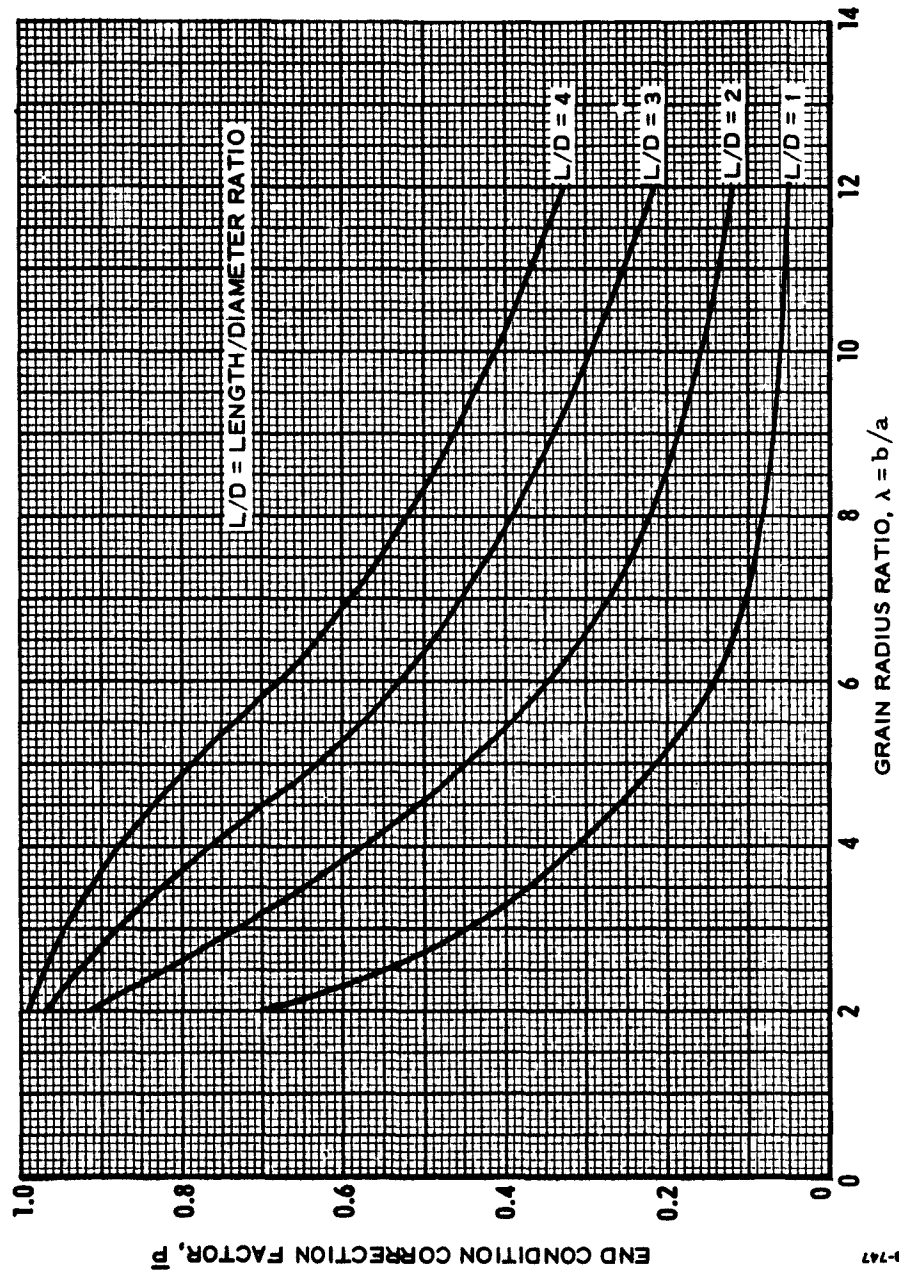


Figure D-2 Parr End Condition Correction Factor for Finite Length Grains, P versus λ

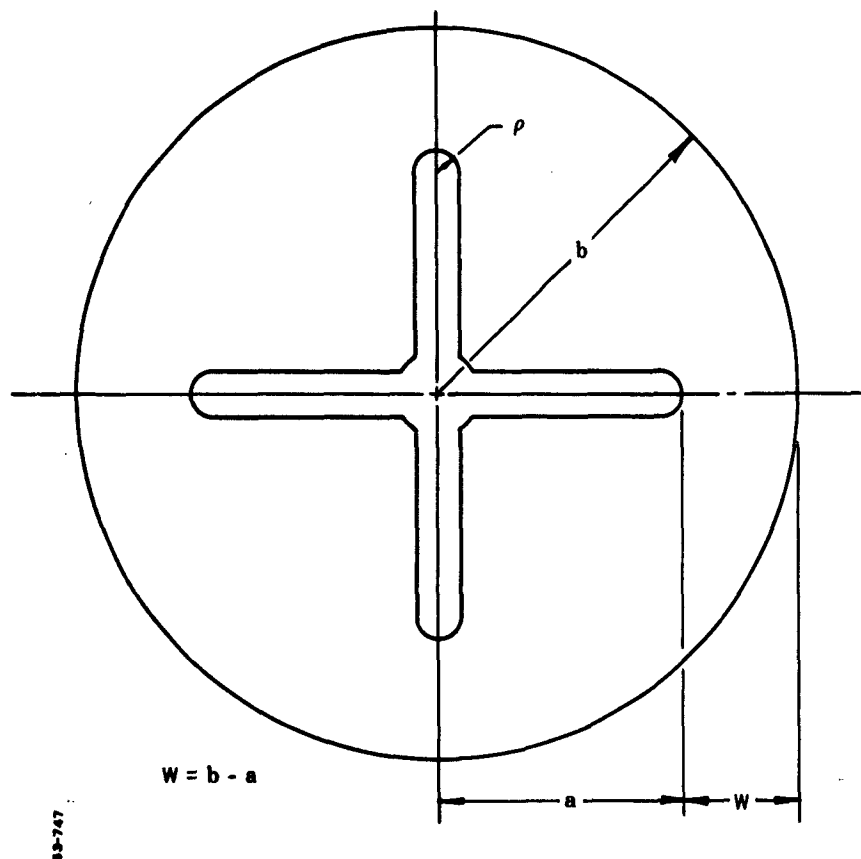


Figure D-3 Nomenclature for Star Valley Stress Concentration Relationships, Figures D-4 through D-8

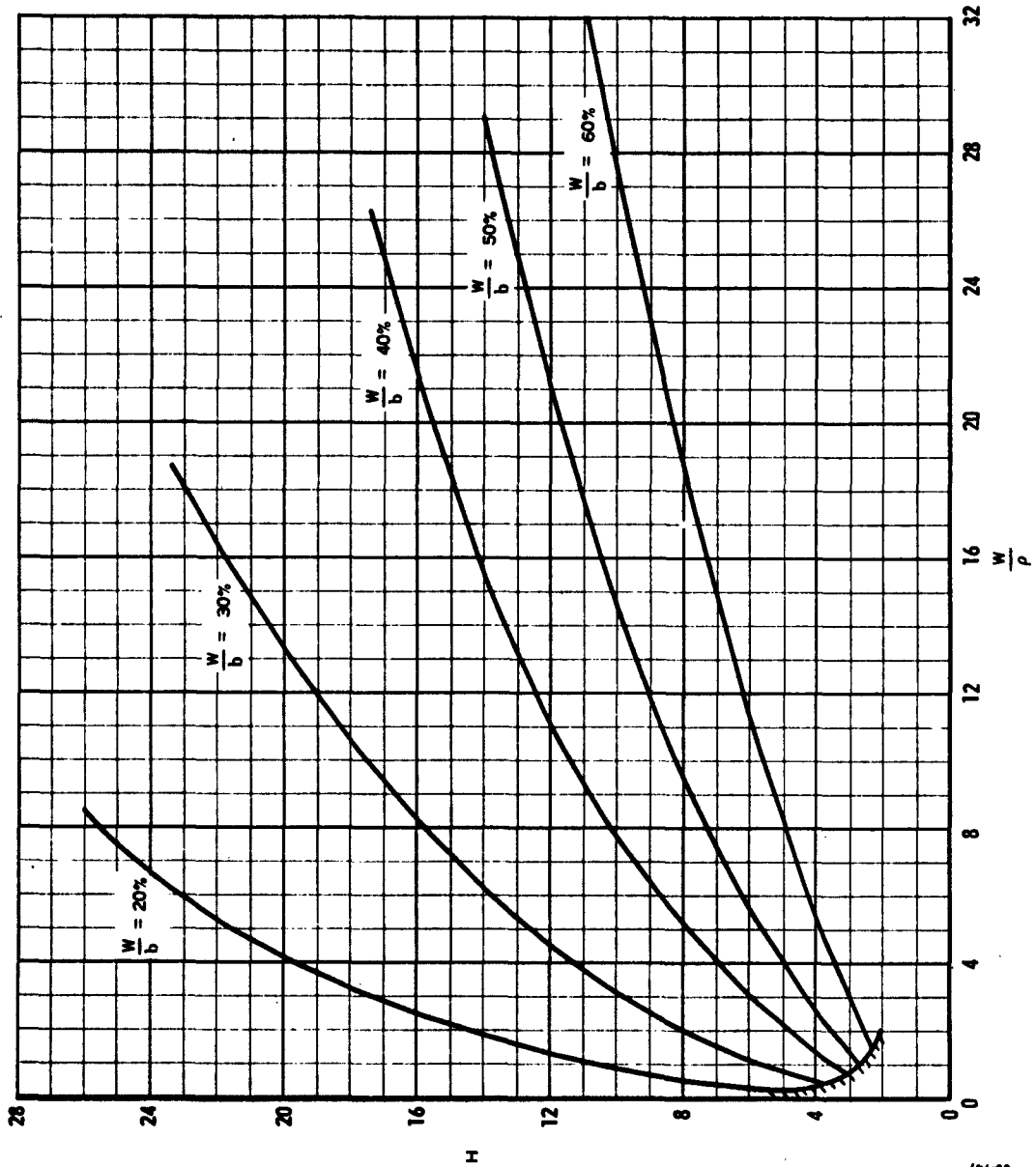


Figure D-4 Star Valley Stress Concentration Factor H for Three-Slotted Grains

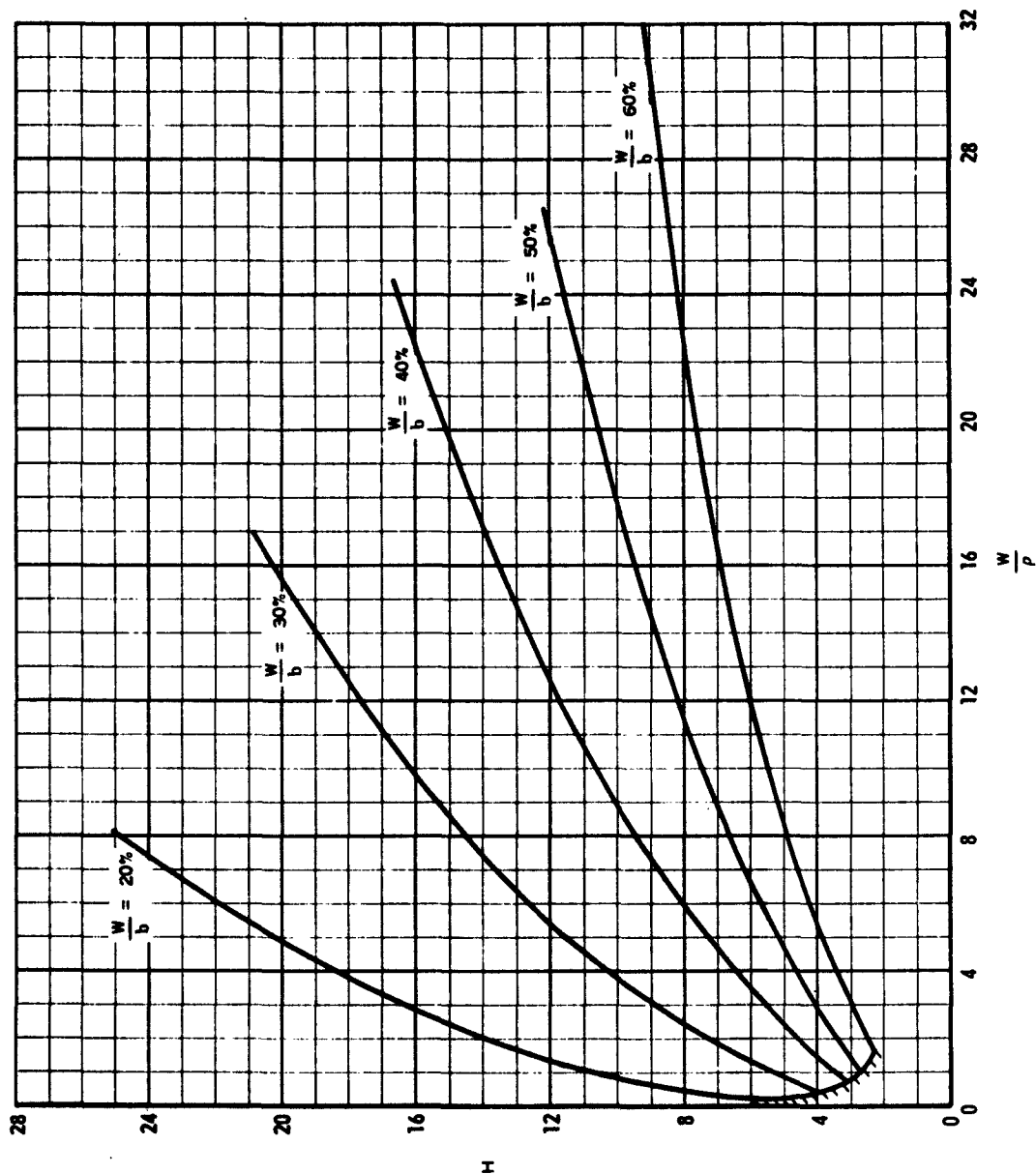


Figure D-5 Star Valley Stress Concentration Factor H for Four-Slotted Grains

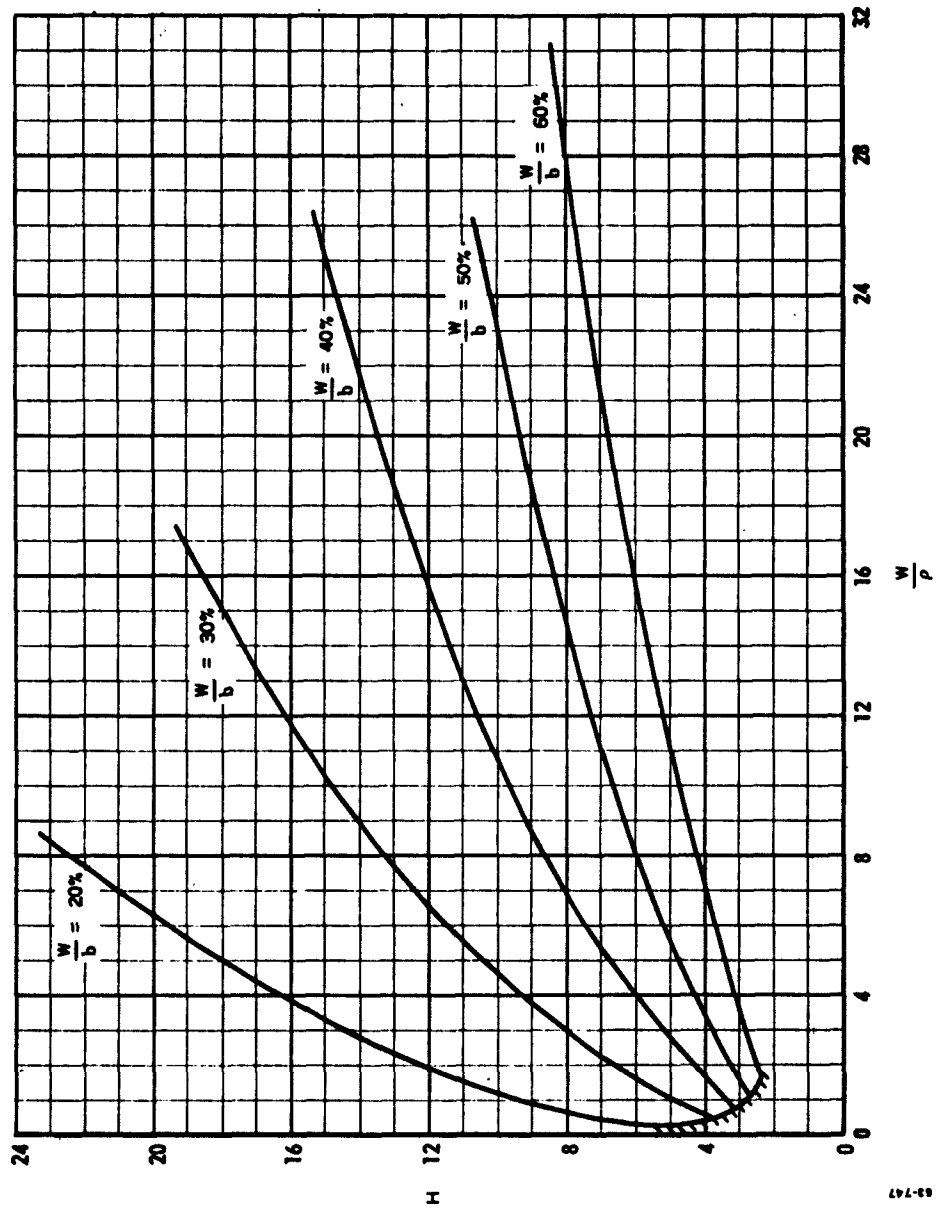


Figure D-6 Star Valley Stress Concentration Factor H for
Five-Slotted Grains

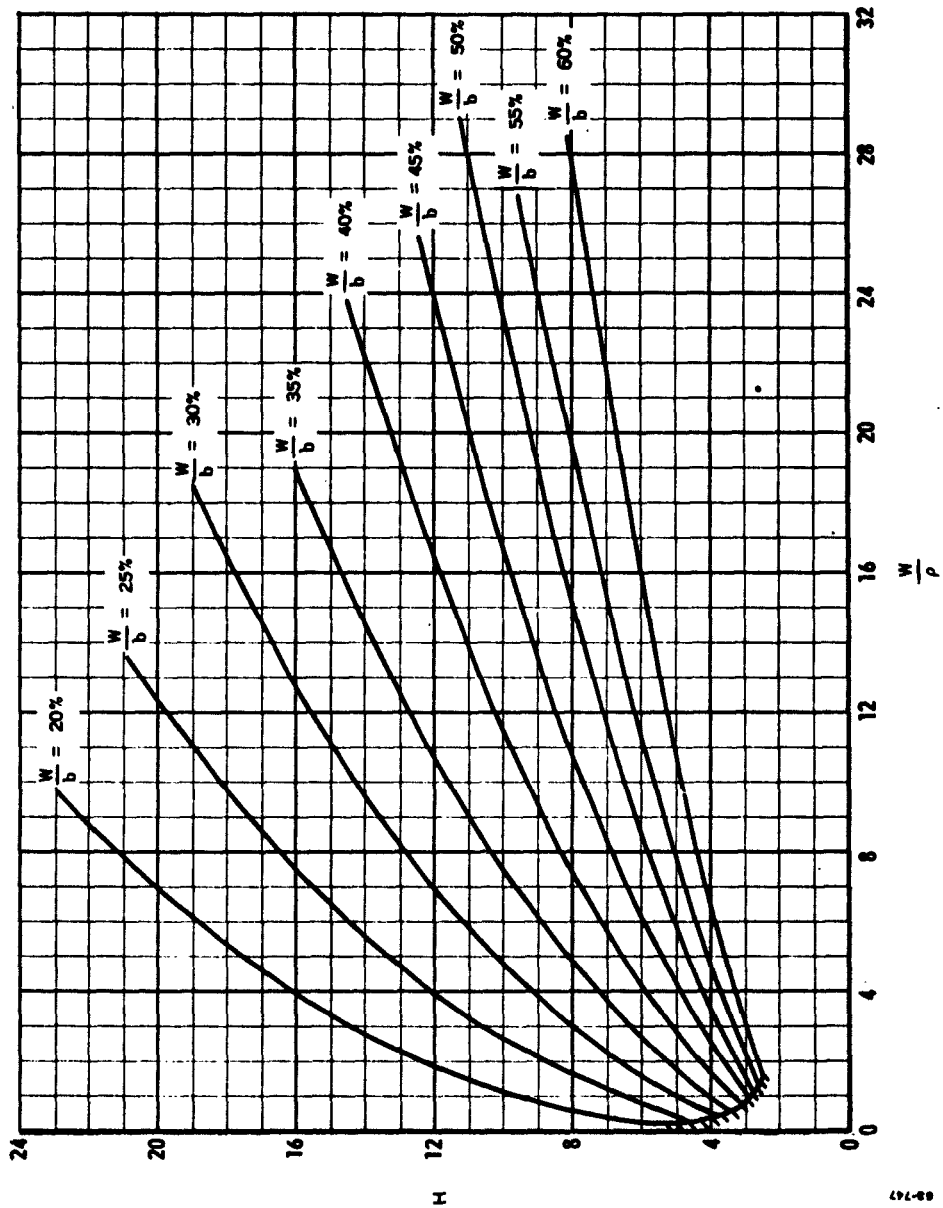


Figure D-7 Star Valley Stress Concentration Factor H for Six-Slotted Grains

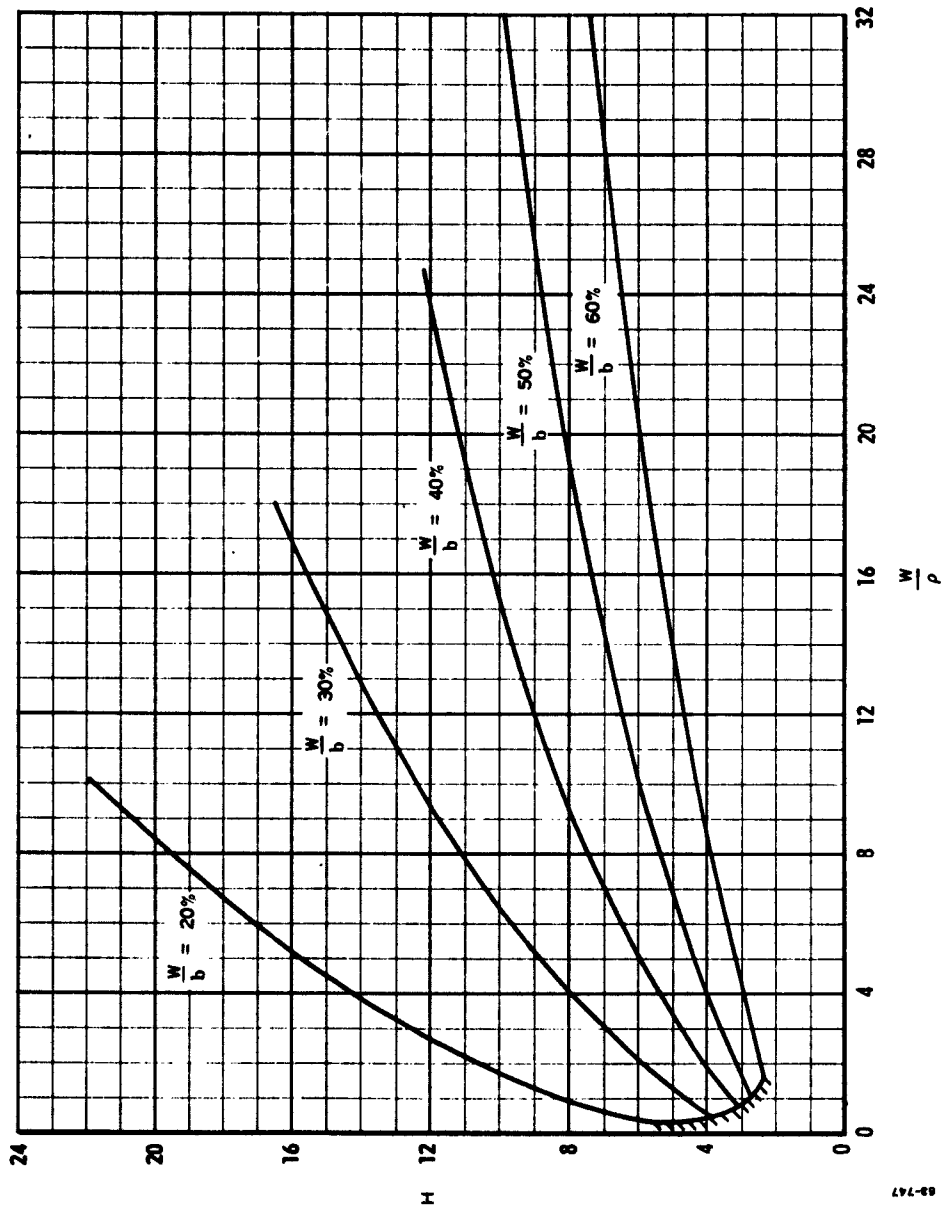


Figure D-8 Star Valley Stress Concentration Factor H for Eight-Slotted Grains

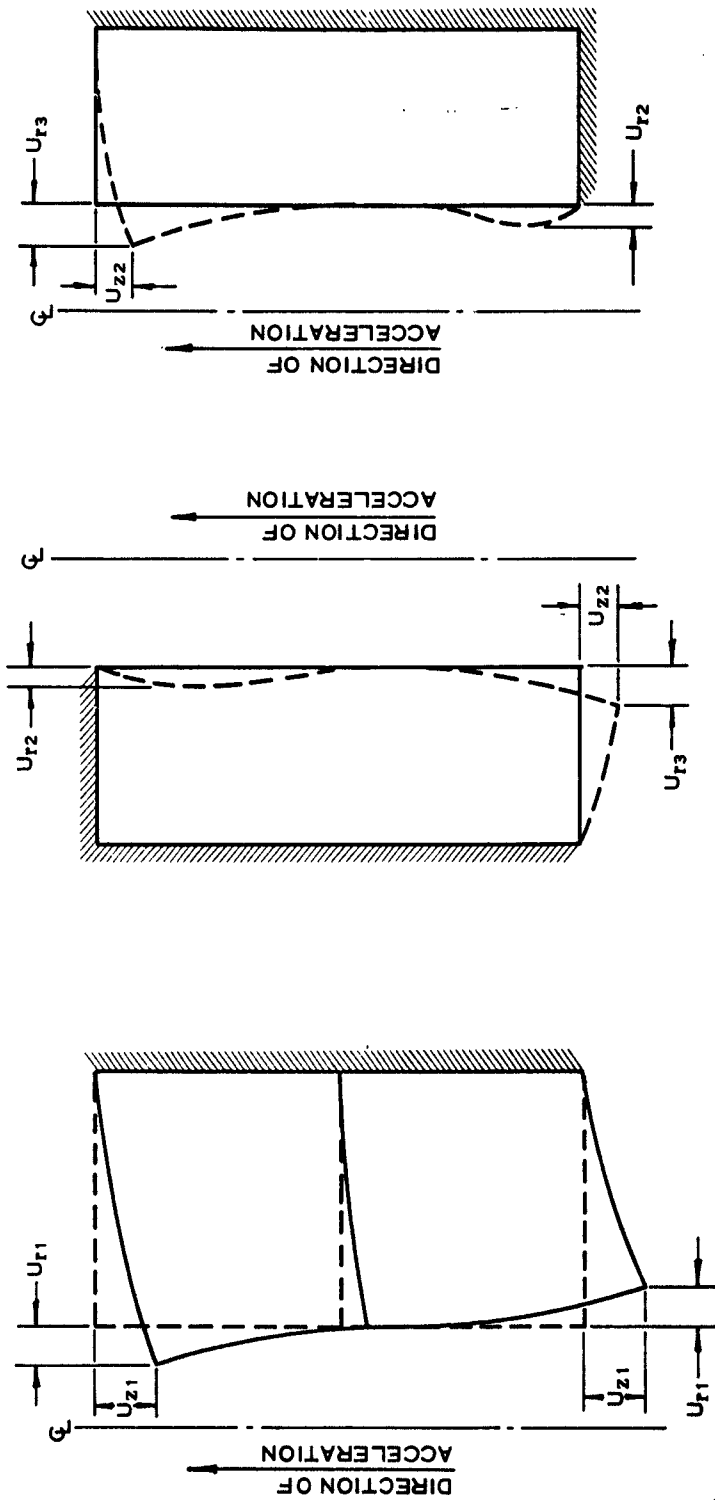


Figure D-9 Nomenclature for Grain Slump Relationships,
Figures D-10 through D-14

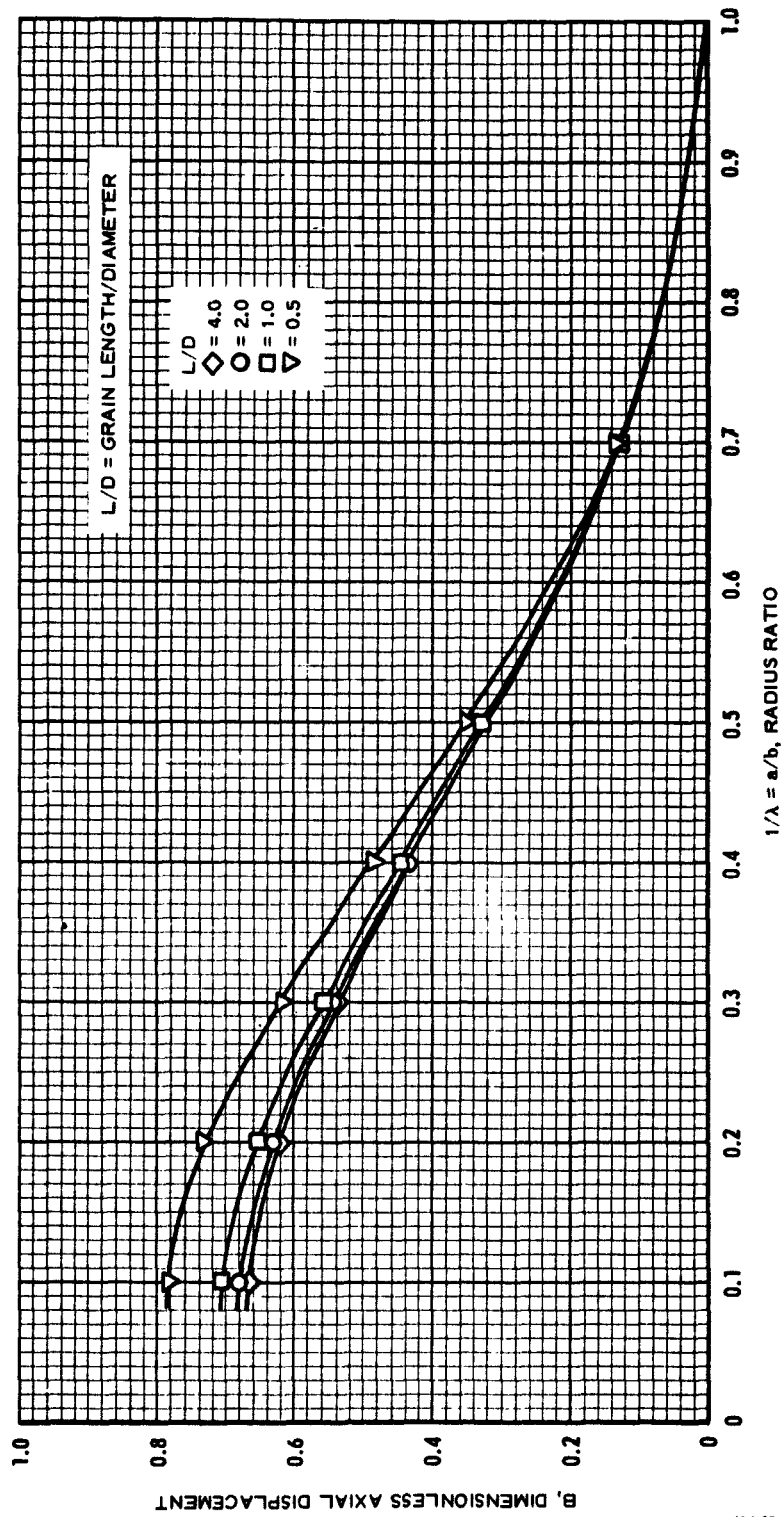


Figure D-10 Dimensionless Axial Displacement U_{z1} of Free Corner of Free-Free Grain

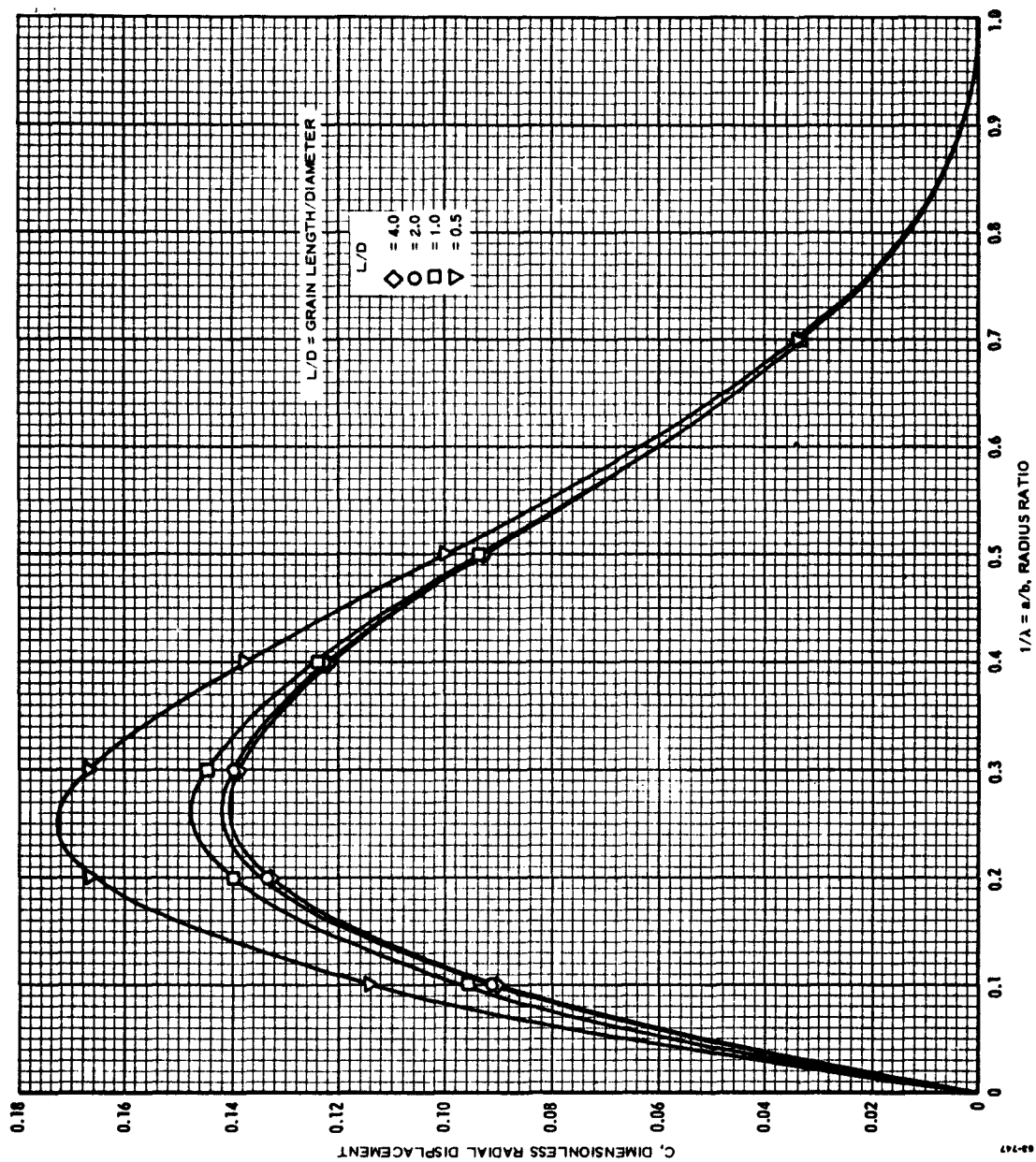


Figure D-11 Dimensionless Radial Displacement U_{r1} of Free Corner of Free-Free Grain

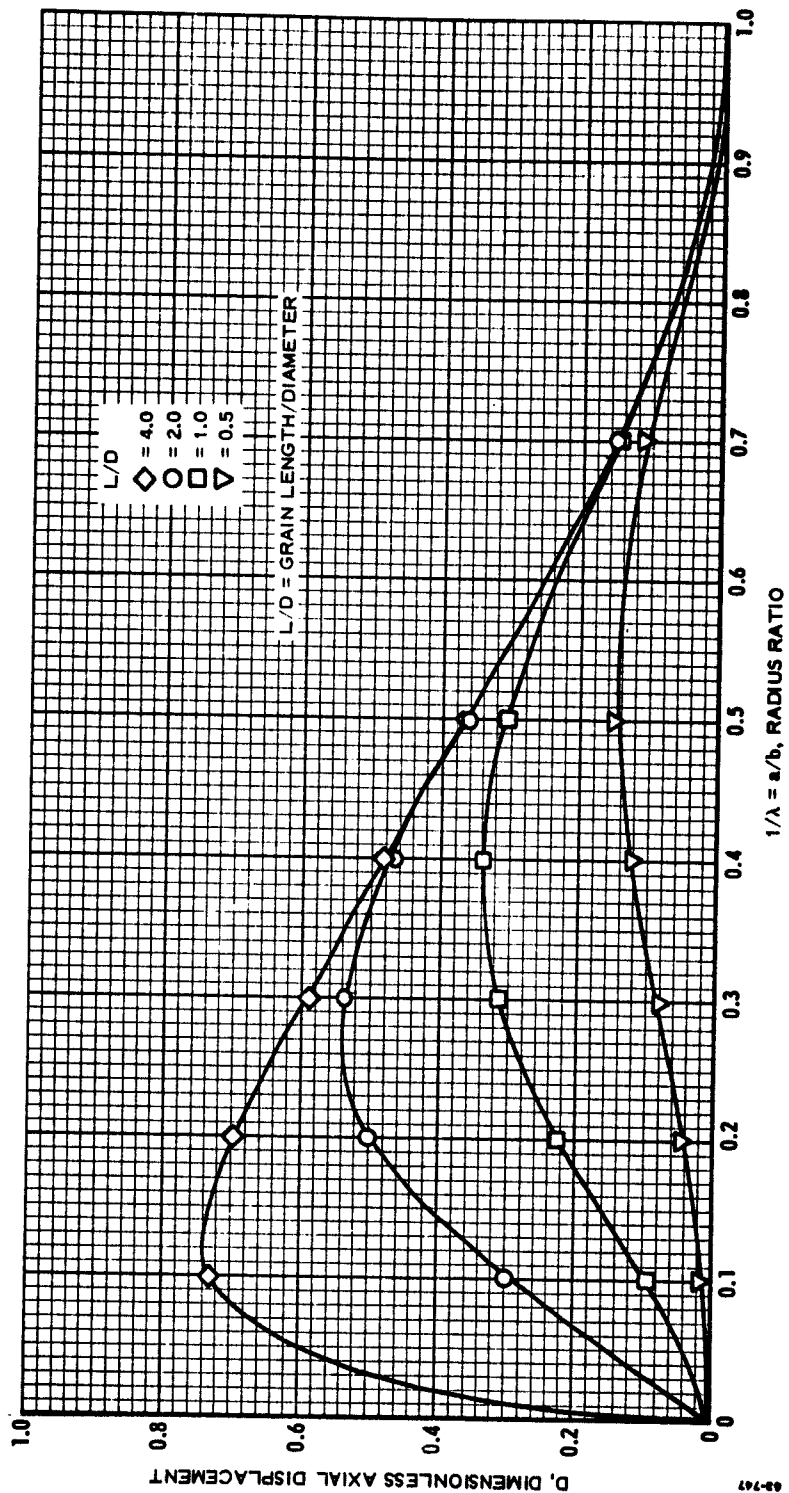


Figure D-12 Dimensionless Axial Displacement U_{zz} of Free Corner of Fixed-Free Grain

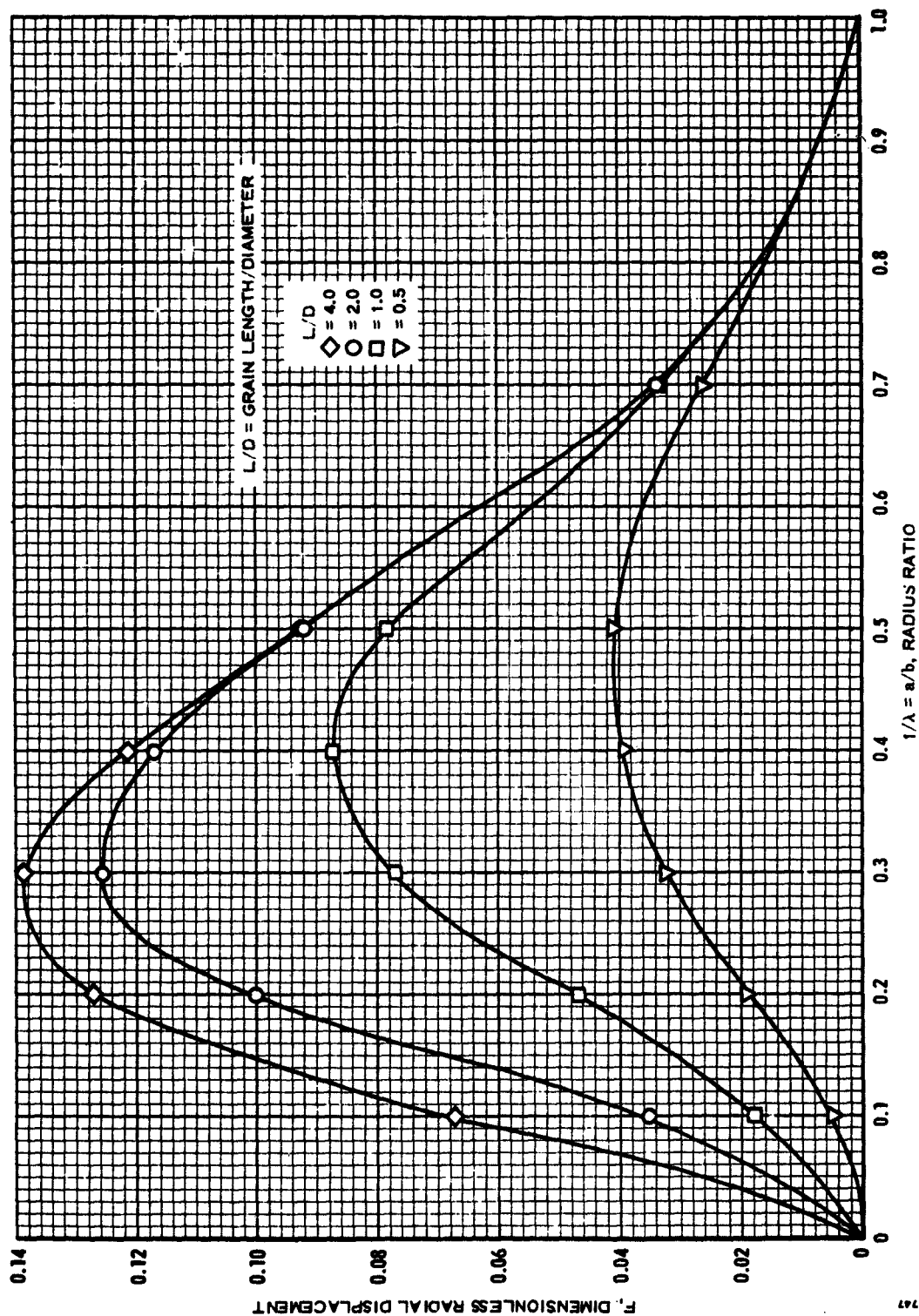


Figure D-13 Dimensionless Radial Displacement U_{r3} of Free Corner of Fixed-Free Grain

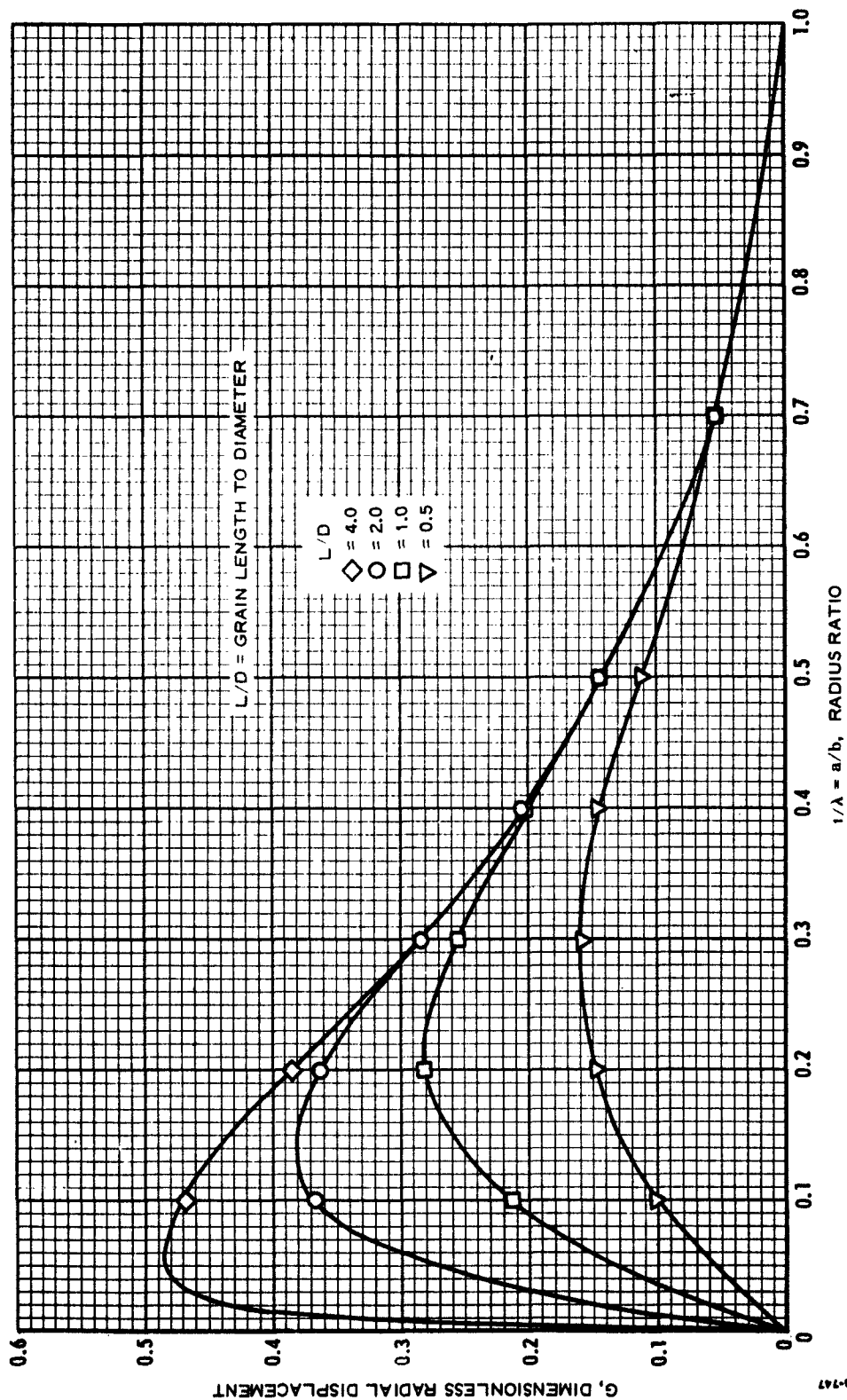


Figure D-14 Dimensionless Radial Displacement, U_{r2} , Near Fixed End of Fixed-Free Grain

REFERENCES

- * Alfrey, T., 1947, Mechanical Behavior of High Polymers, Interscience
- * Billmeyer, F. W., 1962, Textbook of Polymer Science, Interscience

Biot, M. A., 1954, "Theory of Stress-Strain Relations in Anisotropic Viscoelasticity and Relaxation Phenomena," J. Appl. Phys., 25, p. 1385.

Brisbane, J. J., 1962, "Viscoelastic Characterization of Propellant," Interoffice Memo, Rohm and Haas Co., Redstone Arsenal Research Division.
- * Bueche, F., 1962, Physical Properties of Polymers, Interscience

Duerr, T. H., 1961, "Effective Gage Length Measurements in Propellants," Bulletin of 20th Meeting of JANAF Panel on Physical Properties of Propellants, SPIA/pp-14u
- * Eirich, F. R., 1960, Rheology, Volume I, II, III, Academic Press
- * Ferry, J. D., 1961, Viscoelastic Properties of Polymers, Wiley

Fitzgerald, J. E., 1960, Bulletin of 19th Meeting of JANAF Panel on Physical Properties of Propellants, SPIA Publication No. PP-13/SPSP-8

Fitzgerald, J. E., et. al, 1961, "Axial Slump of a Circular Port Grain," Bulletin of 20th Meeting of JANAF Panel on Physical Properties, SPIA/pp-14u

Fourney, M. E., and Parmerter, R. R., 1961, "Stress Concentrations for Internally Perforated Star Grains," Bureau of Naval Weapons, NAV-WEPS Report 7758. (Also, see: Fourney and Parmerter, 1963, "Photoelastic Design Data for Pressure Stresses in Slotted Rocket Grains," AIAA Journal, 1, p. 697.)

Hart, D. A., 1963, "4th Solid-Rocket Conference, a Review," *Astronautics and Aerospace Engineering*, 1, No. 3.
- * ICRPG Solid Propellant Mechanical Behavior Manual, July 1963

Ignatowski, A. J., 1963, "Analog Tests," ICRPG Solid Propellant Mechanical Behavior Manual, Section 4.8. (Also: Rohm and Haas Co., Redstone Arsenal Research Division, Quarterly Progress Report on Interior Ballistics, Report No. P-62-1, 1962.)

Jones, J. W., et. al, 1961, "Propellant Viscoelastic Characterization in Creep and Stress Relaxation Tests," Bulletin of 20th Meeting of JANAF Panel on Physical Properties, SPIA/pp-14u

Jones, J. W., 1963, "Bulletin of the 1st Meeting, Working Group on Mechanical Behavior, Interagency Chemical Rocket Propulsion Group, CPIA Publication No. 2.

REFERENCES (Continued)

- Knauss, Wolfgang, 1963, LPC Structural Integrity Technical Note No. 1.
- Kruse, R. B., and Mahaffey, W. R., 1963, "The Correlation of Viscoelastic Behavior with Model Thermal Testing," ARS Paper No. 2749-63
- * Lee, E. H., 1960, "Solution of Viscoelastic Stress Analysis Problems Using Measured Creep or Relaxation Functions," Interim Technical Report No. 1, Contract Grant DA-ARO(D)-31-124-G54, U.S. Army Research Office Project No. 1892-E
- * Lee, E. H., 1960, "Viscoelastic Stress Analysis," Proceedings of 1st Symposium on Naval Structural Mechanics, Pergamon Press
- * LPC 556-F-1, 1963, "Structural Integrity of Propellant Grains (U)," Final Report, Contract No. DA-04-495-ORD-3260, Lockheed Propulsion Company
- * LPC 578-F-1, 1963, "Thermal Stress Investigation of Solid Propellant Grains," Volume I, Theory and Experiment.
- * Muskhelishvili, N. I., 1953, Some Basic Problems of the Mathematical Theory of Elasticity, Noordhoff.
- Parr, C. H., 1962, "Deformations and Stresses in Case-Bonded Solid Propellant Grains of Finite Length by Numerical Methods," Rohm and Haas Co., Redstone Arsenal Research Division, Quarterly Progress Report on Engineering Research No. P-61-17.
- Parr, C. H., 1963, "Deformations and Stresses in Axially Accelerated Case-Bonded Solid Propellant Grains of Finite Length," Rohm and Haas Co., Redstone Arsenal Research Division, Quarterly Progress Report on Engineering Research No. P-62-27.
- Schapery, R. A., 1962, "Irreversible Thermodynamics and Variational Principles with Applications to Viscoelasticity," Thesis, California Institute of Technology, GALCIT
- Sokolnikoff, I. S., 1956, Mathematical Theory of Elasticity, McGraw-Hill
- Timoshenko, S. and Young, D.H., 1956, Engineering Mechanics, McGraw
- * Timoshenko, and Goodier, 1951, Theory of Elasticity, McGraw
- Tobolsky, A. V., 1956, "Stress Relaxation Studies of the Viscoelastic Properties of Polymers, J. Appl. Phys., 27, p. 673.
- * Tobolsky, A. V., 1960, Properties and Structure of Polymers, Wiley
- * Treloar, L. R. G., 1958, The Physics of Rubber Elasticity, Oxford

REFERENCES (Continued)

Williams, Malcom L., et.al, 1955, "The Temperature Dependence of Relaxation Mechanisms in Amorphous Polymers and Other Glass Forming Liquids," Journal of American Chemical Society, 77, p. 3701

- * Williams, M. L., Blatz, P. J., and Schapery, R. A., 1961, "Fundamental Studies Relating to Systems Analysis of Solid Propellants," Final Report No. SM-61-5, California Institute of Technology.

* General References